January 2011

Cortical Cartography: Mapping Functional Areas Across the Human Brain with Resting State Functional Connectivity MRI

Alexander Cohen
Washington University in St. Louis

WASHINGTON UNIVERSITY IN ST. LOUIS

Division of Biology and Biomedical Sciences

Neurosciences

Dissertation Examination Committee:
Steven Petersen, Chair
Deanna Barch
Kathleen McDermott
Marc Raichle
Brad Schlaggar
David Van Essen

CORTICAL CARTOGRAPHY: MAPPING FUNCTIONAL AREAS ACROSS THE HUMAN BRAIN WITH RESTING STATE FUNCTIONAL CONNECTIVITY MRI

by

Alexander Li Cohen

A dissertation presented to the
Graduate School of Arts and Sciences
of Washington University in
partial fulfillment of the
requirements for the degree
of Doctor of Philosophy

May 2011

Saint Louis, Missouri

ABSTRACT OF THE DISSERTATION

Cortical Cartography:

Mapping functional areas across the human brain

with resting state functional connectivity MRI

by

Alexander Li Cohen

Doctor of Philosophy in Biology and Biomedical Sciences

Neurosciences

Washington University in St. Louis, 2011

Professor Steven E. Petersen, Chairperson

Human behavior and cognition are largely supported by the cerebral cortex, a structure organized at many physical scales ranging from individual neurons up to distributed systems of multiple interconnected “functional areas”. Each functional area possesses a unique combination of inputs, outputs, and internal structure, and is thought to make a distinct contribution to information processing. Thus, the study of each area’s normal function, developmental trajectory, and modified responses following loss or injury may greatly enhance our understanding of cognition. Indeed, one of the (often unsaid) overarching goals of functional neuroimaging is to use differential activity between conditions to identify specific information processing operations reflected in these functional areas. Unfortunately, delineating a complete collection of functional areas in any mammal, let alone non-invasively in humans, is not straightforward and

currently incomplete. Correlations in spontaneous BOLD activity, often referred to as resting state functional connectivity (rs-fcMRI), are especially promising as a way to delineate functional areas since they localize differences in patterns of correlated activity across large expanses of cortex.

Presented here is the exploration, development, initial application, and first order validation of rs-fcMRI mapping, the non-invasive delineation of putative functional areas and boundaries across the cortical surface in individual humans using rs-fcMRI. rs-fcMRI 'contour' maps can be created in individual subjects which delineate sharp transitions and stable locations in correlation patterns. Several of the strongest and most resilient of these features can be consistently detected both across time within subject, are comparable across subject, independent cohort, and scanner, and appear to represent known functional-anatomical divisions. An initial validation of rs-fcMRI mapping against task-related activity, finds consistency with task-related fMRI results for two separate tasks in two groups of subjects, as well as in individual data. These results provide a proof-of-concept for using rs-fcMRI mapping to describe a putative distribution of functional areas and boundaries within single individuals, as well as to potentially improve functional neuroimaging studies in basic, translational, and clinical settings through the independent delineation of functional areas that can be compared across subjects, groups, and studies.

ACKNOWLEDGMENTS

It is a pleasure to thank the many people who made this thesis possible. I would like to begin by expressing my deepest gratitude to my mentor, Dr. Steve Petersen. It has been an honor and a privilege to work on this project with Steve and I am continually amazed by his dedication to scientific objectivity, the high level of rigor to which he holds himself and all of the lab's endeavors, and the meticulous care he takes in teaching and honing the thought process of every one of his students. I could not have asked for a better mentor and his continual support, insight, and challenge to accomplish more than I thought possible have always made me excited to come to work. I can only hope that my future endeavors live up to his standards and expectations. I have also had the privilege of having a second mentor in Dr. Brad Schlaggar. His skill in conducting rigorous science while always considering the clinical applications of the research at hand has made him a tremendous role-model for me as a physician scientist, and I hope that I can someday follow in his footsteps.

I would also like to thank the members of my thesis committee. Dr. Marc Raichle has provided tremendous perspective and many insightful questions that have forced me to think really hard about the implications of the methods and results of this project while my many long discussions with Dr. David Van Essen about the nuts-and-bolts of cortical mapping have certainly impressed upon me the amazing complexity of the thin strip of tissue we call the cerebral cortex. I would also like to extend my humble gratitude to both Dr. Deanna Barch and Dr. Kathleen McDermott; both of whom graciously agreed to be

members of my thesis examination committee with little advance warning. I look forward to hearing their insights into this thesis project.

I would also like to thank Dr. Andreas Burkhalter and Dr. Maurizio Corbetta, each of whom welcomed me into their labs as rotation students. I greatly benefited from their scientific acumen and each provided me with unique insights into cortical organization.

This thesis would not have been possible without the technical expertise and generosity of Fran Miezin, whom I surely bothered endlessly with strange computer error messages, crashed computers, and an endless quest for more hard drive space and processing power. I would also like to thank Mark McAvoy for his continual assistance with Fidl scripts, Avi Snyder for his guidance in image registration and analysis, and John Harwell for his help in implementing new Caret functions. This thesis, of course, relies heavily on the tremendous work of these three invaluable members of our neuroimaging community. I must also extend my thanks to both Donna Dierker and Erin Reid for their patience in training me and answering my innumerable questions on surface-registration.

I also want to thank all of the students and post-docs who have trained alongside me in the Petersen and Schlaggar labs. It has been a joy to work with such an amazing, fun, and extremely talented group of students. They have all been my teachers, my students, my peers, and most importantly, my friends for the past several years and I thank all of them for their insights, their questions, and their camaraderie. I particularly want to thank Steve Nelson, whom I've worked closely with over the past two years. He drove my research into new directions, and our work together has benefited both of us greatly.

I would like to thank Rebecca Coalson and Kelly McVey for all of their assistance in scanning, and Mary Downey-Jones for more things than I could possibly list here. I would also like to thank Brian Sullivan, Shirley McTigue, and the rest of the staff in the MSTP, DBBS, and neuroscience department offices. I must also thank my study participants, without whom this thesis would not be possible.

I would also like to express my deep appreciation and gratitude for my family, whom I've been hundreds of miles away from for quite some time now. My parents, Joseph and Helen Cohen, have been tremendously patient, understanding, and supportive of me in all of my endeavors, and I am indebted to them for all that they have given me. My sister and brother, Jennifer and Jonathan Cohen, both of whom I'm very proud of, have also always supported me, always understanding and never once complaining when I could not be there at graduations or holidays because some big deadline was looming.

This thesis is dedicated to my wonderful and loving wife, Mallika Anand. She has stood beside me and supported me through all of this thesis with tremendous patience and encouragement, and I could not have done it without her.

This research was financially supported by an IGERT Program Fellowship (NSF 0548890), an NRSA Fellowship from NIH/NINDS (F30 NS062489), and by R21 NS061144, R01 NS46424, and the McDonnell Center for Systems Neuroscience.

TABLE OF CONTENTS

LIST OF FIGURES

CHAPTER 1: MAPPING STRUCTURE TO FUNCTION IN THE HUMAN BRAIN WITH RESTING STATE FUNCTIONAL CONNECTIVITY MRI

Cognitive neuroscience is the study of neural substrates underlying mental processes and behavior

One of the perennial goals of both neuroscience and psychology has been understanding how behavior and cognition are implemented by the human brain and the nervous system, giving rise to the shared discipline of cognitive neuroscience. A primary tenet of cognitive neuroscience is that specific cognitive processes correspond to specific physical structures within the nervous system. This is supported by observations of the last 150 years, dating back to John Hughlings Jackson's study of patients with epilepsy (Jackson, 1870) as well as Paul Broca's and Carl Wernicke's parallel work on localization of lesions leading to specific language deficits (Broca, 1861; Wernicke, 1874). However, as knowledge of the brain increased, it became clear that the nervous system is organized at many scales (Figure 1.1), and requires multiple distinct approaches to understand the structures and corresponding functions implemented at each level (Churchland and Sejnowski, 1991).

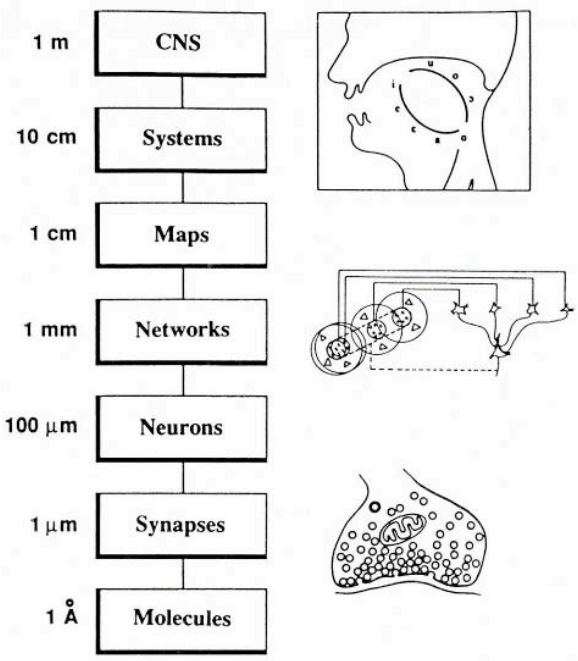

Figure 1.1: Levels of neuroanatomical organization

Churchland and Sejnowski's diagram of the levels of neuroanatomical organization, ranging from the entire central nervous system (CNS) down to the level of individual molecules of neurotransmitters (from (Churchland and Sejnowski, 1991)).

Levels of analysis and methods

Cognitive processes and behaviors are supported by substrates at multiple levels, resulting in components of external behavior or internal cognition, e.g., *motor reflexes* supported by 'networks' of neurons, *visual attention* supported by 'systems' of functional areas (labeled 'maps' in the figure above, see Functional areas… below), or *sadness* likely supported by, or the result of, emergent properties of the collection of 'systems' into conscious awareness. As such, studying the neural implementation of different cognitive processes or behaviors requires access to different levels of neural organization.

As shown in Figure 1.2 below, numerous methods with overlapping capabilities in spatial and temporal resolution can be brought to bear. Of particular note:

- Behavioral studies (not shown in diagram) provide information at the CNS/organism level and insight into the systems level.

- fMRI/PET imaging, non-invasive electrical/magnetic recordings, and the study of lesional deficits are frequently the modality of choice to obtain information at the systems and map levels.
- Invasive electrical, patch clamp and extracellular recordings, and types of optical imaging can access the functional profiles of maps, networks, and neurons.
- At the subcellular level, i.e., synapses/molecules, patch clamp techniques and microscopy techniques such as immunohistochemistry or EM can provide fine-scale detail.
- Alternative methods such as genetic analyses can often impact multiple levels of organization simultaneously.

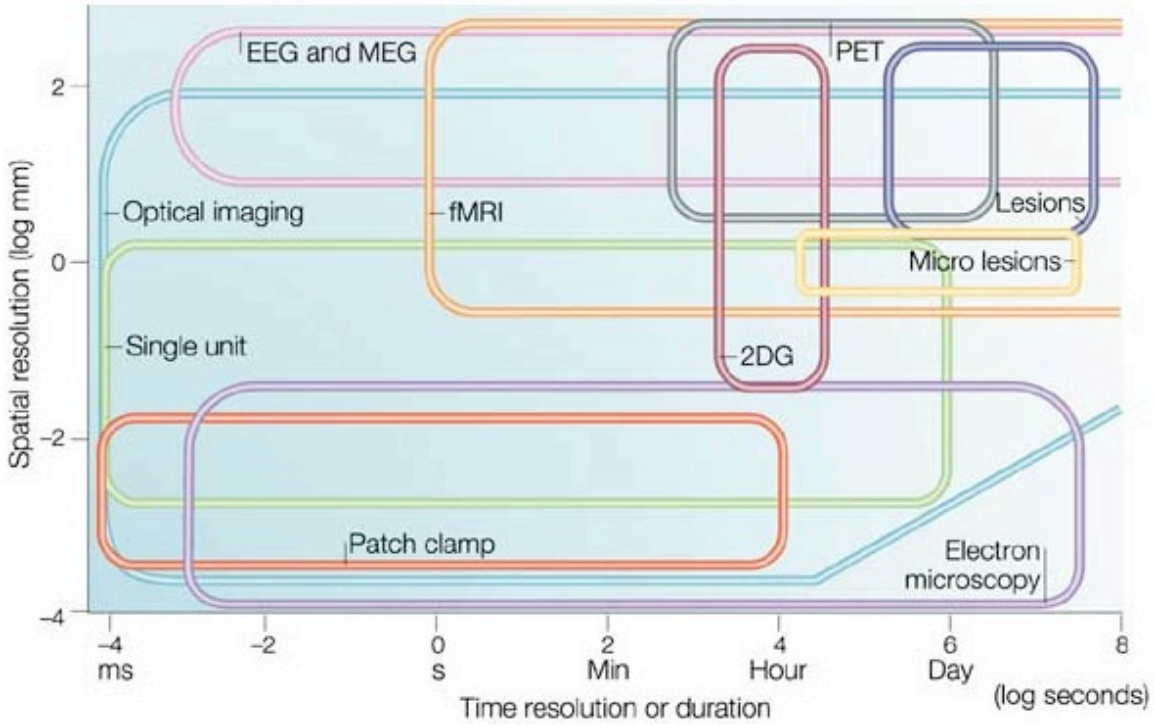

Figure 1.2: The spatial and temporal resolutions of current methods in neuroscience

Grinvald and Hildesheim's diagram comparing the temporal and spatial resolutions of several methods currently in use to study the brain and the nervous system (from (Grinvald and Hildesheim, 2004)).

Studying behavior and cognition in humans is commonly restricted to non-invasive functional neuroimaging techniques, limiting investigation to the levels of CNS, systems, and maps.

Many of the techniques described above are invasive and, in some cases, destructive, limiting their utility in studying human cognition. Since the mid-1980s, however, functional neuroimaging has facilitated progress in cognitive neuroscience by

allowing non-invasive measurement of functional involvement in the brain, with increasing resolution as technology improved.

Functional areas represent separable entities that each may uniquely contribute to information processing.

In Figure 1.2 above, a level labeled "maps" is interposed between networks (i.e., columns) and systems (Churchland and Sejnowski, 1991). They refer to this level as "maps" because many of the most accurately defined entities at this scale (~1 centimeter) are topographically organized cortical areas. Distinct regions, however, have been reported throughout the cortex, including motor (Strick, 1988), and orbitofrontal (Carmichael and Price, 1994) cortex as well as the complete hemispheric partitioning schemes of Brodmann (Brodmann, 1909) and other classical anatomists.

In two seminal papers (Felleman and Van Essen, 1991; Van Essen, 1985), four criteria were proposed for defining functional areas, based mainly on studies of non-human primates: Function (as defined by lesion-behavior or having neurons whose functional properties are distinct from neighboring cortex), Architectonics (having unique arrangements of cells, myelin density, and/or combination of chemical markers, etc.), Connections (having a different combination of inputs and outputs from neighboring cortex), and Topography (having a topographic map that can be used to define boundaries, as between primary visual cortex and V2) - FACT.

Using combinations of these four criteria, many studies have demonstrated that functional areas are distinct and sharply separable regions of cortex, and that this level of differentiation extends across (at least) much of the brain. For instance, sharp borders

have been defined using distinctions between various visual regions such as MT and DL, DL and DM, and DM and M in the owl monkey (Allman et al., 1981). Developmentally, functional areas have been demonstrated to arise from neural tissue with common potential for differentiation, yet still result in sharply demarcated functional areas with distinct functional, architectonic, and connectional properties (O'Leary et al., 1994; Schlaggar and O'Leary, 1991). Clear distinctions are also seen in somatosensory cortex (Drevets et al., 1995; Kaas et al., 1979; Merzenich et al., 1987). Forms of topography have been used to define multiple maps/areas in auditory cortex (Brugge and Reale, 1985; Imig et al., 1977), motor representations (Passingham et al., 2002; Strick, 1988), and for parietal cortex (Lewis and Van Essen, 2000b). In macaques, separable distinct cortical regions have been identified in orbital and medial prefrontal cortex (Carmichael and Price, 1994), consistent with the suggestion that functional distinctions extend beyond sensory and motor regions (Felleman and Van Essen, 1991).

Many of these studies (e.g., (Lewis and Van Essen, 2000a)) note that while these areas are sharply defined within individuals, the variability in folding patterns, area size, and position across subjects drives the use of probabilistic atlases on the group level. It is important to note that this does not symbolize a lack in abrupt borders between areas within the individual.

Since these maps, or functional areas, possess unique combinations of inputs, outputs, and internal structure, each functional area is thought to make a distinct contribution to information processing. Thus, the study of each area’s normal function, developmental trajectory, and modified responses following loss or injury, would greatly

enhance our understanding of typical and disordered cognition. Indeed, one of the (often unsaid) overarching goals of functional neuroimaging is to use differential activity between conditions to identify specific information processing operations reflected in separate functional areas (e.g., (Posner et al., 1988)).

The ability to non-invasively define functional areas in humans is currently limited.

Using the criteria specified above, ascertaining and delineating a complete collection of functional areas in any mammal, let alone non-invasively in humans, is not straightforward and currently incomplete for all species (Levitt, 2003; Van Essen, 2004a). In particular, the ability to define functional areas by these criteria in human cerebral cortex is inadequate, as many of the methods used to generate relatively precise delineations in nonhuman animals are not available for studies of living humans.

Function

fMRI and lesion studies provide some localization ability, but their precision is relatively low. fMRI, for instance, often has difficulty in distinguishing between adjacent regions with similar functional profiles, even within single individuals where the problem of registration is removed. For example, the use of visual motion stimuli to define a putative human MT+ (the plus indicating the tentative inclusion of adjacent functional areas such as MST) (Swallow et al., 2003) admits the incompleteness of the enterprise, and hopes for a time when we have accurate functional localizers for more of cerebral cortex.

Architectonics

Historic architectonic partitioning schemes, such as the rendition of areas introduced by Korbinian Brodmann (Brodmann, 1909), often contain incorrect boundaries and do not address individual variation of location and extent (see (Van Essen and Dierker, 2007a)). Although many (but not all) of Brodmann's areas have now been further subdivided using additional techniques (Van Essen, 1985), the placement of Brodmann's cortical parcellation schema into stereotactic atlases has led to their pervasive use as anatomic labels.

Albeit helpful for providing a general picture of where a region of interest may lie, any current labeling system does not and should not substitute for actual identification of specific functional areas. In practice, this lack of specificity can lead to regions as far apart as 4 cm in stereotactic space, one quarter the anterior-posterior length of the average brain, being referred to by the same name, and considered as part of the same functional entity (e.g., the application of the name "dorsolateral prefrontal cortex" in Kerns et al. (Kerns, 2006) and Luks et al. (Luks et al., 2007)). This lack of specificity not only confuses the field, but is inconsistent with any neurobiological basis of cortical organization. However, without the availability of more precise regional definitions, this common practice is necessary in order to have a common descriptive language. Additionally, obtaining architectonic measurements in living humans remains limited to a restricted set of areas (Scheperjans et al., 2007).

Connectivity

Until recently, the analysis of anatomical connections between different pieces of cortex in living humans could not be approached, although some progress certainly has been made (Amunts and Zilles, 2001; Zilles et al., 2002). As an alternative, diffusion imaging, which measures the directional diffusion of water within a voxel, can reveal local anisotropic differences in fiber bundles in neighboring regions of cortex in living humans, and has recently been used to delineate some human cortical areas (Beckmann et al., 2009; Behrens et al., 2006; Croxson et al., 2005; Hua et al., 2009; Johansen-Berg et al., 2004; Johansen-Berg et al., 2005; Klein et al., 2007). The use of probabilistic fiber bundle differences in diffusion tractography is, in some respects, analogous to the use of blunt dissection to identify major fiber bundles in humans.

Topography

Because the early visual system is topographically organized, topographic mapping has been used in a large number of human imaging studies to localize separate visual functional areas for study (DeYoe et al., 1995; Jack et al., 2006; Sereno et al., 1995). However, while retinotopic maps in early visual areas make the definition of topographic boundaries relatively straightforward, topography degrades higher in the cortical hierarchy making area boundaries based on this method less discernible. As such, while there have been some recent efforts to apply topography mapping to frontal and parietal regions (Silver and Kastner, 2009), the viability of topographic mapping, in humans as in animals, is mostly restricted to early sensory and motor areas.

A new method for obtaining functional areas in humans may be possible using resting state functional connectivity MRI (rs-fcMRI): a rapidly-acquired and non-invasive assay of "seed" functional identity.

Definition

Resting state functional connectivity (rs-fcMRI) is a method for evaluating regional interactions that occur when a subject is not performing an explicit task (Achard et al., 2006; Beckmann et al., 2005; Biswal et al., 1995; Damoiseaux et al., 2006; Dosenbach et al., 2007; Fair et al., 2007a; Fair et al., 2007b; Fox et al., 2005; Greicius et al., 2003; Lowe et al., 1998; Nir et al., 2006; Salvador et al., 2005). It is based on the discovery that low-frequency (< ~0.1 Hz) BOLD fluctuations in distant, but apparently functionally related grey matter regions, show strong correlations at rest (Biswal et al., 1995; Damoiseaux et al., 2006; Lowe et al., 1998; Nir et al., 2006). These low frequency BOLD fluctuations are presumed to relate to spontaneous neural activity (Biswal et al., 1995; Leopold et al., 2003; Nir et al., 2006) and are continuous across multiple 'resting' states, such as eyes-open, eyes-closed, and fixation (Fox et al., 2005; Margulies et al., 2007), as well as across individuals and sessions (Damoiseaux et al., 2006), and, to some extent, across species (Vincent et al., 2007). Cross-correlating the time series of a particular brain region ('seed' region) with all other voxels in the brain can illuminate which voxels are "functionally connected" with the seed region, in that their timecourses are highly correlated. For example, a seed region in the left primary motor cortex shows "functional connections" with the right primary motor cortex as well as supplementary motor area (SMA), and other regions (Biswal et al., 1995).

These voxel-wise correlation maps can be generated for individual subjects (Fox et al., 2006b) as well as for groups (Fair et al., 2007b). The specific mechanisms relating neural activity to these very slow (>10 sec.) fluctuations in the BOLD response are not known, but the spatial patterns of correlation are very similar to the spatial patterns revealed by functional activations and deactivations across multiple tasks: regions that co-activate tend to have positively correlated rs-fcMRI signals, while regions that become negative when a seed region activates tend to be negatively correlated with the seed region (Fox et al., 2005; Fransson, 2005).

Replication of fMRI results

Multiple studies have demonstrated the ability of rs-fcMRI to identify regions and networks of regions that are functionally related. In pioneering work, Biswal et al. demonstrated strong functional connectivity among motor regions (Biswal et al., 1995). More recently, Greicius (Greicius et al., 2003) and other groups (reviewed in (Raichle and Snyder, 2007)) have replicated the 'default' set of regions (i.e., regions active at rest) as being functionally connected by rs-fcMRI. Fox et al. used rs-fcMRI to identify and distinguish between dorsal and ventral attention networks (Fox et al., 2006a), Hampson et al. found significant correlations between the strength of specific functional connections and performance on a working memory task (Hampson et al., 2006a). Functionally defined networks known to be involved in reading show strong rs-fcMRI correlations as well (Hampson et al., 2006b; Mencl et al., 2000). Our own lab has shown that rs-fcMRI delineates and differentiates between two separable executive control networks (Dosenbach et al., 2007). Across all of these studies the common result appears to be that

correlations seen with rs-fcMRI reflect some aspect of common function, potentially a history of co-activation. These correlations are not driven by common metabolic demands or vascular distribution (unpublished results).

rs-fcMRI has recently generated considerable interest for several reasons (Vincent et al., 2006). First, resting state BOLD fluctuations allow descriptions of connectivity patterns even in individual subjects. Second, rs-fcMRI unburdens experimental design, subject compliance, and training demands, making it attractive for studies of development and clinical populations (Bokde et al., 2006; Castellanos et al., 2008; Fair et al., 2007a; Greicius et al., 2007; Greicius et al., 2004; Rombouts and Scheltens, 2005; Tian et al., 2006; Whalley et al., 2005). Lastly, resting state functional connectivity, particularly the methods described in this proposal, may provide a basis for comparisons between species (Vincent et al., 2006).

Since rs-fcMRI measures correlated activity, it might in principle reflect mainly direct (monosynaptic) anatomical connections. Empirically, though, the linkage between highly correlated regions can evidently be indirect, through one or more intermediate regions or merely common input (Vincent et al., 2007). Regardless of functional connectivity's equivalence to anatomical connectivity, a functional area's history of interaction with other areas is likely to be consistent across its spatial extent, barring topographically-organized areas, and distinct between separate areas. As such, rs-fcMRI may be well suited for delineating the location and boundaries of a large number of functional areas.

rs-fcMRI may be useful as a functionally-defined analogous assay of connectional tracing in humans.

While rs-fcMRI may not reveal anatomical connections of the kind seen in tract-tracing studies (Vincent et al., 2007); it has the potential to be exploited in the same fashion for the purpose of defining functional areas. rs-fcMRI "seeds" can be placed in any cortical or sub-cortical location and the pattern of correlations with that seed point calculated for the rest of the brain. As such, recent work analyzing these correlation maps has shown some promise in finding boundaries in group data (Kim et al., 2009; Margulies et al., 2007; Roy et al., 2009; Schubotz et al., 2009) as well as some initial utility in locating specific functional areas in distorted anatomies, i.e., due to stroke or tumor growth (Zhang et al., 2009a). These works, however, have typically relied on anatomically defined regions of interest, either over the whole brain, or in one hemisphere to analyze the contralateral side. An ideal mapping solution could hopefully produce putative functional area locations across the entire hemisphere simultaneously.

Can a "rs-fcMRI mapping" methodology be developed that can non-invasively delineate functional areas in individual human brains?

The goal of this thesis is to explore the feasibility and validity of generating a non-invasive rs-fcMRI-based functional area parcellation method. The subsequent chapters of this thesis will describe an exploration of the potential for using rs-fcMRI in defining functional areas (Chapter 2) and the subsequent development of an analysis procedure that results in rs-fcMRI contour maps that span cortical hemispheres (Chapter 3). This is followed by an internal validation and extension of the methods developed in

Chapter 3 by viewing the rs-fcMRI mapping results from multiple subjects, independent cohorts, and data collected on different MRI scanners (Chapter 4). Then, an initial cross-validation of rs-fcMRI mapping, via comparison with task-related fMRI results acquired within the same subjects, is presented in Chapter 5. Finally, a discussion of potential extensions and applications of rs-fcMRI mapping is presented (Chapter 6).

CHAPTER 2: THE POTENTIAL FOR DEFINING FUNCTIONAL AREAS IN INDIVIDUAL HUMAN BRAINS USING RS-FCMRI

NOTE: This chapter was independently published as Cohen et al., Defining functional areas in individual human brains using resting functional connectivity MRI, NeuroImage, 2008. (doi:10.1016/j.neuroimage.2008.01.066). As such, much of the introduction to this chapter is redundant with the previous Chapter 1.

Introduction

In Churchland and Sejnowski's famous diagram showing the levels of neuroanatomical organization, a level labeled "maps" is interposed between networks (i.e., columns) and systems (Churchland and Sejnowski, 1991). This level was called "maps" because many of the most accurately defined entities at this scale (~ 1 cm) are topographically organized cortical areas. Classic examples include the multiple retinotopic maps of primary and extrastriate visual cortex, where each map constitutes a separate representation of the visual field and contains neurons with a distinctive collection of functional characteristics.

Organization at this scale is not limited to visual cortical regions, nor to topographically organized somatosensory (Clark et al., 1988) or auditory (Langers et al., 2007) maps. Distinct subregions have been reported throughout the cortex, including motor (Strick, 1988), and orbitofrontal (Carmichael and Price, 1994) cortex as well as the complete hemispheric partitioning schemes of Brodmann (Brodmann, 1909) and other classical anatomists. Although topography is not seen in every region, it can be combined with other attributes, as suggested by Passingham and colleagues for frontal and motor

regions (Passingham et al., 2002), to provide a distinct "fingerprint" that can be used for the identification of individual regions.

For the remainder of this report, regions that represent separable functional domains of cortex will be referred to as "functional areas". This is in distinction to a more general term, "region", or "region of interest", which may encompass all or part of several functional areas. Because functional areas possess unique combinations of inputs, outputs, and internal structure, each functional area is thought to make a distinct contribution to information processing. Thus, the study of each area's normal function, developmental trajectory, and modified responses following loss or injury, can be greatly aided by the ability to accurately and reliably define the location and boundaries of functional areas in individual living humans.

Four criteria have been proposed for defining cortical areas, based mainly on studies of non-human primates (Felleman and Van Essen, 1991; Van Essen, 1985): Function (as defined by lesion-behavior or having neurons whose functional properties are distinct from neighboring cortex), Architectonics (having unique arrangements of cells, myelin density, and/or combinations of chemical markers, etc.), Connections (having a different combination of inputs and outputs from neighboring cortex), and Topography (having a topographic map that can be used to define boundaries, for example between primary visual cortex and V2).

Unfortunately, the current ability to define functional areas by these criteria in human cerebral cortex is inadequate. fMRI and lesion studies provide some localization ability, but their precision is relatively low. Historic architectonic partitioning schemes,

such as the rendition of areas introduced by Korbinian Brodmann, unfortunately often contain incorrect boundaries and do not address individual variation of location and extent (see (Van Essen and Dierker, 2007a)). Promising methodologies such as architectonic measurements in living humans (Scheperjans et al., 2007) and connectional studies using DTI (Klein et al., 2007) are currently still limited to a small set of areas. Mapping of topographic organization is mostly restricted to sensory and motor areas.

Recently, measures of correlation between resting brain regions (so-called resting-state functional connectivity, or rs-fcMRI) have demonstrated promise in describing boundaries between functional areas in limited regions of cortex (Margulies et al., 2007). Resting state functional connectivity is a method for evaluating regional interactions that occur when a subject is not performing an explicit task (Achard et al., 2006; Beckmann et al., 2005; Biswal et al., 1995; Damoiseaux et al., 2006; Dosenbach et al., 2007; Fair et al., 2007a; Fair et al., 2007b; Fox et al., 2005; Greicius et al., 2003; Lowe et al., 1998; Nir et al., 2006; Salvador et al., 2005). It is based on the discovery that low-frequency (< ~0.1 Hz) BOLD fluctuations in distant, but apparently functionally related grey matter regions, show strong correlations at rest (Biswal et al., 1995; Damoiseaux et al., 2006; Lowe et al., 1998; Nir et al., 2006). These low frequency BOLD fluctuations are presumed to relate to spontaneous neural activity (Biswal et al., 1995; Leopold et al., 2003; Nir et al., 2006). Additionally, since rs-fcMRI does not require active engagement in a behavioral task, it unburdens experimental design, subject compliance, and training demands, making it attractive for studies of development, aging, and clinical populations (Bokde et

al., 2006; Castellanos et al., 2008; Greicius, 2008; Greicius et al., 2007; Rombouts and Scheltens, 2005; Tian et al., 2006; Whalley et al., 2005).

Cross-correlating the time series of a particular brain region (seed region) with all other voxels in the brain can illuminate which voxels are "functionally connected" with the seed region, in that their timecourses are highly correlated. For example, a seed region in the left primary motor cortex shows "functional connections" with the right primary motor cortex as well as supplementary motor area (SMA) (Biswal et al., 1995), and other regions. These voxel-wise correlation maps can be generated for individual subjects (Fox et al., 2006b). The specific mechanisms relating neural activity to these very slow (>10 sec.) fluctuations in the BOLD response are not known, but the spatial patterns are similar to those revealed by the signal functional activation data: regions that co-activate tend to have correlated rs-fcMRI signals while regions that become negative when a seed regions activates tend to be negatively correlated with the seed region (Fox et al., 2006a; Greicius et al., 2003).

Because "seeds" can be placed in any cortical or subcortical location, development of methods for analyzing these correlation maps could provide a basis for delineating the location and boundaries of a large number of functional areas in single individuals. The analyses presented below provide evidence that rs-fcMRI can aid in the delineation of a large number of functional area boundaries in individual human cortex. They show that: (i) Changes in correlation maps occur abruptly as the seed location moves systematically across the cortical sheet, suggesting the presence of a boundary rather than a smooth gradation. (ii) These transitions occur in many locations in

individual subjects. (iii) Customized image processing techniques can be used to identify putative boundaries and bounded regions across large expanses of cortex. (iv) The boundaries appear reliable when assessed with independent measurements. (v) The overall map has the appropriate granularity to reflect area-level cortical parcellation.

Methods

Overview

The aim of the analysis stream presented here is to identify locations on the cortex where the pattern of rs-fcMRI changes rapidly, potentially representing boundaries between functional areas. Our approach utilizes established fcMRI voxel-wise correlation methods, coupled to several novel analysis techniques that are performed on a surface representation of the cortex. These include established edge detection and image segmentation algorithms used in computer vision and image analysis programs. These surface-based operations treat the brain as a 2D sheet, while volume-based analyses treat the brain as a 3D volume.

The flowchart in Figure 2.1 describes the major steps involved in our analysis stream. Annotations refer to specific parts of the Methods section that describe each portion of our approach and Figures that display the various intermediate steps of the analysis. This methodology can be applied to any set of fcMRI data see (Fair et al., 2007b), but the current analysis involves continuous resting state/relaxed fixation data.

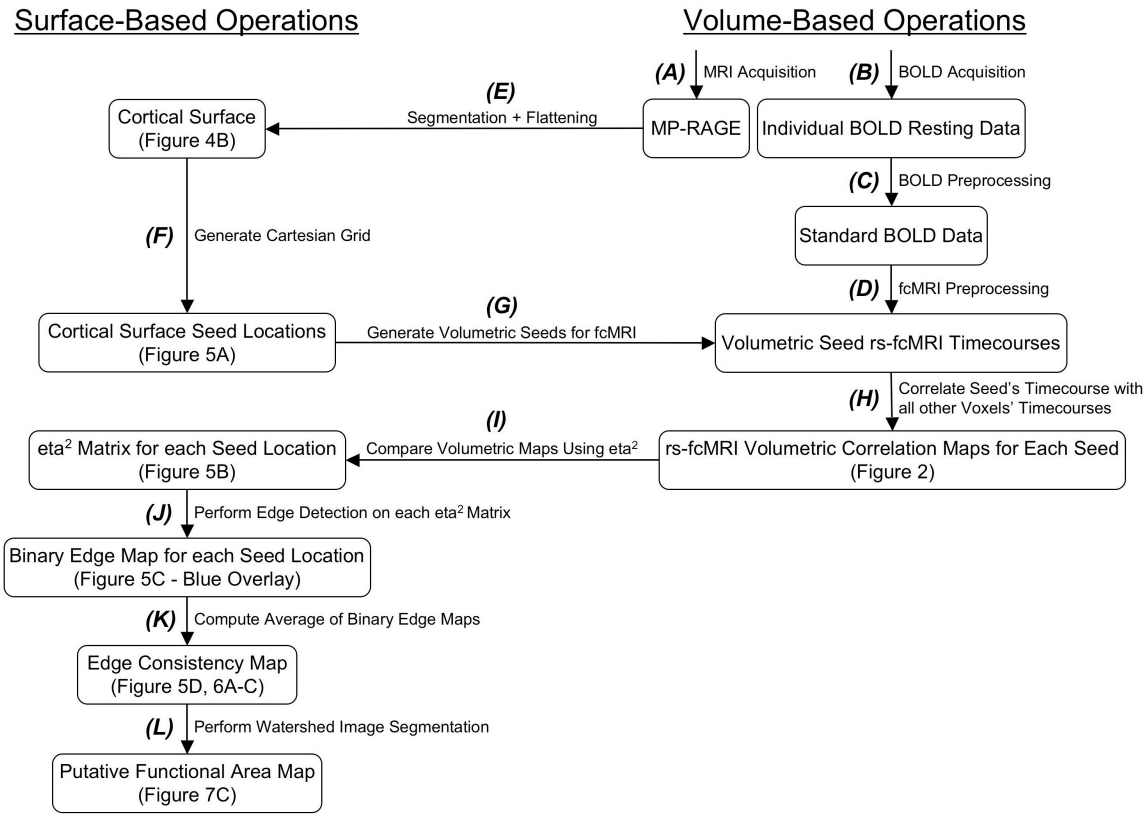

Figure 2.1: rs-fcMRI analysis stream flowchart

Flowchart outlining the analysis stream presented here and the techniques involved. Bolded letters refer to specific portions of the Methods section that describe each procedural operation. Examples of several steps in the procedure are denoted by the Figure where they can be found.

Data acquisition

fMRI data were acquired on a Siemens 1.5 Tesla MAGNETOM Vision system (Erlangen, Germany). (A) Structural images were obtained using a sagittal magnetization-prepared rapid gradient echo (MP-RAGE) three-dimensional T1-weighted sequence (TE=4 ms, TR=9.7 ms, TI=300 ms, flip angle=12 deg, 128 slices with 1.25 x 1

x 1 mm voxels). (B) Functional images were obtained using an asymmetric spin echo echo-planar sequence sensitive to blood oxygen level-dependent (BOLD) contrast (T2* evolution time=50 ms, α=90°, in-plane resolution 3.75x3.75 mm). Whole brain coverage was obtained with 16 contiguous interleaved 8 mm axial slices acquired parallel to the plane transecting the anterior and posterior commissure (AC-PC plane). Steady state magnetization was assumed after 4 frames (~ 10 s). 128 whole brain images (TR=2.5s) were acquired per BOLD run across 6 runs for our single subject (23yo female). For the population-average analysis, 32 whole brain images (TR=2.5s) were extracted from the rest blocks from a mixed blocked/event-related design per BOLD run across 8 runs for 31 subjects (avg. 24.4yo, 17F).

Data preprocessing

Standard fMRI preprocessing

(C) Functional images were processed to reduce artifacts (Fair et al., 2007b; Miezin et al., 2000). These steps included: (i) removal of a central spike caused by MR signal offset, (ii) correction of odd vs. even slice intensity differences attributable to interleaved acquisition without gaps, (iii) correction for head movement within and across runs and (iv) across-run intensity normalization to a whole brain mode value of 1000.

Several of the temporal nuisance signals that need to be regressed out to examine the resting state signal are related to anatomical structures, such as white matter and the ventricles (see rs-fcMRI preprocessing below). This entails registering the data for each subject to an atlas space, so that common imaging masks and fcMRI seeds can be used to

define these nuisance signals in each subject. This transformation of the functional data to atlas space, in this case, 711-2B (Buckner et al., 2004; Ojemann et al., 1997; Talairach and Tournoux, 1988) was computed for each individual via the MP-RAGE scan. Each run then was resampled in atlas space (Talairach and Tournoux, 1988) on an isotropic grid (3 mm voxels) combining movement correction and atlas transformation in one interpolation (Lancaster et al., 1995; Snyder, 1996). This single interpolation procedure eliminates blurring that would be introduced by multiple interpolations. All subsequent operations were performed on the atlas-transformed volumetric timeseries.

rs-fcMRI specific preprocessing

(D) Pre-processing for functional connectivity analyses was performed on the fMRI data, as in Fox et. al. (Fox et al., 2005), to optimize the time-series data and remove spurious variance. These steps include removal of the linear trend, temporal band-pass filtering (0.009 Hz < f < 0.08 Hz), spatial smoothing (6 mm full width at half maximum), as well as regression of several "nuisance" signals and their time-based first order derivatives, including six motion parameters, and whole brain, ventricular, and white matter signals.

Cortical surface generation from anatomical MRI data using Caret

(E) The structural MRI volume for the single-subject analysis was spatially normalized to the 711-2B volumetric MRI atlas (Lancaster et al., 1995; Snyder, 1996) and resampled to 1 mm^3 voxels. Segmentation of the cortical mid-thickness as well as surface reconstruction was done using Caret 5.3 software (Van Essen et al., 2001). Surface flattening was accomplished by making cuts along five standardized trajectories

that help minimize distortions (see Figure 2.2 and (Van Essen, 2005)). This flattened surface was then used to generate a grid of seed points, or patch, which was then used to generate rs-fcMRI correlation maps as described below.

rs-fcMRI boundary generation

Cortical seed and rs-fcMRI correlation map generation

(F) On the flat map of the subject's cortex, a Cartesian 3 mm point grid was created using Caret to define a set of seeds representing a patch of the cortical surface that respects cortical folding patterns (as shown in Figure 2.5A). This allowed us to treat the cortex as a 2D structure and use standard 2D image processing techniques. (G) The corresponding 3D stereotactic coordinates for each Cartesian grid point were used to generate 3 mm diameter spherical regions of interest around each volumetric seed voxel. This sampling density provides a fine-grained map without excessive oversampling of the fMRI data (3 mm voxel size, but with 6 mm FWHM smoothing). While each seed point is 3 mm apart on the flattened representation, the folding pattern of the brain results in some seeds being further than 3mm apart in the underlying volume, while others are closer than 3mm in the underlying volume. (H) For each seed, volumetric correlation maps were generated as in Fox et al. (Fox et al., 2005) and Fair et al. (Fair et al., 2007b) by correlating the timecourse of this region of interest with the timecourses of all other voxels over the entire volume of the brain. This creates a volumetric correlation map for each seed, where the intensity at each voxel is the Fisher Z-transformed correlation (r) between that voxel and the seed region for the volume.

eta² matrix creation for each seed

(I) To compute the similarity between seed locations, an eta² coefficient was calculated for every seed pair. eta² is equal to the fraction of the variance in one signal accounted for by variance in a second signal where comparisons are done on a point by point basis. The more similar two signals, or in this case, images, are, the higher the eta² coefficient between them. eta² can vary in value from 0 (no similarity) to 1 (identical). To determine the similarity or difference between the large-scale correlational structure of two seed locations, eta² is calculated between the two volumetric correlation maps (a and b) generated from these two seed locations and equals:

$$eta^2 = 1 - \frac{SS_{Within}}{SS_{Total}} = 1 - \frac{\sum_{i=1}^{n}\left[(a_i - m_i)^2 + (b_i - m_i)^2\right]}{\sum_{i=1}^{n}\left[(a_i - \overline{M})^2 + (b_i - \overline{M})^2\right]}$$

where a_i and b_i represent the values at position i in maps a and b respectively. m_i is the mean value of the two images at position i, $(a_i+b_i)/2$, and M-bar is the grand mean value across the mean image, m, or across all locations in both correlation maps. eta² measures the difference in the values at corresponding points in the two images, not strictly whether the points vary in similar ways, and can detect differences and similarities in the volumetric correlation maps using information from all of the voxels of the entire volume. The eta² coefficients are stored in a series of matrices (the same size and shape as the patch of seeds) such that each seed has a corresponding matrix

representing the eta^2 coefficients of that seed's volumetric correlation map compared to the volumetric correlation maps of all other seeds in the patch (as shown in Figure 2.5B).

We use eta^2 to compare images instead of correlation, *r*, because our goal is to quantify the similarity of the two images, not the correlational relationship between them. While correlation is often used for similarity description, there are instances where the correlation coefficient between images is unaffected by changes in the two images which make them more or less similar from each other. Two examples where this is readily apparent are scaling and offset; if the value of each voxel in one map is exactly double the value of another, they will have a correlation coefficient of 1, but are still different from one another at every point and will have eta^2 values that may be much less than unity. Similarly, if the value of each voxel in one map is 100 units greater than another, they will again have a correlation coefficient of 1, even though every voxel is different. In fact, the correlation coefficient will not change from 1 if the scaling factor increases or decreases in the first case, or if the offset factor increases or decreases in the second case. In both cases, however, eta^2 will measure and detect these differences and will vary as a scaling factor, offset, or another form of variation changes the difference between the two maps. The eta^2 coefficient will only equal 1 if they are, in fact, identical at every point.

Edge detection algorithms

(J) Since the aforementioned matrix of eta^2 coefficients (i.e., eta^2 profile) is a 2D array of values across the cortical surface, it can be treated as flat image data. To find salient edges in these arrays, the Canny edge detection algorithm (Canny, 1986), implemented in the Image Processing Toolbox (v7.2) of the MATLAB software suite,

was applied to each seed's eta^2 profile 'image'. The Canny method smoothes the image with a Gaussian filter to reduce noise, and then creates a gradient image that locates regions with high spatial derivatives. High gradient values represent locations where the original image was rapidly changing (i.e., peaks in the first derivative). After eliminating pixels in the 2D array that are not local maxima in the gradient image, the algorithm tracks along the highlighted regions of the image and, using high and low thresholds, categorizes each location as an edge or not. To prevent hysteresis, if the magnitude of the pixel is below the low threshold, it is set to zero, while if the magnitude is above the high threshold, it is considered an edge. If the magnitude of the pixel is between the two thresholds, then the location is only considered an edge if there is a neighboring pixel that itself had a gradient above the high threshold.

Our current implementation uses the default MATLAB algorithm to generate the two thresholds such that the high threshold is calculated to be the lowest value at which no more than 30% of the pixels are detected as edges, and the low threshold is defined as 40% of the high threshold. The use of edge detection here is purely to find the gradient peaks that are spatially stable across short stretches of each of the eta^2 profile 'images'. Thus, the specific thresholds for the edge detection algorithm do not have to be manually set each time. The primary goal is to identify and differentiate locations with strong, spatially coherent peaks as being different from locations that are relatively smooth or have incoherent gradient peaks, across some or most of the eta^2 profiles. The present adaptive threshold algorithm evidently performs this function adequately.

The result of processing the eta^2 profile set with an edge detection algorithm is a set of binary images representing the locations of rapid changes in each grid point's eta^2 profile (blue overlay in Figure 2.5C).

Putative areal boundary map generation

(K) Since the edge determination is binary, averaging across the entire set of seed matrix images at each location gives the relative likelihood that a particular location was determined to be an edge across the set of seed matrices. This gives a probabilistic or putative edge location map in which the intensity represents how likely a location is actually a functional border (Figure 2.5D).

Putative functional area identification

(L) Since the intensity of the putative edge map represents the likelihood that a given location is not a member of a functional area, our data can be transformed into regions of interest that represent putative functional areas using the morphology-based watershed transform (Vincent and Soille, 1991). This method treats each low intensity (low probability of edge) region as a 'valley' that progressively fills until reaching ambiguous locations between regions (in this case putative edges in the overall edge map) (Figure 2.7).

Results

We first demonstrate that rs-fcMRI patterns can be strikingly different in a population-average dataset even when the seed regions are relatively close (2.08 cm). We then explore the ramifications of this observation more systematically in single-subject

data, expanding on the implications this has for defining functional areas across the cortex.

rs-fcMRI of closely apposed seed regions shows putative areal boundaries where map patterns change abruptly.

Voxel-wise correlations were performed on interleaved resting state fMRI data see (Fair et al., 2007b) acquired from 31 healthy adult subjects using functionally defined seed regions (12mm-diameter spheres surrounding the peaks of activation) placed in the nearby supramarginal (-52, -42, +24) and angular (-49, -62, +29) gyri. These regions of interest, whose centers are separated by 2.08 cm (vector distance in 3D), were derived from a study investigating the development of lexical processing that showed these nearby regions to have similar but dissociable developmental profiles for a set of lexical tasks (Church et al., 2008a).

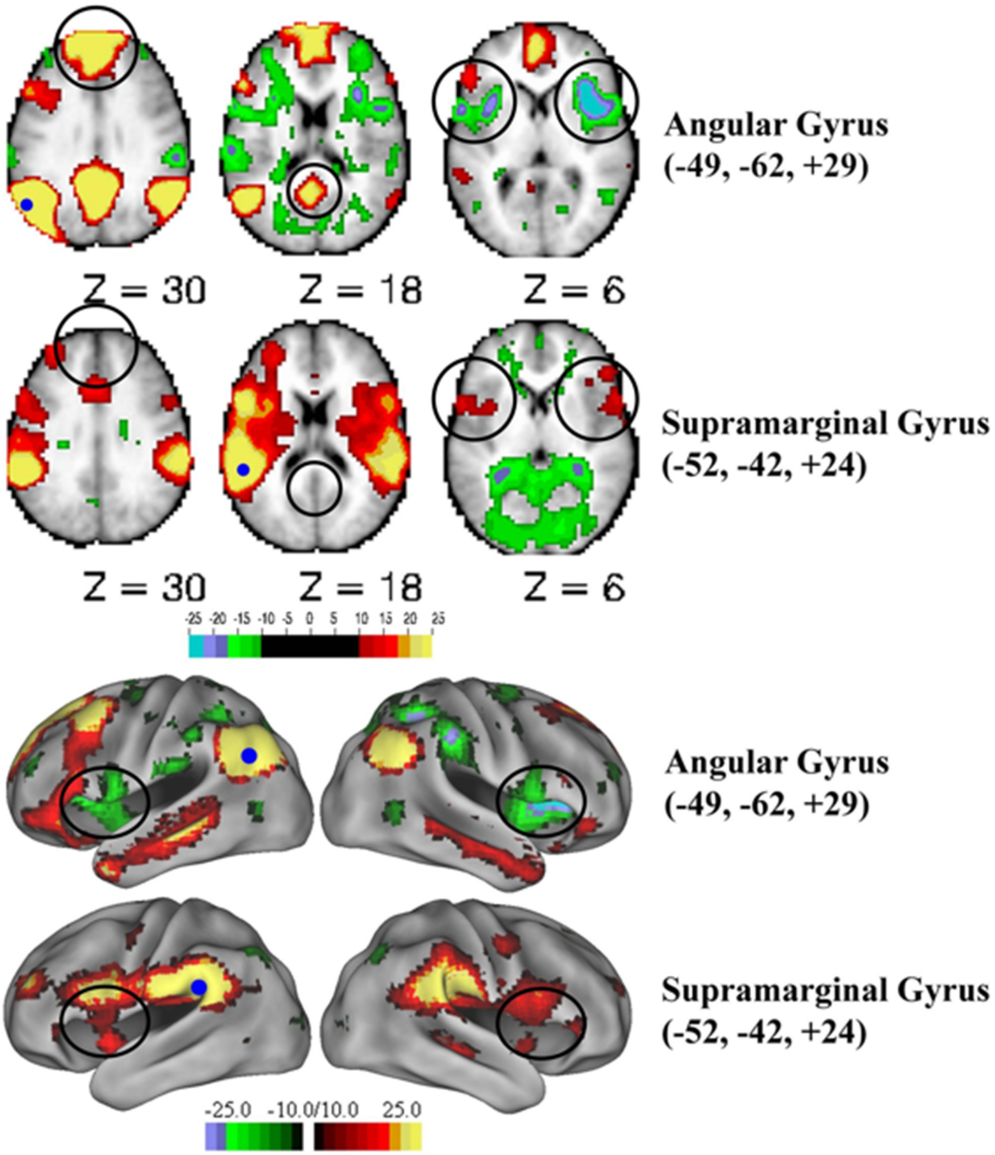

Figure 2.2: rs-fcMRI correlation maps from angular and supramarginal gyrus seeds

Shown are transverse sections and lateral hemispheric views, mapped to the PALS human cortical atlas (Van Essen, 2005), showing the functional connectivity patterns of regions of interest in the angular (upper slice and lateral view) and supramarginal gyrus (lower slice and lateral view). Highlighted (circles) are a few of the salient differences. Seed regions are indicated with filled dark blue circles. The strength of positive and negative correlations is shown in warm and cool colors respectively.

The angular and supramarginal gyri seed regions (small blue spheres in left hemispheres in Figure 2.2) show markedly different functional connectivity profiles, indicating that rs-fcMRI can be remarkably different between nearby functional areas. Regions having positive correlations (warm colors) with the angular gyrus seed (top rows of volume and surface views) show very little overlap with regions showing positive correlations with the supramarginal gyrus seed (bottom rows of volume and surface views). Derived from group data, these results are consistent with previous studies demonstrating that correlation patterns are reliable across subjects and investigators.

Although correlation maps from nearby seeds can be quite different, delineating boundaries necessitates that these differences do not progress smoothly across the brain, but rather show abrupt local changes, similar to those seen in connectional anatomy and functional properties (e.g., (Felleman and Van Essen, 1991; Maunsell and Van Essen, 1983)). To test for such a transition, a series of spherical seed regions (3 mm diameter) were generated between the centers of the supramarginal and angular gyri regions from group data (Figure 2.3A and B). The locations for these intermediate regions were delineated on the PALS atlas flat map and projected to the volume via the PALS 'average fiducial surface' (Van Essen, 2005).

We analyzed the correlation maps for the series of seed regions by visual inspection and by computing the similarity of each correlation maps to each of the other correlation maps using an eta^2 coefficient. While a correlation coefficient measures the relationship between changes in two images, the eta^2 coefficient provides a better measure of the overall similarity or difference between images (see Methods for details).

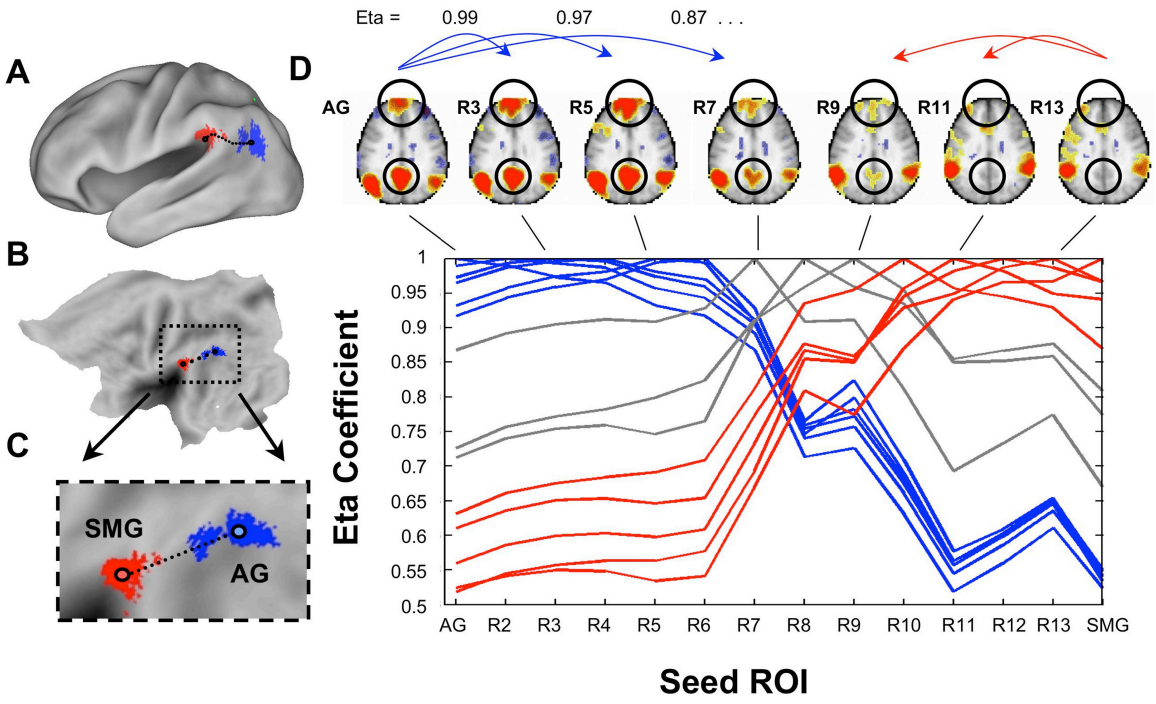

Figure 2.3: rs-fcMRI correlation maps from a line of seeds extending from angular gyrus to supramarginal gyrus

Panels A-C show the locations of the angular (blue) and supramarginal (red) regions. Black dots in C indicate the seed regions used. Panel D (upper panel) shows some of the connectivity maps derived from the series of seed regions. Encircled are particular differences that highlight the changing connectivity patterns. Panel D (lower panel) represents the eta^2 values derived when comparing the AG map with all other maps (first blue line), the SMG map with all other maps (last red line), and so forth for all maps…

As shown in Figure 2.3D, the eta^2 coefficients demonstrate a transition between the locations of seeds R7, R8, and R9, as the profile of eta^2 coefficients drastically changes within 1cm (3 map-mm separation, (Van Essen and Drury, 1997)). Thus, the eta^2 profiles can be divided into three groups: AG-R6 (blue), R10-SMG (red), and an

intermediate zone R7-R9 (grey) that is a putative transition region between the other two groups. The transition region found here is wider than typical transition between architectonically defined areas (Zilles et al., 2002), but this may reflect individual variability in the location of areal boundaries in the contributing population.

rs-fcMRI in a single subject can delineate multiple putative areal boundaries simultaneously.

Feasibility using single subject data is important, as the group data are inherently blurred by imperfect registration across subjects. Thus, a surface-based "fiducial" representation of the cortical mid-thickness was obtained for a single subject using the SureFit cortical segmentation algorithm available in the CARET software package (Van Essen et al., 2001). Correlation (volume) maps were generated for a set of 3 mm diameter spherical seed regions along the left cingulate sulcus and adjacent medial cortex (3 map-mm separation along a line on the flat map. For each of the 25 seed locations, its correlation map was compared to the correlation maps for the 24 other seed locations along this line, yielding a profile that peaked at unity for the given seed location.

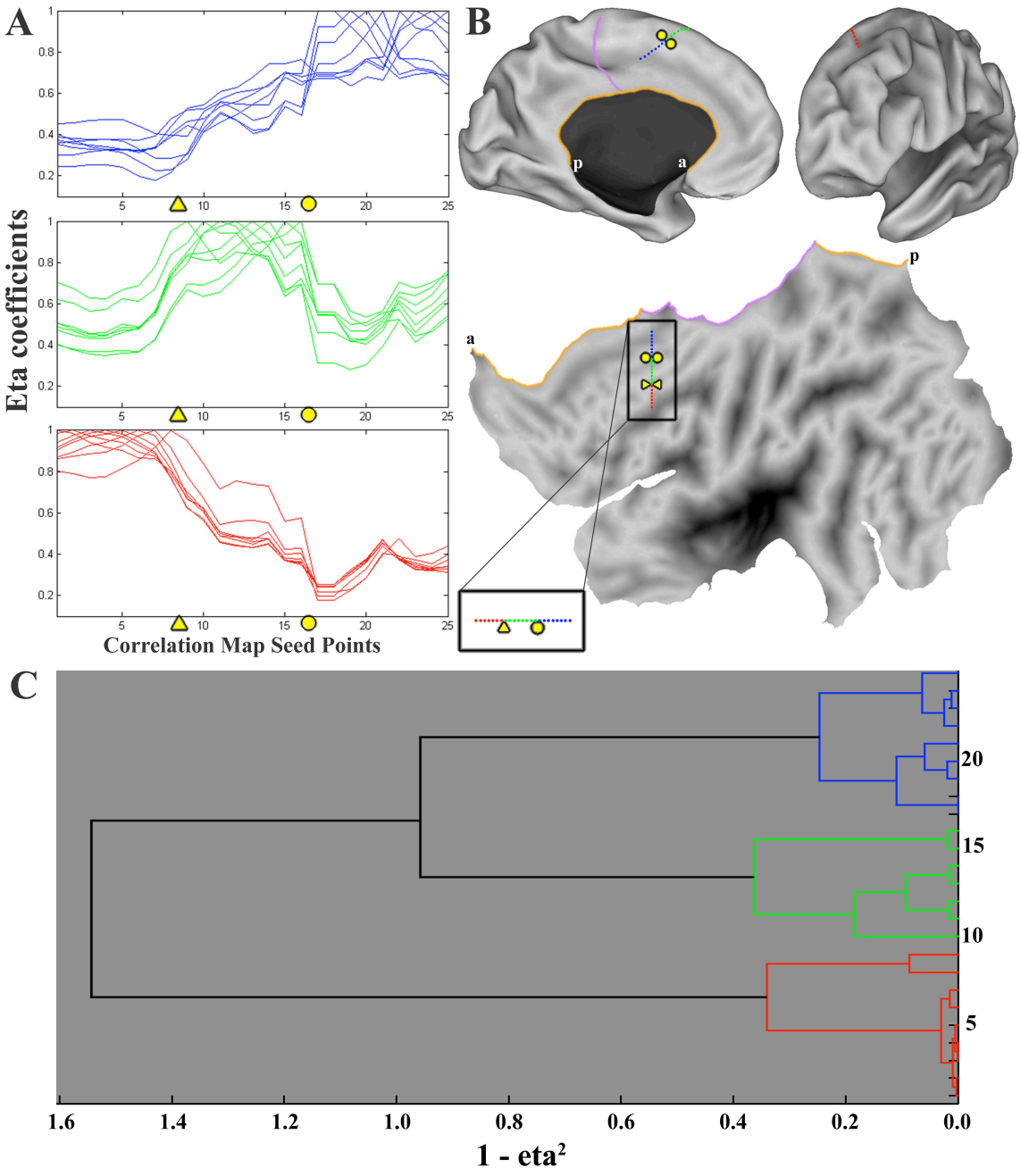

Figure 2.4: rs-fcMRI correlation maps from a line of seeds in cingulate cortex in a single individual

Panel A displays the eta² coefficients between each seed point's correlation maps, as in Figure 2.3D. Triangle and circle designate locations of rapid change. Panel B shows the location of the line of seed points on the left hemisphere, as well as the nearby artificial

'cuts' created during the process of flattening the cortex. The medial wall hole is shown in orange, with 'a' and 'p' designating anterior and posterior ends of the anterior medial wall cut. The cingulate cut is shown in purple on both the inflated medial view and the flattened view. Panel C shows the results of hierarchical clustering the eta^2 profiles shown in Panel A.

To objectively separate the eta^2 profiles into groups, as done in Figure 2.3, hierarchical clustering analysis was performed on the eta^2 profiles to find any strong divisions among the set (Cordes et al., 2002; Dosenbach et al., 2007; Salvador et al., 2005). A '1-eta^2' calculation was used as a distance measure between the profiles. The commonly chosen UPGMA (Unweighted Paired Group Method with Arithmetic mean) hierarchical clustering method (Eisen et al., 1998; Handl et al., 2005) sorted the eta^2 profiles for each seed's correlation map into three main groups (Figure 2.4C), which recapitulates the anatomical ordering as well as the distinct shape differences seen in Figure 2.4A (blue curves vs green curves vs red curves). Further inspection of the clusters reveals two abrupt changes in the green curves (triangle and circle locations), which occurred at similar locations for the other curves, indicating functional transitions that are candidates for areal boundaries. While there is a general decrease in eta^2 coefficient with distance from the comparison point, abrupt changes are concentrated at specific locations along the line regardless of which comparison points are chosen. Thus, rs-fcMRI functional transitions can be derived from individual subject data, and multiple transitions are evident even in this relatively limited view.

Sharp transition zones, or "edges", can be mapped across the 2D cortical surface using automated image processing techniques.

The line-based approach above provides proof of principle that rs-fcMRI measures can delineate putative cortical boundaries in individual subjects. However, mapping functional transitions throughout the cortex using this approach would be highly time-consuming and inefficient. Therefore, it was important to develop a computational approach that takes advantage of the information in rs-fcMRI data more efficiently.

Using a 2D grid of seed regions (i.e., a "patch") on the cortical surface (Figure 2.5A), eta^2 coefficients were computed for all pairs of seed regions within the patch, yielding a 2D eta^2 profile map for each of the seed regions comprising the patch. Each 2D eta^2 profile map (Figure 2.5B) was processed with a Canny edge detection algorithm (Canny, 1986), a method for rapid automated discrimination of strong gradients (edges), creating a binary "edge map" for each seed (Figure 2.5C, blue overlay). These binary maps were averaged to generate an 'edge consistency map' for the grid, where intensity at each location represents the fraction of maps in which that location was considered an edge (Figure 2.5D). The line-based and edge-detection-based approaches are consistent with one another. The transitions obtained in the line analysis described above (circles and triangles), spatially align with the putative edges determined by the edge consistency analysis, as indicated by the bright red pixels crossing the line of seed points.

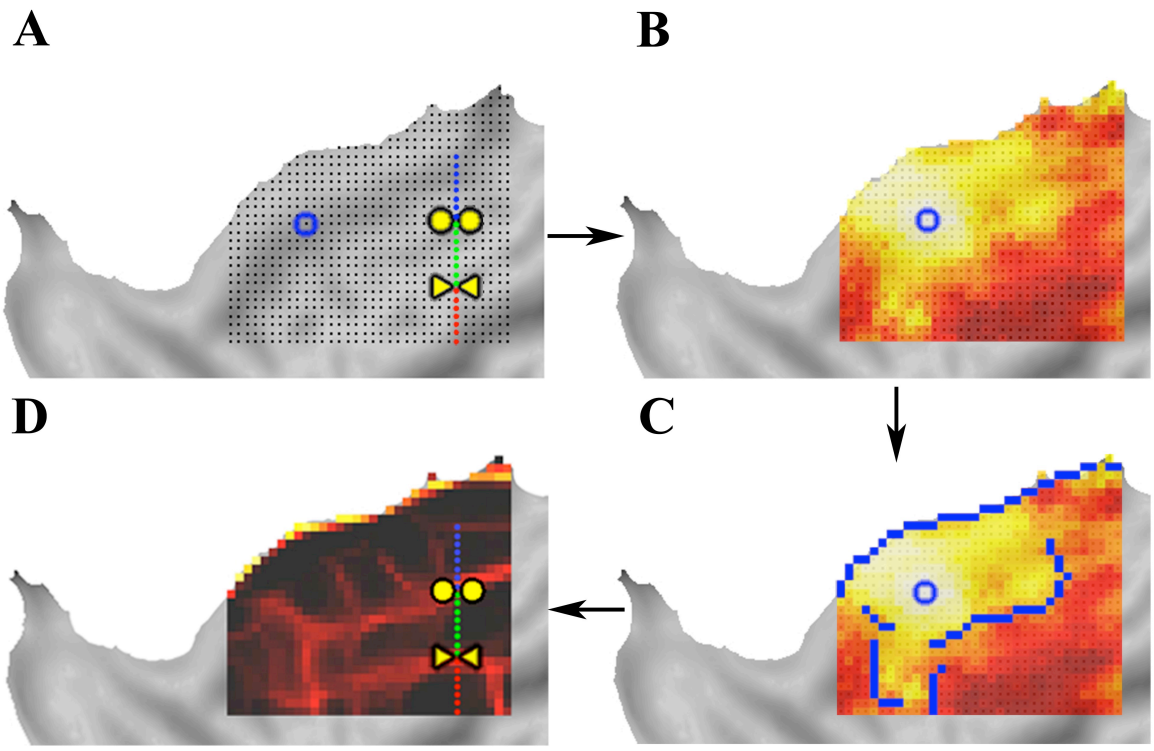

Figure 2.5: 2D "patch" eta² matrix and rs-fcMRI contour map construction

Panel A shows the 2D patch of seed regions on this subject's flattened cortex (Note: The line of points and boundary locations from Figure 2.4 are plotted in panels A and D for comparison). The eta² profile for one of the seeds (blue circle) is shown in panel B. Each of these eta² maps are then analyzed with an automated edge-detection algorithm that generates borders, blue overlay in panel C. Averaging all of the detected edge maps (binary blue overlay in panel C) results in the putative edge map shown in panel D, where intensity of each location reflects the fraction of maps in which that location was considered an edge.

As seen in Figure 2.5D, the set of candidate boundaries derived using this method extend over regions of the flat map that are appropriate in size and trajectory for cortical

area boundaries, Thus, processing large portions of the brain can be done much more efficiently using an automated computational approach. In addition, because the analysis is sensitive to gradients in any direction along the cortical sheet, it is inherently more appropriate for systematic identification of cortical area boundaries.

Several putative areas in Figure 2.5D are only partially enclosed by the presently detected boundaries. This might in part reflect a non-optimal thresholding strategy in the current algorithm but it may also represent a lack of differentiation between functional areas based on resting functional connectivity. If two neighboring functional areas have similar connectivity profiles, the eta^2 coefficient between maps in the two areas will be high, and such boundaries may not be detected by our current methods. Thus, convergence across methods and a combination of different approaches may be needed to elucidate the entire set of cortical functional areas.

Boundaries generated from adjacent cortical surface patches yield consistent results.

Since the edge consistency map is derived from the correlation maps for a particular set of cortical loci, it is conceivable that the resultant pattern is specific to the chosen patch and is unrelated to cortical areal boundaries. We assessed this possibility by analyzing two additional patches, or sets of cortical seed points. First, a patch of dorso-medial cortex adjacent to that used above (blue box, Figure 2.6A and B), was analyzed to test whether an independent dataset would show continuity with the pattern of edge locations seen previously. Second, an overlapping patch corresponding to half of the original dataset and half of the new independent dataset (green box, Figure 2.6A and C)

was used. The same edge detection analyses were applied to both new sets to find putative edge locations.

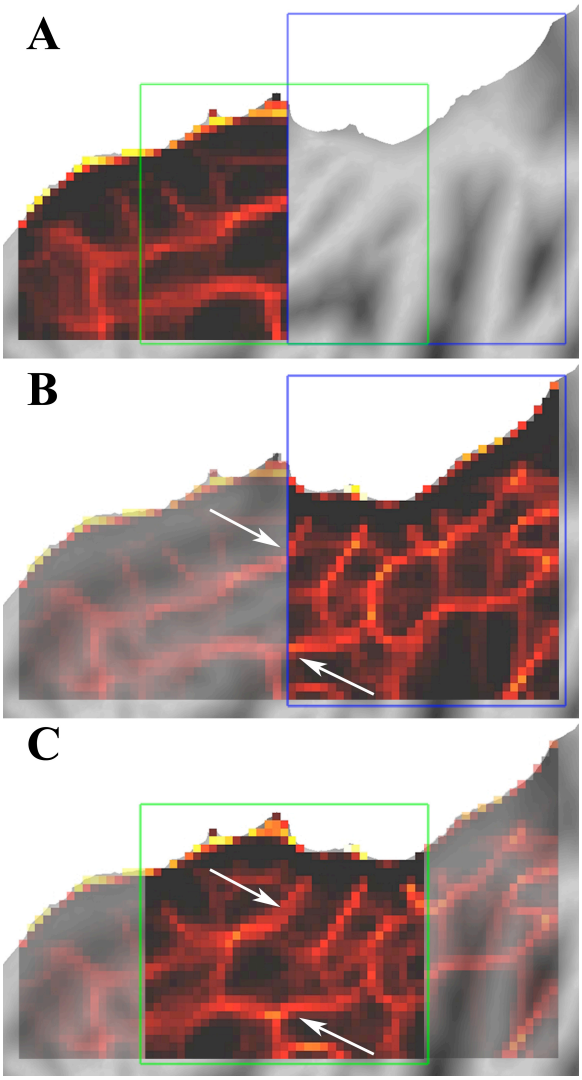

Figure 2.6: rs-fcMRI contour maps from overlapping and adjacent "patches" of cortex

Panel A shows the original patch of the left cingulate cortex shown in Figure 2.5. Panel B demonstrates that edge locations identified in the neighboring posterior patch align with those in the original patch, even though the two datasets do not share seed points or correlation maps. Panel C shows that the independently analyzed overlapping patch is consistent with the matching regions of A and B.

As seen in Figure 2.6B, edge consistency maps generated using a completely separate but adjacent set of seed point sets reveal consistent edges that align with one another. When superimposing the edge maps from two independent or overlapping patches onto the same surface, considerable consistency is noted, including the continuous boundaries marked with arrows in Figure 2.6B and C.

These results provide qualitative evidence that our approach can consistently identify boundary contours across the cortex in a single human subject.

Generating boundaries allows automatic definition of putative functional areas.

Since the edge consistency maps show continuity across extended regions of cortex, it should be possible to group contiguous seed points surrounded by putative edges into putative functional areas, using existing image segmentation algorithms. A watershed segmentation algorithm (Vincent and Soille, 1991) was applied to the edge consistency map. Figure 2.7 demonstrates the progression from edges (panel A) to bounded and labeled "areas" (panel C).

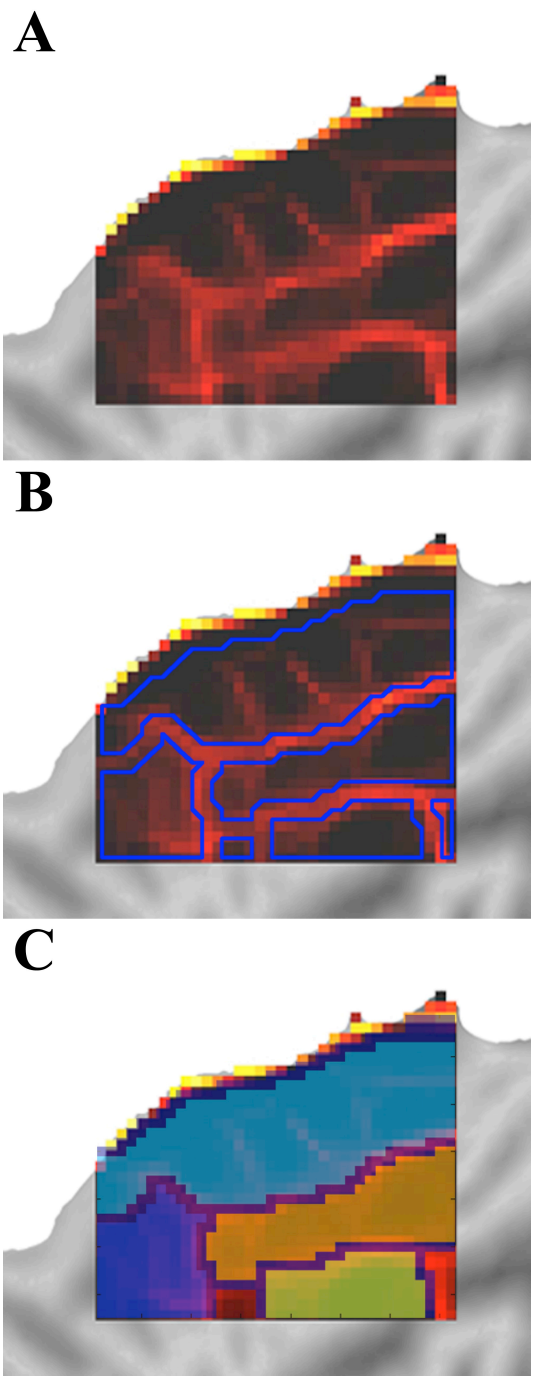

Figure 2.7: Putative area generation from rs-fcMRI contour maps

Panel A shows the rs-fcMRI derived boundaries generated above. Applying a watershed image segmentation algorithm parses the patch into contiguous non-overlapping regions least likely to be edges (i.e., most likely to be areas) shown in panel B, which can then be individually identified and labeled for investigation and validation as shown in panel C.

Using a putative edge map, a patch of cortex can be segmented into several bounded and partially bounded areas by a watershed algorithm. This suggests that rs-fcMRI derived putative edges and standard imaging segmentation methods should allow parcellation of an individual's cortical surface into putative functional areas. While these bounded areas may in some cases represent only a part of one or more than one functional area, it allows for the generation of ROIs that can be validated using complementary methods.

Discussion

Imaging and functional areas

Since the mid 1980s, functional neuroimaging has facilitated progress in cognitive neuroscience - the study of neural substrates underlying mental processes and behavior. Typically, functional neuroimaging identifies brain regions that are differentially activated by different task states or affected by specified behavioral events. We use the terms “regions” and “regions of interest” advisedly whenever we are unsure whether functional imaging has identified differential activation in a whole and distinct functional area. We recommend that the term “area” be reserved for “functional areas” and that “region” be used for a collection of voxels or otherwise defined region of interest.

One of the overarching goals of functional neuroimaging is to use differential activity between conditions to identify specific information processing operations reflected in separate functional areas (e.g., (Posner et al., 1988)). Ascertaining a large-scale collection of functional areas in any mammal, let alone humans, is not straightforward and currently incomplete (Levitt, 2003; Van Essen, 2004b).

A fundamental problem in trying to identify functional areas in humans is that many of the methods used to generate the relatively precise definitions available in nonhuman animals are not available for studies in living humans, as noted above. Recently, the use of areal connections to define areas has been employed in humans. Diffusion tensor imaging (DTI) tractography, which measures the directional diffusion of water within a voxel, can reveal local anisotropic differences in fiber bundles in neighboring regions of cortex in living humans, and was recently used to delineate some

human cortical areas (Behrens et al., 2006; Croxson et al., 2005; Johansen-Berg et al., 2004; Johansen-Berg et al., 2005; Klein et al., 2007). The use of probabilistic fiber bundle differences in diffusion tractography is in some respects analogous to the use of blunt dissection to identify major fiber bundles in humans. However, the challenge of accurately dissociating crossing bundles of fibers with DTI speaks to the need for a converging method of areal definition.

Since rs-fcMRI measures correlated activity, it might in principle reflect mainly direct (monosynaptic) anatomical connections. Empirically, though, the linkage between highly correlated regions can evidently be indirect, through one or more intermediate regions or common external input (Vincent et al., 2007). Even if functional connectivity is not directly equivalent to monosynaptic anatomical connections, a functional area's history of interaction with other areas is likely to be consistent across its extent, and distinct between separate areas. Thus, this method may be well suited for delineating the location and boundaries of a large number of functional areas.

Overcoming individual variation

Individual variation must be considered when comparing functional areas across subjects or populations of subjects (i.e., in cross-sectional development and aging studies, or between patient populations). To address this problem, investigators have implemented neuroimaging approaches that rely upon improved registration techniques (volumetric or surface-based), presuming that alignment of anatomical features will improve the alignment of functional areas. The most advanced registration methods available attempt to compensate for individual variation in brain surface shape, size, and folding pattern

(Lyttelton et al., 2007; Van Essen, 2005; Van Essen and Dierker, 2007b). However, this approach does not provide an ideal solution because the location and extent of each functional area varies substantially from person to person, irrespective of anatomical landmarks (Amunts et al., 2000; Amunts et al., 1999; Andrews et al., 1997; Uylings et al., 2005; Van Essen et al., 1984). Our current work is performed on a within subject basis, but future across subject comparisons will be made through the PALS B12 atlas (Van Essen and Dierker, 2007b) using CARET which can account for more individual differences than volumetric averaging. We hope to then directly examine inter-subject variation of areal location and how this can be used to additionally refine registration.

To overcome the difficulties with regards to individual variability, many studies use a large number of subjects such that, after alignment, the activated brain region common to the majority of subjects will emerge as the active focal point (e.g., (Dosenbach et al., 2006)). This gives a "best guess" approximation of the centroid of the common activated brain region, presumably located within an actual functional area (Lancaster et al., 1995), but "blurs" the variability in location and extent of areas across individuals.

In some cases, a lack of specificity can lead to regions as far apart as 4 cm in stereotactic space, one quarter the anterior-posterior length of the average brain, being referred to by the same name, and considered as part of the same functional entity (e.g., the application of the name "dorsolateral prefrontal cortex" in Kerns et al. (Kerns, 2006) and Luks et al. (Luks et al., 2007)). However, without the availability of more precise

regional definitions, this common practice is unavoidable in order to have a common descriptive language.

Another method utilized to overcome individual variability is to use the average activation of many repetitions of a region-specific "localizer" task in individuals (e.g., (Swallow et al., 2003)). Analyses can then be performed on a subject-by-subject basis using the activation-delineated peak. However, such localizer tasks exist for relatively few locations in the brain, and the considerable similarity in the functional properties of many neighboring functional areas often makes it difficult to differentiate areas based solely on their activation to a particular task or stimulus set (e.g., (Swallow et al., 2003)).

Therefore, functional activations and fcMRI seeds are currently most commonly referred to by their stereotactic coordinates or anatomic (gyral and sulcal) locations. The generation of cortex-wide maps of functional areas for individuals would allow for more accurate and functionally meaningful labels to be applied without relying on stereotaxis with its added concerns about individual areal variation.

rs-fcMRI functional area definition

We have demonstrated that rs-fcMRI patterns can abruptly change between putative functional areas and that this signal is strong enough to be detected in individual subjects as well as in group data. Additionally, combining surface-based analysis techniques with image processing algorithms allows for the simultaneous delineation of candidate/putative area borders across expanses of cortex in automated fashion without the need for prior information about a region's function or topography. We have also shown that putative borders generated from independent data from a separate portion of

cortex yield similar and consistent results with our initial dataset. Finally, defining borders with these methods provides usable and biologically plausible putative areas for use as region masks for functional studies or as seeds for use in functional connectivity studies.

Our approach combines several disparate methods that aid the currently used analyses: (i) Due to the ease of acquisition, rs-fcMRI can be accurately acquired from typical and atypical populations. (ii) The use of widespread surface-equidistant seed regions removes the need for prior stipulations about the location of specific functional areas. Surface-based definition of areas also greatly decreases the amount of processing needed, while still defining salient and meaningful functional boundaries and areas across the cortex. (iii) eta^2 is a useful similarity index for comparing fcMRI maps, as it captures the difference or similarity between two images as distinct from the correlation between them, (Pearson's *r* statistic), and allows for rapid analysis of differences. (iv) The inclusion of automated image processing techniques allows for hypothesis-independent generation of functional areas across wide expanses of cortex in rapid fashion. Specifically, the Canny edge detection algorithm permits the detection of continuous yet near-threshold borders, while excluding spurious noise. (v) Regions identified in individual subjects can be easily labeled and transferred to standard fMRI region generation programs used for analysis of functional data from task paradigms, presumably increasing the signal-to-noise ratio over group-average defined regions. Additionally, the combination of existing methods used in this study can also be extended to other efforts in brain mapping. The methods described here and elsewhere

(Margulies et al., 2007), may also provide a basis for comparisons between species (Buckner and Vincent, 2007; Vincent et al., 2007). Clearly, more work remains to refine the methods presented here.

Future directions/caveats

Functional validation

While our rs-fcMRI derived boundaries and areas are within a plausible range in size for known cortical areas (Van Essen and Dierker, 2007a) and have a biologically plausible distribution, validation against functional data is essential and is currently in progress. Test-retest validation needs to be performed by scanning the same subjects in different sessions separated by several days or weeks. Since the location of functional areas should not change over time, even if their fcMRI patterns change, we anticipate being able to detect the same borders across multiple scans separated after months or years. The borders generated using rs-fcMRI can be directly compared to functional activations in the same individual for areas where there is topographic organization. For example, the borders of early visual areas can be activated using visual meridia stimuli for retinotopy. Additionally, robust localizers, such as eye-movement for the frontal eye fields (FEF), should generate peaks of activity that localize within putative rs-fcMRI functional areas and not across detected boundaries. Finally, comparison across subjects for the above validations can be performed to determine if the fidelity of detecting borders is variable across subjects.

Method refinement

While we have currently performed our analysis on the cortical surface, these algorithms could potentially be expanded to work in 3 dimensions for parcellation of deep brain nuclei. We focus here on surface-based definition of areas as it greatly decreases the amount of processing needed, while providing salient boundaries and areas across the cortex.

Using flat maps to delineate seed locations is problematic where there are artificial cuts (discontinuities) such as that in the cingulate sulcus (Figure 2.4B – purple line) or near the natural boundary of the medial wall, which exists even when closed topologies are used. This can be resolved in future analyses using overlapping patches defined on closed topologies (e.g., defined on a spherical or very inflated surface). Also, the watershed algorithm, by design, will always produce closed boundaries, however, as clear from Figure 2.6, some of these putative areas extend beyond a single patch. Thus, while demonstrated here on a local scale, watershed segmentation should preferably be performed on the entire cortical surface at once.

The methods used in this report describe biologically plausible functional areas, but alternative analysis methods may enhance the robustness of the results. For instance, edge detection on the initial eta^2 profiles is currently performed by the Canny algorithm, but many other edge detection techniques are also available, including the Roberts-Cross, Prewitt, Sobel, Marr-Hildreth, zero-crossings of the 2nd derivative method, and the Rothwell method (Lim, 1990; Parker, 1997). Additionally, it may prove advantageous to utilize the entire range of the underlying gradient magnitudes to produce a probabilistic

boundary map, retaining much of the information that is discarded when creating binary edge maps of the initial eta^2 maps for each location. Therefore, methods that do not require edge detection will be explored as well.

Converging methods in the field

In addition to our own efforts at defining areal borders, several other groups are working on converging methods that should allow cross-modality validation and increased confidence in the borders that overlap across methodologies. Johansen-Berg et al. (Johansen-Berg et al., 2004; Johansen-Berg et al., 2005) and Rushworth et. al. (Rushworth et al., 2006) have used DTI to separate specific functional areas based on the underlying tractography. Margulies et. al., (Margulies et al., 2007) have recently shown regional differences in resting state connectivity across large sections of the anterior cingulate gyrus.

The maturation of the above methods (Johansen-Berg et al., 2004; Johansen-Berg et al., 2005; Margulies et al., 2007; Nir et al., 2006) and those used in this manuscript, could radically change the way functional neuroimaging data are analyzed in basic, translational, and clinical settings. If functional areas could be reliably identified within individual subjects, spatially normalizing individual brains using probabilistic atlases could be supplanted by the individual's own functional area locations as constraints on the registration process. The ability to delineate an individual's functional areas would greatly improve the utility of fMRI for clinical diagnosis and prognosis. Such capabilities would herald a new era of non-invasive investigation of brain area function.

CHAPTER 3: RS-FCMRI MAPPING OF INDIVIDUAL HUMAN CORTEX

Introduction

Understanding the organization of functional areas across the cerebral cortex is a current challenge in neuroimaging.

As previously discussed, the cerebral cortex is organized at multiple levels, with functional areas and the networks they constitute being of particular interest to cognitive neuroscience. Neuroimaging has advanced cognitive neuroscience by allowing the non-invasive study of the processing contributions, developmental trajectory, and modified responses following loss or injury of various regions in the brain. However, many of these regions may include part of, or more than one, functional area, and in many parts of the brain the field is still relatively blind to the location and distribution of the underlying functional areas, hindering the appropriate ascription of functional distinctions. Additionally, localizing even these 'regions' within single subjects is still quite difficult. Being able to rapidly identify and characterize functional areas in *individual* subjects will allow for a multitude of parameters to be examined and compared against individual differences in task-evoked responses as well as individual behavioral measures.

On a larger scale, recent efforts to analyze large-scale neural networks have provided insight into the general organization of the brain (Dosenbach et al., 2007; Fair et al., 2008; Hagmann et al., 2008). However, the non-invasive delineation of biologically appropriate nodes for these types of analyses is the single largest challenge in constructing a useful and complete description of human large scale networks. Thus, the

establishment of individual methods or combinations thereof that can be used to to define such regions will surely be of use to a large range of current and future investigations.

A moderate amount of individual variation in both structural and functional anatomy makes it desirable to determine a unique map of each individual's organization of functional areas.

As previously discussed in Chapter 2, the specific folding patterns of each subject are variable, leading to inaccuracy in applying standardized anatomical labels to particular sections of cortex. A related problem is that regions referred to by the same name are often considered as part of the same functional entity, despite sometimes having significantly different structural locations (e.g., the application of the name "dorsolateral prefrontal cortex" in Kerns et al. (Kerns, 2006) and Luks et al. (Luks et al., 2007) to regions that are 4cm apart in stereotactic space). Until it is possible to apply more precise and, when necessary, individualized regional definitions, uncertainty will remain when using anatomical labels or stereotactic coordinates to decide whether results from multiple experiments are supported by a common neuroanatomical structure.

Beyond differences in folding and anatomical landmarks, the location and extent of each functional area varies substantially from person to person, (Amunts et al., 2000; Amunts et al., 1999; Andrews et al., 1997; Uylings et al., 2005; Van Essen et al., 1984). Thus, the generation of areal maps for individual subjects that respects this functional variation would be an ideal solution.

The average activation of many repetitions of a region-specific "localizer" task in individuals can be used to identify functional areas within single subjects (e.g., (Swallow

et al., 2003)). However, such localizer tasks exist for relatively few regions of the brain, and the considerable similarity in the functional properties of many neighboring functional areas often makes it difficult to differentiate areas based solely on their activation to a particular task or stimulus set (e.g., (Swallow et al., 2003)). Additionally, to do a reasonable set of localizer tasks requires many bold runs (Drobyshevsky et al., 2006) while ~10 minutes of rs-fcMRI data may be sufficient to capture (Van Dijk et al., 2009).

rs-fcMRI mapping may provide a functionally-defined delineation of many, if not all, putative functional areas in individual subjects.

In Cohen et al., ((Cohen et al., 2008) or Chapter 2), we demonstrated the potential for using resting-state functional connectivity MRI (rs-fcMRI) to differentiate between spatially adjacent pieces of cortex. Extending this concept, it should be possible to identify locations of rapid transition in rs-fcMRI profile across the entire cortical surface. It may then be possible to identify regions of cortex that share similar rs-fcMRI correlational patterns with the rest of the brain and are distinct from surrounding cortex, i.e., putative functional areas.

rs-fcMRI correlation patterns appear to recapitulate relationships between regions seen in many functional activation studies, i.e., sensorimotor networks (He et al., 2009), networks related to control (Dosenbach et al., 2007), and the default network (Raichle and Snyder, 2007). It is therefore reasonable to assume that putative functional areas and boundaries found with rs-fcMRI would also have a similar relationship to evoked functional activity. Thus, rs-fcMRI mapping may provide a means for generating

unbiased regions of interest that can be applied on an individual subject basis to evoked-activity neuroimaging data, mitigating the need for arduous localizer studies to locate activated regions, and even potentially providing a full or partial description of a set of putative functional areas in individual subjects.

Here, we apply rs-fcMRI mapping to full hemispheric surfaces, identify putative functional areas based on rs-fcMRI mapping, and examine the within-subject reliability of putative areas over time.

The analyses presented below show that: (i) rs-fcMRI mapping can be performed on large extended grids to analyze an entire cortical hemisphere. (ii) This large-scale map can be used to identify locations of putative functional areas and putative functional boundaries. (iii) These putative functional area locations and the underlying rs-fcMRI contour maps are reliable over time within subject. (iv) rs-fcMRI mapping can be used to analyze the strength of boundaries (as indexed by gradient calculation) between neighboring putative areas as well as their location (as indexed with edge detection algorithms).

Methods

Overview

The analysis stream presented here extends the stream described in chapter 2 to operate on an entire cortical hemisphere . Thus, while the methods have been expanded in scope, the approach remains the same, utilizing both established seed-based rs-fcMRI voxel-wise correlation methods and several image processing techniques that are

performed on a surface representation of the cortex. These techniques include established edge detection and image segmentation algorithms available in MATLAB as well as several novel functions to examine the effects of various steps involved in edge detection. These surface-based operations treat the cortex as a 2D sheet, while the volume-based analyses treat the brain as a 3D volume.

In Chapter 2, a focused "patch" applied to medial frontal/cingulate cortex detected multiple putative functional boundaries and areas simultaneously, but it was not computationally feasible at the time to generalize those results to larger grids. Several algorithmic advances and increased computing resources allow us to now derive entire rs-fcMRI maps for a high-resolution grid covering the entire hemisphere in under 6 hours.

Subjects

rs-fcMRI data was collected from subjects (n = 8, 3F, age 24-27 years) instructed to relax while fixating on a black crosshair against a white background. Four runs (2.5s TR, 132 frames per run) were acquired on two separate days with an average of 20 days (SD=16 days, minimum of 7 days) intervening between the two scan sessions.

Data acquisition

Images were acquired in adherence to a standard protocol. To help stabilize head position, each subject was fitted with a thermoplastic mask fastened to holders on the head coil. All images were obtained with a Siemens MAGNETOM Trio Tim 3.0T Scanner (Erlangen, Germany) and a Siemens 12 channel Head Matrix Coil. A T1-weighted sagittal MPRAGE structural image was obtained (TE=3.08ms, TR(partition) =2.4 s, TI =1000ms, flip angle=8 degrees, 176 slices with 1x1x1 mm voxels) (Mugler

and Brookeman, 1990). An auto align pulse sequence protocol provided in the Siemens software was used to align the acquisition slices of the functional scans parallel to the anterior commissure-posterior commissure (AC-PC) plane and centered on the brain. This plane is parallel to the slices in the Talairach atlas (Talairach and Tournoux, 1988). Functional imaging was performed using a blood oxygenation level-dependent (BOLD) contrast sensitive gradient echo echo-planar sequence (TE =27 ms, flip angle=90°, in-plane resolution= 4x4 mm). Whole brain EPI volumes (MR frames) of 32 contiguous, 4 mm-thick axial slices were obtained every 2.5 seconds. A T2-weighted turbo spin echo structural image (TE=84ms, TR=6.8 s, 32 slices with 1 x 1 x 4 mm voxels) in the same anatomical planes as the BOLD images was also obtained to improve alignment to an atlas.

Data preprocessing

Standard fMRI preprocessing

Imaging data from each subject were pre-processed to remove noise and artifacts as in Chapter 2.

rs-fcMRI specific preprocessing

Pre-processing for functional connectivity analyses was also performed on the fMRI data as in Chapter 2.

Surface preprocessing

Cortical surface generation from anatomical MRI data using Freesurfer

Following the volumetric registration procedures described in Chapter 2, the atlas-registered MP-RAGE anatomical image for each subject was processed through the Freesurfer analysis pipeline (Freesurfer 4.5 (Dale et al., 1999; Dale and Sereno, 1993; Fischl et al., 2001; Fischl et al., 1999; Ségonne et al., 2004; Ségonne et al., 2005)) to generate white matter, pial, and spherical surfaces for each subject. A grey mid-thickness surface was generated by averaging the pial and white matter surfaces.

Surface-based registration to the PALS atlas using Caret

The surfaces generated by Freesurfer were resampled from ~150K nodes to ~74K nodes and converted into Caret-appropriate sets of files, with translation to re-align surfaces to the standard Caret origin and orientation (Caret 5.612 (Van Essen et al., 2001)). Surface flattening was accomplished by making cuts along five standardized trajectories that help minimize distortions (Van Essen, 2005). The six PALS landmarks were then defined for each subject based on their individual anatomy and these landmarks used to register each subject to the PALS atlas family of surfaces through spherical deformation and registration. This allows the use of the PALS surfaces as an intermediary to identify similar locations across the subjects' cortical surfaces, in relation to each subject's set of anatomical landmarks.

Cortical seed and rs-fcMRI correlation map generation

In Chapter 2, seeds were defined directly on the individual subject's flattened cortical representation. Here, the PALS atlas family of surfaces were used as a starting point to obtain common surface coordinates to use across our group of subjects (Van

Essen, 2005). A 3 ‘map-mm’ Cartesian grid was generated on the flattened PALS surface that covered the entire available surface of a hemisphere. Alternatively, a limited section (patch) was generated on the spherical surface to examine specific portions of the cortex. These grids were then projected through the PALS surface-registration process to the corresponding cortical locations on each subject’s grey mid-thickness fiducial surface.

The 3D stereotactic coordinates for each grid point in each subject were used to obtain the voxel (3x3x3mm resolution) containing each point. These voxels were then used as seeds for rs-fcMRI analysis. Thus, for the remainder of this thesis, the terms ‘seed’, ‘seed voxel’, ‘seed region’, and ‘node’ are generally interchangeable. This sampling density provides as fine-grained map as currently possible without excessive oversampling of the fMRI data (4x4x4mm acquisition voxels resampled to 3x3x3mm, with 6mm FWHM smoothing occurring during rs-fcMRI preprocessing (Fox et al., 2005)). While each seed region is 3 ‘map-mm’ apart on the flattened representation, the folded nature of the cortex results in some regions being further than 3mm apart in the underlying volume, while some points may actually refer to the same voxel in the underlying volume. This is an unavoidable consequence of using a high-resolution surface-based Cartesian grid with the constraint that the distance between ‘neighboring’ nodes always be less than the effective resolution of the data.

For each seed region, then, in each subject, Z-transformed volumetric correlation maps were generated as in Chapter 2.

eta^2 matrix creation for each seed

eta^2 coefficients were calculated for all possible pairs of volumetric correlation maps, generating an *n* x *n* eta^2 matrix where each column represents the similarities between a particular node's volumetric correlation map and all other nodes' volumetric correlation maps. The full *n* x *n* eta^2 matrix was then re-organized into a series of *n* 2D matrices, as in Chapter 2, such that each new matrix contains a spatially-arranged, 'PALS flat map-shaped', eta^2 matrix containing the eta^2 coefficients to a particular node.

Analysis of contrast information in eta^2 matrices

The aim of our contrast analysis is to identify locations on the cortex where the pattern of rs-fcMRI correlations changes rapidly, potentially representing boundaries between functional areas. In addition, we want to locate regions of high consistency, i.e., where rs-fcMRI correlation maps are very stable, potentially representing putative functional areas. Initially, the eta^2 matrix for each of the seed points is processed separately through the following four steps and then combined to form a single map.

eta^2 matrix preparation for image processing

Since the shape of the flattened full cortical sheet is designed to minimize distortion and not to produce a particular shape, the Cartesian grid of eta^2 values is embedded in a slightly larger, but rectangular, matrix to ease the use of image processing algorithms. To prevent the shape of an embedded eta^2 matrix being detected as a putative functional area border, locations outside of the embedded eta^2 matrix are iteratively filled with the average of neighboring locations that do contain data, smoothly filling in the remainder of the rectangular matrix and removing any contrast between the embedded matrix and the surrounding background. These extra locations are masked out after

gradient calculations are complete. As the first step in image processing, each eta^2 matrix is then slightly smoothed with a gaussian filter (FWHM=2 pixels / 6 'map-mm') before the calculations described below.

Gradient magnitude derivation

The numerical gradient for the eta^2 matrix is calculated across every point for both horizontal and vertical directions in the 'image'. The magnitude of the gradient vector at all points was then computed as the combination of the horizontal and vertical components. The direction of the gradient vector is maintained in a gradient orientation matrix for the following calculation.

Non-maxima suppression (NMS)

Assuming that edges can be defined as local maxima in the gradient image, we can then suppress all locations in the gradient image that are *not* local maxima to obtain the most likely locations of boundaries in the original image (Canny, 1986). Thus, the gradient magnitude image and the gradient orientation map are used to determine whether each location is a local maxima along the direction of the of the calculated gradient vector at each location. The NMS map is a matrix of the gradient values at locations detected as local maxima, i.e., likely edges, with a value of zero at all other locations.

Canny edge detection

The Canny edge detection algorithm as described here, follows the above steps with an edge tracing procedure to detect edge locations in the eta^2 matrices. Edge tracing, with hysteresis control, uses both a high and low threshold. Under the assumption that

salient edges should be along continuous curves, a high threshold is used to mark locations sure to be edges. The lower threshold is then used to mark locations of probable edges that are neighbors of locations that pass the more stringent threshold. This procedure results in a binary map of the probable edges and is identical to that performed in Chapter 2, but further explicated here to discuss the merits of each step of the Canny edge detection algorithm.

Construction of rs-fcMRI contour maps based on compiled contrast information

Described above are three sequential steps that result in Canny algorithm 'edge map'; gradient magnitude calculation, non-maxima suppression, and edge tracing. Instead of averaging the final 'edge maps' from each eta^2 matrix to generate rs-fcMRI contour maps, as was done in Chapter 2, it is possible to stop after an earlier sequential step, e.g., gradient magnitude calculation, and jump directly to combining the results. Thus, you can make rs-fcMRI contour maps that represent:

- the average rate of change at each location using the gradient magnitude maps,
- the average gradient values of *just* maxima locations using the non-maxima suppressed gradient maps,
- or the relative likelihood that a particular location was determined to be an edge using the full Canny algorithm 'edge maps'.

Since each step removed information from the data, to isolate specifically edge locations, the resulting rs-fcMRI contour maps represent either the strength or the location of putative boundaries, or in the case of the non-maxima suppressed maps, a

combination of how likely a location is actually a putative functional border and the strength of the putative border at that location.

Putative functional area detection and analysis using local extrema locations

Local extrema detection on rs-fcMRI cortical contour maps

To find putative functional area locations (i.e., locations with stable and distinct rs-fcMRI patterns), the following procedure was assembled: 1) inversion of the rs-fcMRI contour map such that putative areas are now represented as 'peaks' in the image, 2) additional Gaussian filtering to obtain spatially stable peaks, 3) local extrema detection using freely available MATLAB code (Aguilera, 2005), 4) thresholding of the obtained list of local maxima to restrict the number, minimum 'height' (which corresponds to the relative amount of stability), and minimum distance between peaks. The set of filtered peak locations can then be used to generate regions of interest for further analyses by either extending regions across the surface or growing regions volumetrically.

Volumetric region of interest (ROI) and rs-fcMRI correlation map generation for each putative functional area

To analyze the rs-fcMRI pattern from each putative area, seed regions were created at the volumetric coordinates corresponding to each putative area's location on the surface and used to create rs-fcMRI correlation maps. The watershed parcellation approach described in Chapter 2 was not performed here. As can be seen in Figures 3.1 and 3.2, many of the local minima in the full hemispheric maps are not circumscribed by complete borders. Thus putative functional areas were obtained by simply generating

small spherical regions at the volumetric locations corresponding to the detected peaks of rs-fcMRI stability.

For the analyses below, the detected peaks in rs-fcMRI contour maps were projected into volume space and extended into 6mm spherical ROIs (7 voxels in 3x3x3mm space) to generate rs-fcMRI correlation maps at known stable locations across the cortex.

Analysis of rs-fcMRI consistency across time within single subjects

Comparison of contour gradient and statistical maps across day within individual subjects

To analyze the consistency across time of the final gradient maps generated from each individual, a spatial correlation was computed comparing the detected average gradient value for each location in the two maps across the cortical surface. This correlation can be compared to the spatial correlation of each subject's average gradient map to the other subjects' average gradient maps to demonstrate the greater consistency within than between subjects.

Comparison of detected putative functional area locations across day within individual subjects

To determine whether detected putative areas, i.e., peaks of rs-fcMRI stability, can be consistently detected across time within single individuals, putative areas were independently determined from two separate days of data, and the rs-fcMRI correlation map for each detected putative area generated. The two sets of correlation maps were

compared to each other to find the spatial correlation between each possible Day 1-Day 2 (D1-D2) pair of putative areas. Since the correlation maps being compared are from two separate datasets, and the correlation values within the maps may be increased or decreased depending on the SNR of the scan session, spatial correlation is used here to compare correlation maps across time instead of eta^2.

For each putative area from each day, the putative area on the other day with the most highly correlated rs-fcMRI correlation map was considered to be the highest likelihood 'partner' for that putative area. To reduce spurious matches that were implausibly distant yet numerically slightly more correlated than a closer possible 'partner', all pair-wise spatial correlations were normalized by a Gaussian displacement factor with a FWHM of 20 map-mm, such that each pair-wise correlation value is multiplied by the fractional height of a gaussian curve at the distance between the two putative area locations. Thus, the pair-wise correlation between two putative areas detected at identical locations would be unchanged, a pair separated by 10 map-mm would have their pair-wise correlation divided by 2, and as the displacement between putative areas increases, the pair-wise spatial correlations is multiplied by a smaller and smaller scaling factor.

Thus, potential pairs of putative areas that are spatially far from each other must have stronger spatial correlations between their rs-fcMRI correlation maps than a spatially close pairing of similar pre-normalized strength to be designated the highest likelihood 'partner'. When a D1-D2 pair of putative areas 'agreed' that the other is most likely to be the identical putative area, a positive match was declared. Liberal thresholds

for the minimum allowable pair-wise spatial correlation and the maximum distance between the two putative areas were then applied to remove pairings for regions that were not detected on the other day, resulting in non-plausible pair-wise distances or spatial correlations.

Results

rs-fcMRI contour maps can be extended to cover a full hemisphere and can be used to determine locations of putative functional areas.

Beginning with the procedure outlined in Chapter 2, the methods for constructing rs-fcMRI contour maps have been expanded to allow for a significant improvement in automaticity and tremendous reduction in the time required to produce results. Additionally, while the patches produced in Chapter 2 were derived from the subject's own flat cortical map, all of the data shown below were derived from the PALS atlas set of surfaces, and all subjects have been both volumetrically registered and surface-based registered to allow rapid generation of common grids that can be used for all subjects. Thus, rs-fcMRI contour maps can now be rapidly generated that extend across the entire cortical hemisphere, as shown in Figure 3.1.

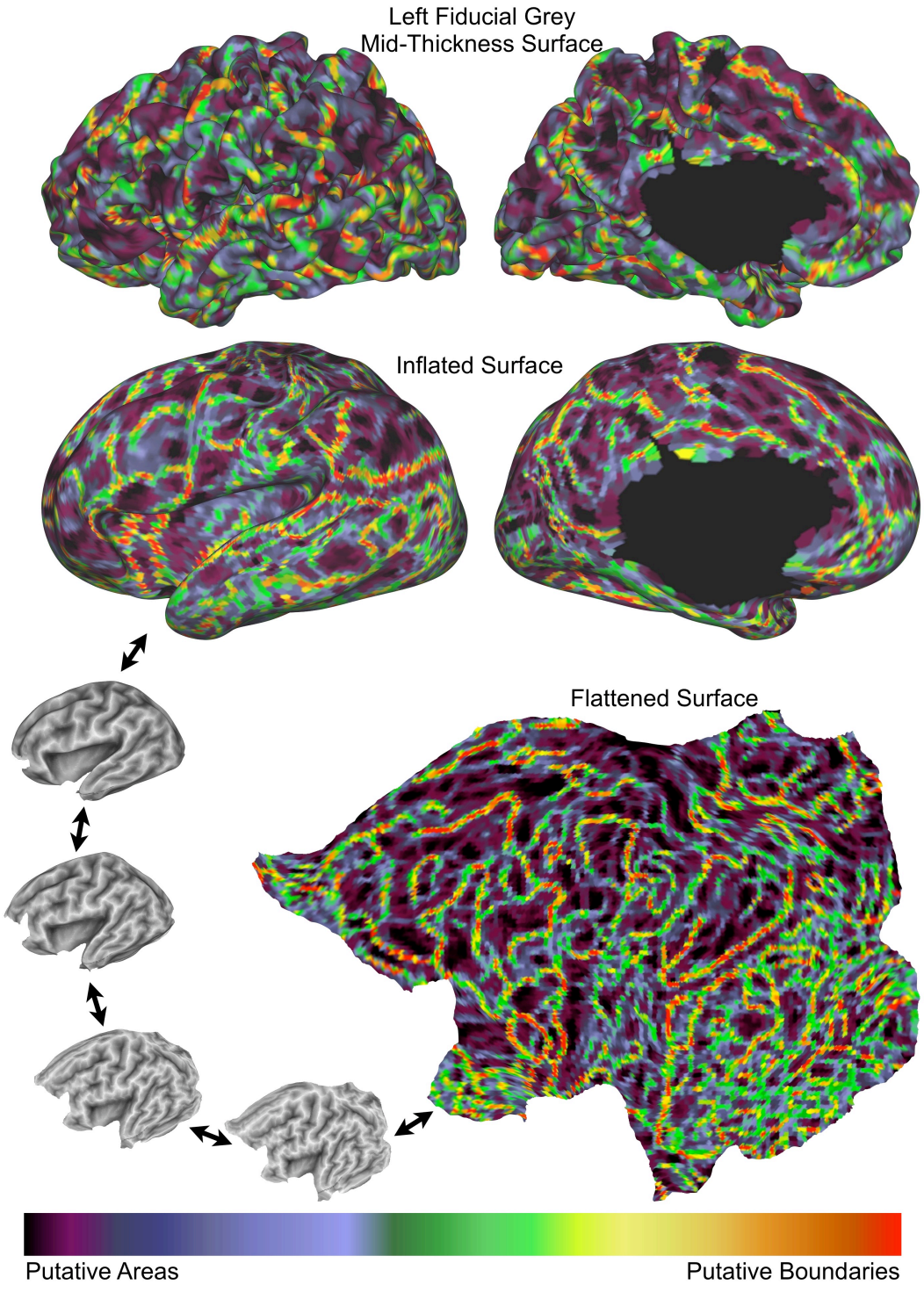

Figure 3.1: rs-fcMRI mapping of the entire left hemisphere in a single individual

Shown are lateral and medial fiducial, lateral and medial inflated, and flat views of the rs-fcMRI contour map for the left hemisphere of a single subject, processed through the

Canny edge detection algorithm described in the Chapter 2 and above. In this representation, 'hot' colors represent strong, consistent edge locations, while 'cool' colors represent locations where edges are rarely, if ever, detected. Inset to the lower are transitional views of the cortical 'flattening' procedure to demonstrate the alignment between the inflated and flat representations used throughout.

One remarkable feature of the rs-fcMRI contour map shown here is that there are locations where edges are very rarely, if ever, detected across the set of underlying eta^2 matrices, indicated by the dark locations on the surfaces of Figure 3.1. Just as strong boundaries represent locations of marked change in rs-fcMRI profiles, locations of strong consistency result from stability in the underlying rs-fcMRI patterns, as would be expected from putative functional areas. As such, stable locations that are potentially distinct from the surrounding cortex may represent the individual subject's functional areas. A set of putative area centroid locations across the cortical surface can be easily derived using local extrema finding techniques and projected back into volume space to generate regions of interest for further analysis. Figure 3.2 demonstrates the results of this procedure for the single subject shown in Figure 3.1.

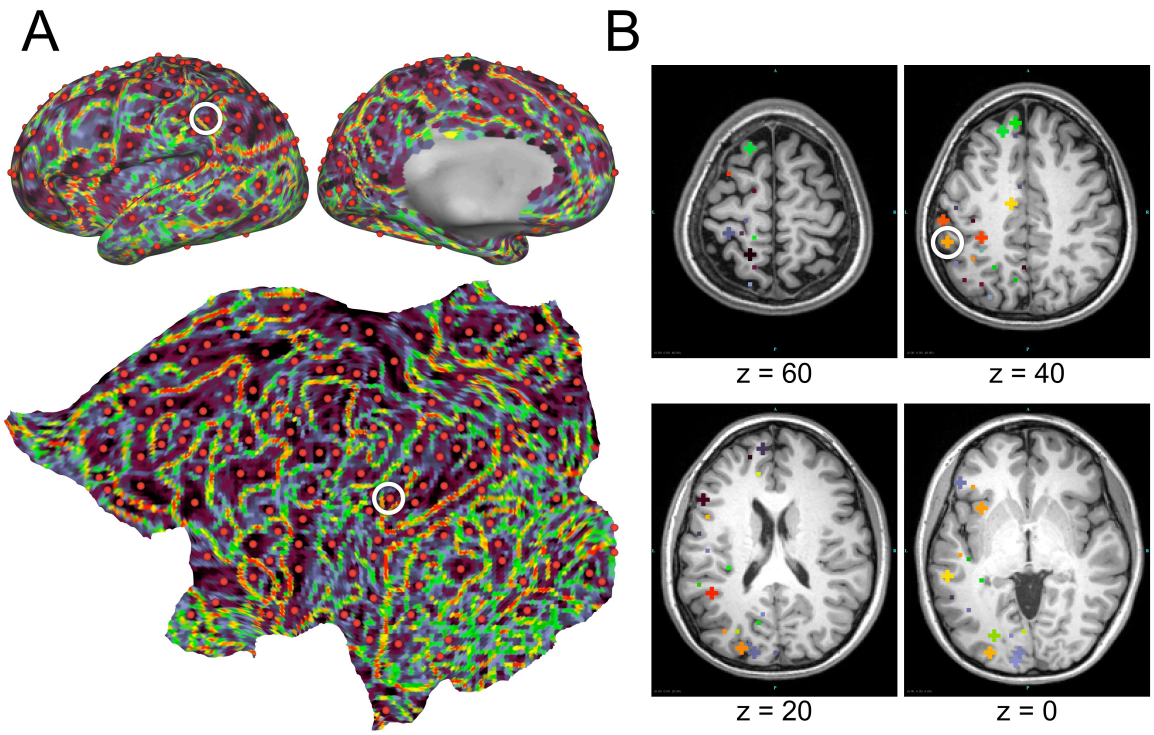

Figure 3.2: Surface and volumetric putative areas created from rs-fcMRI mapping

Panel A shows 150 detected peak locations (red dots) on the lateral, medial, and flat representations of the left hemisphere of a single subject, respectively. Panel B shows representative slices of this single subject's anatomy with the corresponding volumetric regions of interest overlaid in random colors to distinguish regions from one another. Circled in white is a single region, shown on both inflated and flat surfaces, as well as in volume space. Note that 6mm diameter spherical regions resolve to 7 voxel 'stars' in 3x3x3mm space, and appear as crosses when a region is centered on the same z-plane as the image, and as a single voxel when the region is centered above or below the plane of the image.

Thus, a set of regions which contain stable rs-fcMRI profiles distinct from surrounding cortex can be generated for individual subjects. Importantly, these regions are always centered on each subject's grey matter mid-thickness, as opposed to a region defined from a group average, which may not be centered on any particular individual's cortical surface. This set of regions represent a candidate list of functional areas for the entire cortical hemisphere which can then be evaluated.

rs-fcMRI contour maps provide largely stable results independent of patch location and size, up to and including entire cortical hemispheres.

Since rs-fcMRI contour is based on the *relative* differences in the examined set of volumetric correlation maps, using a spatially restricted set of seeds for correlation maps may enhance subtle differences based on the differential involvement of the seed locations in a 'patch' (Figure 3.3). A theoretical example is that a control region in frontal cortex may not differentiate between two occipital visual regions, while a nearby third visual region would. Since including correlation maps from the frontal region would not increase the detection of a boundary between the two occipital visual regions, excluding it would increase sensitivity. In general, patches that are restricted to potentially functionally related cortical surface *may* reveal functional distinctions not seen by averaging gradient results from grids covering the entire cortical hemisphere. Conversely, computing contour maps extending over the full hemisphere (Figure 3.1 and Figure 3.3, Panel A) provide a global view of spatial boundaries across the brain and may still identify spatially contiguous regions that have similar correlation patterns.

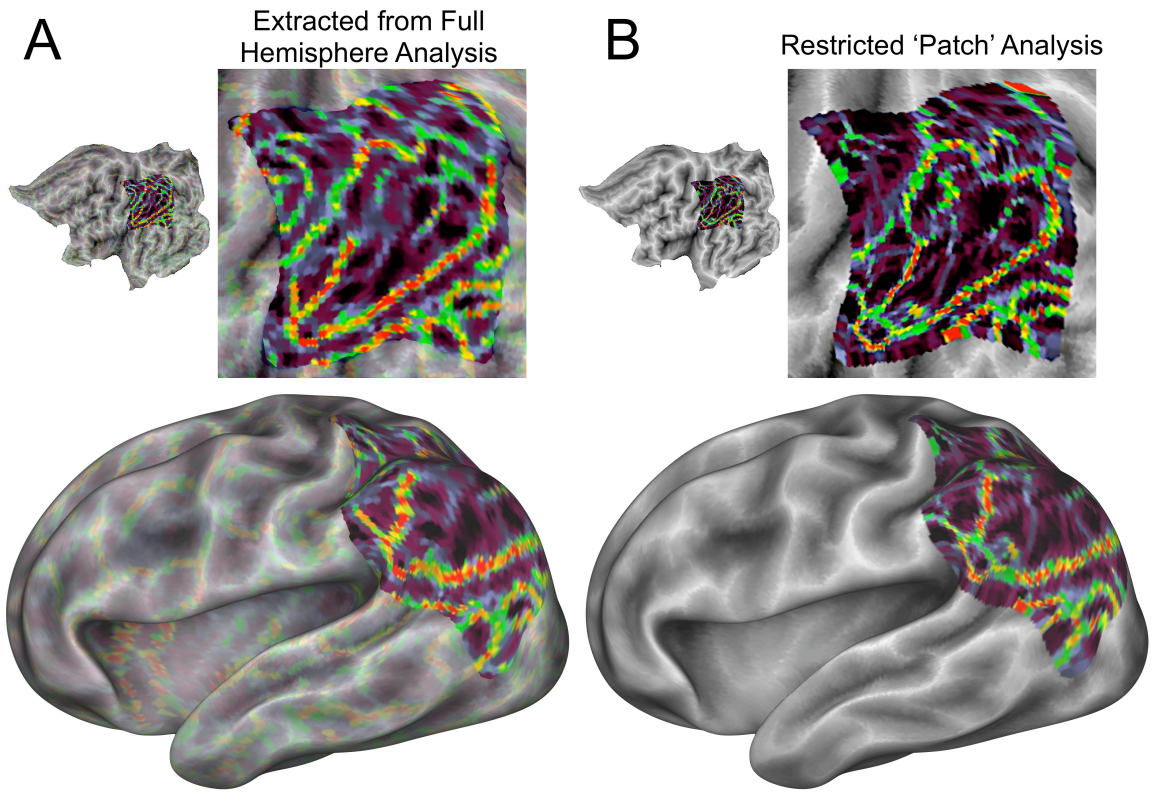

Figure 3.3: Full hemispheric vs. restricted "patch" rs-fcMRI contour maps in left lateral parietal cortex

Shown are flat and lateral inflated views of the rs-fcMRI contours in lateral parietal cortex in the full hemispheric contour map (Panel A), and in a restricted patch placed over left lateral parietal cortex. In this representation, 'hot' colors represent strong, consistent edge locations, while 'cool' colors represent locations where edges are rarely, if ever, detected.

Compared to the lateral parietal portion of the full cortical grid (Figure 3.3, Panel A), a restricted patch placed over lateral parietal cortex (Figure 3.3, Panel B) shows some finer detail within and around the strongly bounded regions in lateral parietal cortex. Comparing the peak detection results shown in Figure 3.2 for the full hemispheric grid

(Figure 3.4, Panel A) with the results of performing peak detection on the restricted lateral parietal patch (Figure 3.4, Panel B) finds many of the same putative area locations, but also finds a few additional local maxima locations, i.e., putative area locations that were not clearly seen in the full hemispheric rs-fcMRI contour map. This indicates the possibility for obtaining increased detail in rs-fcMRI contour maps by taking into account the distance between seed locations and the delineation of putative boundaries based on their rs-fcMRI correlation maps.

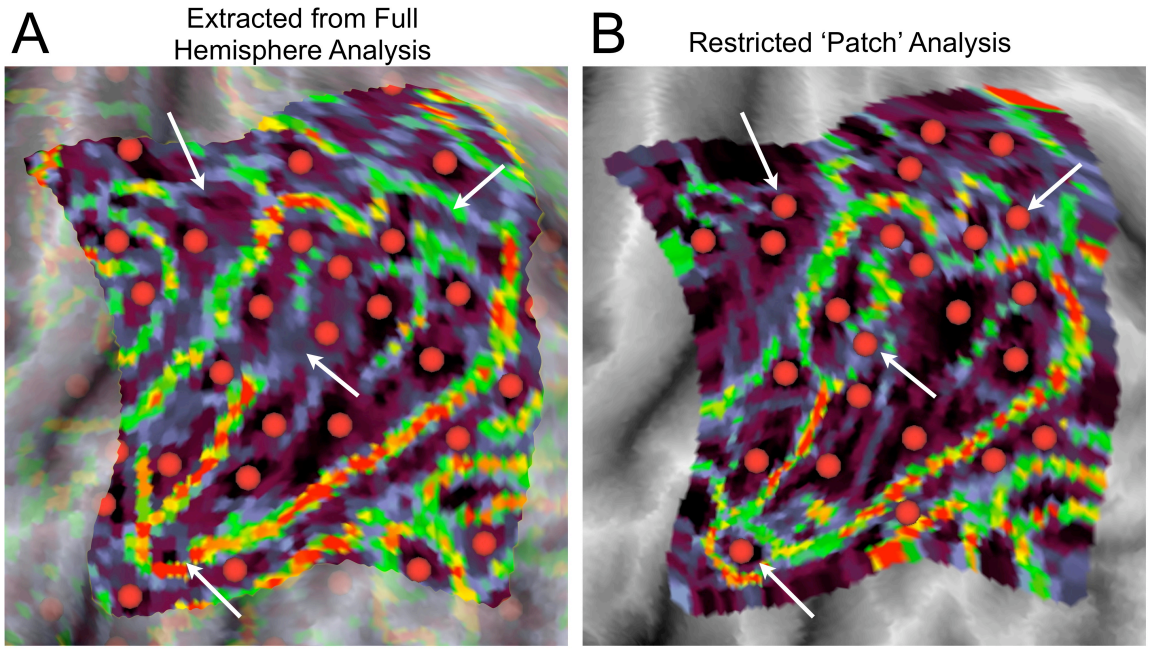

Figure 3.4: Putative areas generated from full hemispheric vs. restricted "patch" rs-fcMRI contour maps in left lateral parietal cortex

Shown are the rs-fcMRI contours and detected peak locations (red circles) from a magnified flat view of a selected portion of the full hemispheric grid over left lateral parietal cortex (Panel A) and a restricted patch placed over left lateral parietal cortex

(Panel B). White arrows highlight putative area locations that are detected in the patch-based analysis but not the full hemisphere analysis. Note that identical settings were used in both cases. 'Hot' colors represent strong, consistent edge locations, while 'cool' colors represent locations where edges are rarely, if ever, detected.

rs-fcMRI contour maps and putative functional area locations are reliable across time within an individual subject.

If rs-fcMRI contour represents the spatial organization of functional areas, then it should be relatively stable over time. Shown below (Figure 3.5, Panel A) is a comparison of the rs-fcMRI contour map shown previously (Figure 3.1) with a map generated from data acquired 53 days later from the same subject. The spatial correlation between the entirety of the two rs-fcMRI contour maps is r=0.52, displaying a moderate level of consistency between the two days' data.

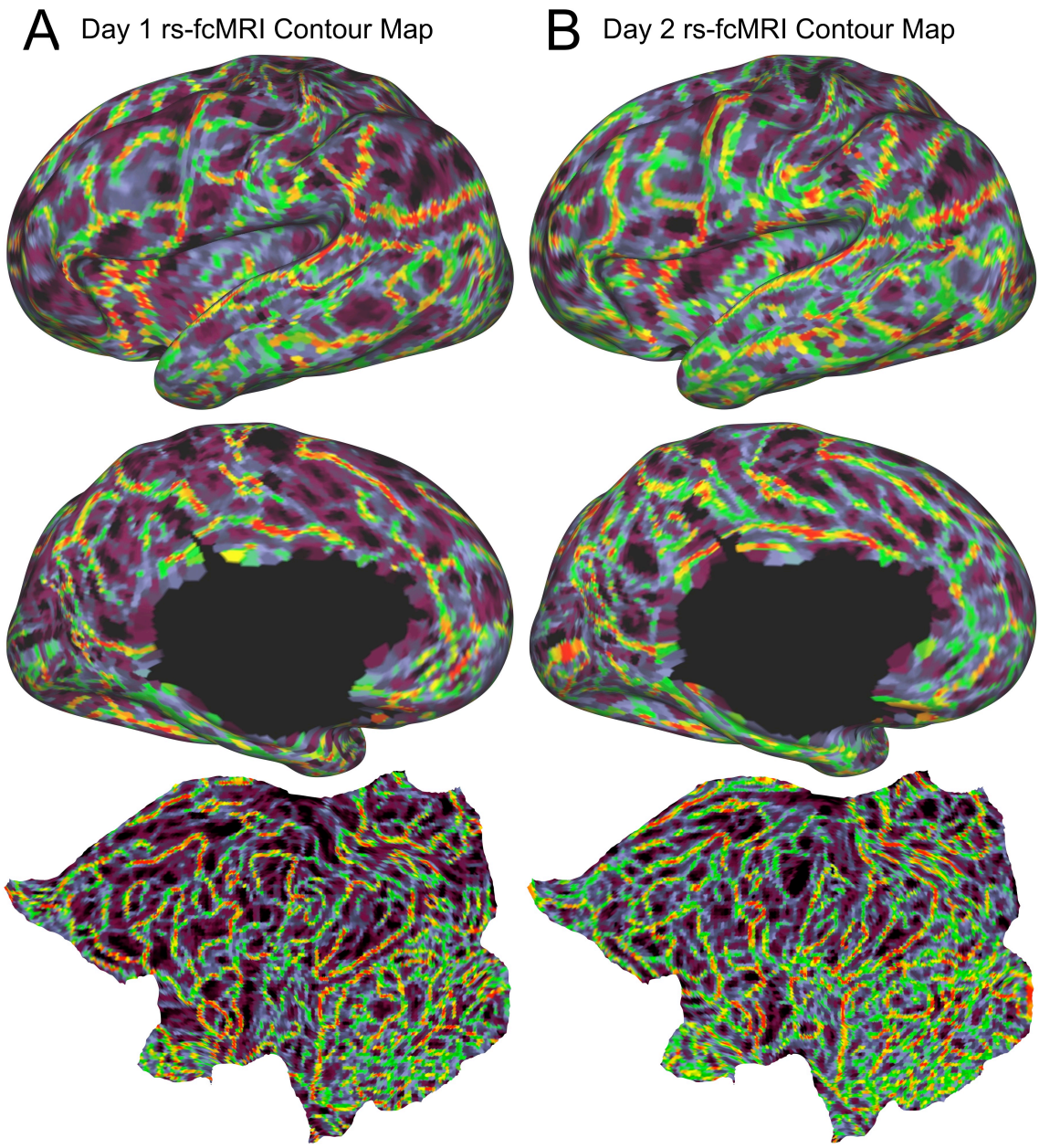

Figure 3.5: Comparison of full hemispheric rs-fcMRI contour map from two separate days in a single individual

Shown in Panel A are inflated and flat views of the rs-fcMRI contour map for the left hemisphere of a single subject from the first scan session, used for Figures 3.1-4. Shown in Panel B are inflated and flat views of a rs-fcMRI contour map generated from a second

scan session, 53 days later. In Both Panels, 'hot' colors represent stronger gradient values, while 'cool' colors represent weaker gradient values.

To specifically test the reliability of the detected putative functional area locations, correlation maps were generated from all of the putative functional area locations from each day's data and compared spatially across day. 109 of the 150 putative areas detected on each day were determined to be high likelihood matches across days, using the correlation of the pair's rs-fcMRI maps, weighted by a Gaussian kernel of the spatial displacement between the pair as a cost function (Figure 3.6).

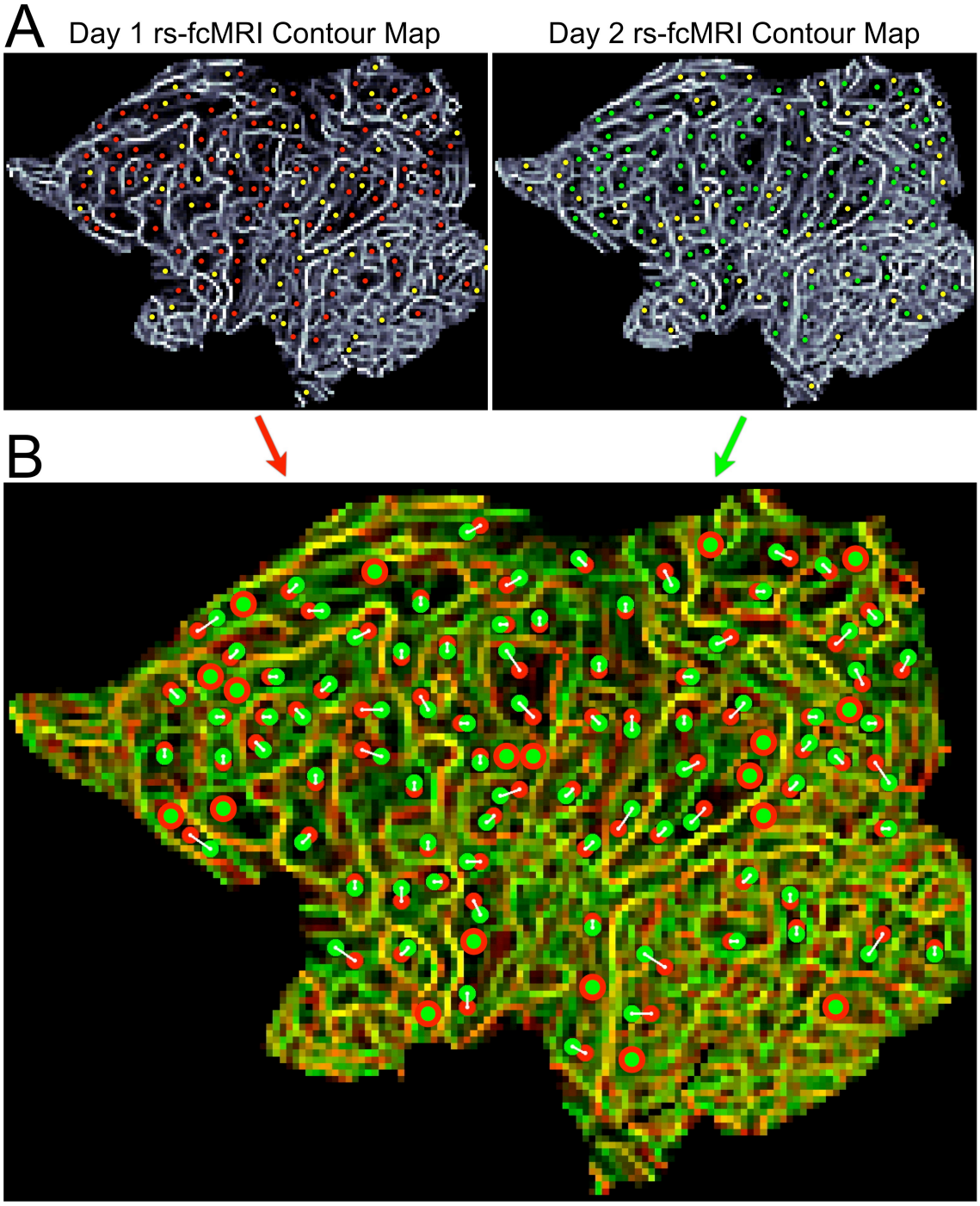

Figure 3.6: Comparison of putative areas generated from two separate days in a single individual

Panel A shows flat views of the left hemisphere rs-fcMRI contour map for a single subject from two separate days, 53 days apart. Detected probable functional area locations that

had high likelihood matches across days are indicated by red (Day 1) or green (Day 2) markers. Yellow markers (Day 1 and Day 2) indicate regions found in individual days, but not matched to a putative area found in the other day. Panel B combines the two days' rs-fcMRI contour maps into a single map with rs-fcMRI contour map shown in red (Day 1) green (Day 2). The 109 matched pairs of putative area locations are superimposed (Day 1: red circles, Day 2: green circles) with white lines drawn between matched putative areas. Note that matched putative area pairs that were detected to be in identical locations are displayed as green/red concentric circles. In Panel A, white represents stronger gradient values, while black represents weaker gradient values; this is mapped to the red and green channels of the underlay in Panel B.

Given the resolution of fMRI acquisition (4x4x4mm), the potential for the subject to be in a slightly different position in the scanner field, and the amount of blurring performed on fcMRI data (6mm FWHM volumetric Gaussian blur), there is the possibility for a small amount of misalignment across days, yet the average distance for the 109 matched pairs is 4.9 "map-mm" across the surface, or 6mm in volume space between the two days. Even though distance is part of the cost function used to define the matched pairs, the average distance between paired regions across days can be used as a measure of alignment, i.e., stable results should not have an average displacement much larger than the resolution of the data. The reproducibility of regions' locations and the relatively small discrepancies between them indicates that this procedure can isolate putative functional area locations that are largely stable over time for further analyses.

Sequentially applying image processing techniques provides a trade-off between robust detection of putative functional areas and boundary strength representation.

While the process described above produces reliable putative area and boundary locations, this approach removes significant information about the spatially dynamic structure of the brain's resting state patterns. Indeed, the relative strength of boundaries and stability of putative areas can also be obtained by altering the analysis stream. Each step of processing in the Canny edge detection algorithm (noise suppression through Gaussian filtering, spatial gradient calculation, non-maxima suppression, and edge tracing with hysteresis control) selectively removes information from the underlying image to derive a specific map of probable edge locations in the image. As used above, this process isolates continuous boundaries of rapid change in each of the underlying eta^2 matrices (representing changes in overall rs-fcMRI patterns) and the results together produce the contour maps seen in Figures 3.1-6. Here, we show that sequentially applying the filtering steps, stopping at each point and combining the produced gradient maps allows us to retain potentially useful information on the spatially dynamic structure of the brain's resting state patterns at the cost of decreased selectivity to edge locations. Figure 3.7 demonstrates the effects of each step of the Canny edge detection algorithm on an eta^2 matrix from a single seed location, while Figure 3.8 demonstrates the effect of using the results from each step, for all 9,916 eta^2 matrices, and producing the rs-fcMRI contour map using that data.

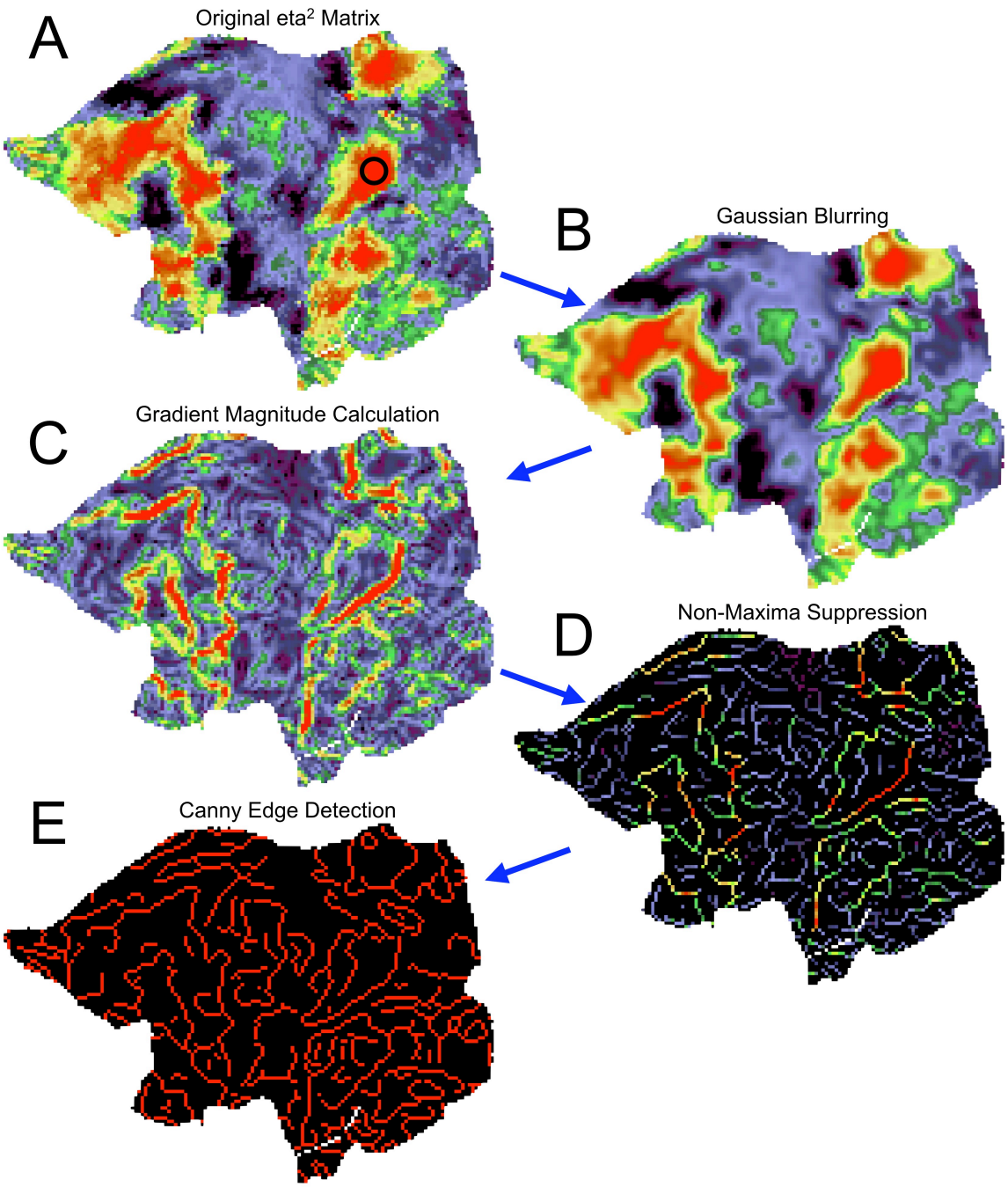

Figure 3.7: The progression of image processing methods applied to eta² matrices to obtain putative boundaries

Shown are flat views of the left hemisphere derived from a single eta² matrix of a single subject (Panel A, seed location shown as black circle), processed through our current

complete algorithm, demonstrating the initial gaussian smoothing (Panel B), gradient magnitude map (Panel C), the non-maxima suppressed (NMS) gradient map (Panel D), and the Canny edge detection map (Panel E) of this eta^2 matrix. In Panels A-B, 'hot' colors represent greater similarity to the target seed's rs-fcMRI correlation map while 'cool's colors represent dissimilarity. In Panels C-E, 'hot' colors represent stronger gradient values, while 'cool' colors represent weaker gradient values.

Gradient Magnitude Calculation

Gradient magnitude images (Figure 3.7, Panel C) provide the least filtered view of the spatial dynamics of the eta^2 matrix, but also provide the least contrast, compared to the later steps. Due to the lack of filtering, locations with potentially spurious amounts of gradient information may remain in the data and it can become difficult to parse the fine-grain detail of the putative area level organization. Locating the exact boundary locations within these maps is also difficult, as locations of rapid transition appear as wider, or blurred, versions of what they theoretically may be. However, since there is valued information at all points, statistics performed on these maps can provide a meaningful account of the stability or variation of locations.

An additional advantage of using gradient magnitudes is the retention of information about the relative strengths of gradients across extended regions of cortex, providing a way to determine the expected difference between data derived from either side of a boundary.

Non-Maxima Suppression

By only retaining the values of those locations that are local maxima in the gradient image, the most probable boundary locations can be identified without having to sacrifice information about the strength of those boundaries (Figure 3.7, Panel D). This elimination of a large proportion of the image allows for the rapid identification of boundary locations, but, by focusing solely on the boundary locations, removes a significant amount of information from the rest of the spatial map. While using data derived from processing up through this point may prove to be a useful intermediate compromise between averaging gradient magnitudes and averaging Canny binary maps, i.e., increased detection while retaining strength information, for now we will treat it simply as a transitional step.

Canny Edge Detection

As previously described, the full Canny edge detection process follows the above steps with hysteresis thresholding, produces a map that can define continuous edges, even if they are weak, and reject a moderate level of noise in the gradient map (Figure 3.7, Panel E).

Creation of rs-fcMRI contour maps from the above contrast analysis methods

Given the differences in the three maps shown above (Figure 3.7, Panels C-E) for a single eta^2 matrix, combining the sets of contrast maps based on either the full amount of contrast information, the contrast information solely from local maxima, or only information on the probable locations of edges should lead to rs-fcMRI contour maps with markedly different interpretations. Shown in Figure 3.8 below are the three rs-

fcMRI contour maps created for each of the two days of data for this subject. It is easily seen that while the ability to derive putative functional area locations vs the strength/ reliability of edges from the three maps is different, the large-scale character of the data is quite similar.

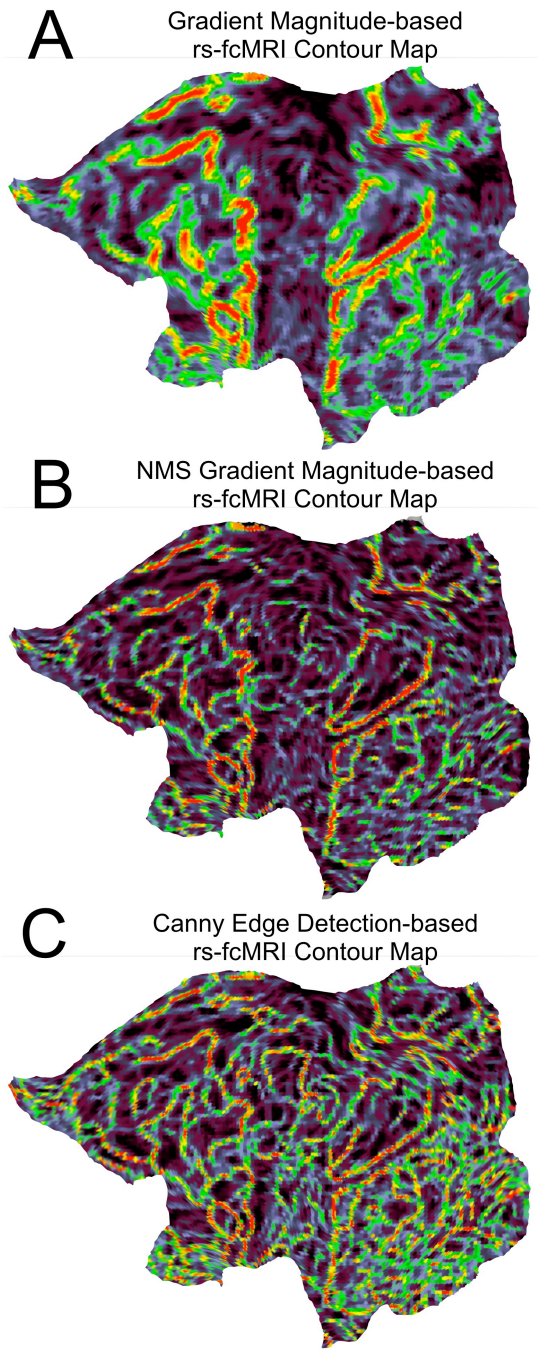

Figure 3.8: Three types of rs-fcMRI contour maps emphasizing different aspects of spatial dynamics across the cortex

Shown are flat views of the left hemisphere for a single subject, processed to various points of our current algorithm and then combined into a single rs-fcMRI contour map, demonstrating the average of the gradient magnitude maps (Panel A), the average of the non-maxima suppressed (NMS) gradient maps (Panel B), and the average of the Canny edge detection maps (Panel C). In these representations, 'hot' colors represent stronger gradient values, while 'cool' colors represent weaker gradient values, or higher and lower probabilities of being detected as an edge for the Canny edge detection method.

Gradient magnitude-based rs-fcMRI contour maps can be used to predict distinctions between spatially nearby regions of interest.

Combining the results described above, the putative area locations derived from the Canny-based rs-fcMRI contour maps can be overlaid on the gradient magnitude-based rs-fcMRI contour maps as shown below (Figure 3.9). In this configuration, predictions can be made and tested about how similar or different 'adjacent' putative functional areas' rs-fcMRI correlation maps should be based on the intensity of the boundary between them, i.e., two putative areas separated by a strong boundary should be quite distinct, while two putative areas with minimal boundaries found between them should be quite similar.

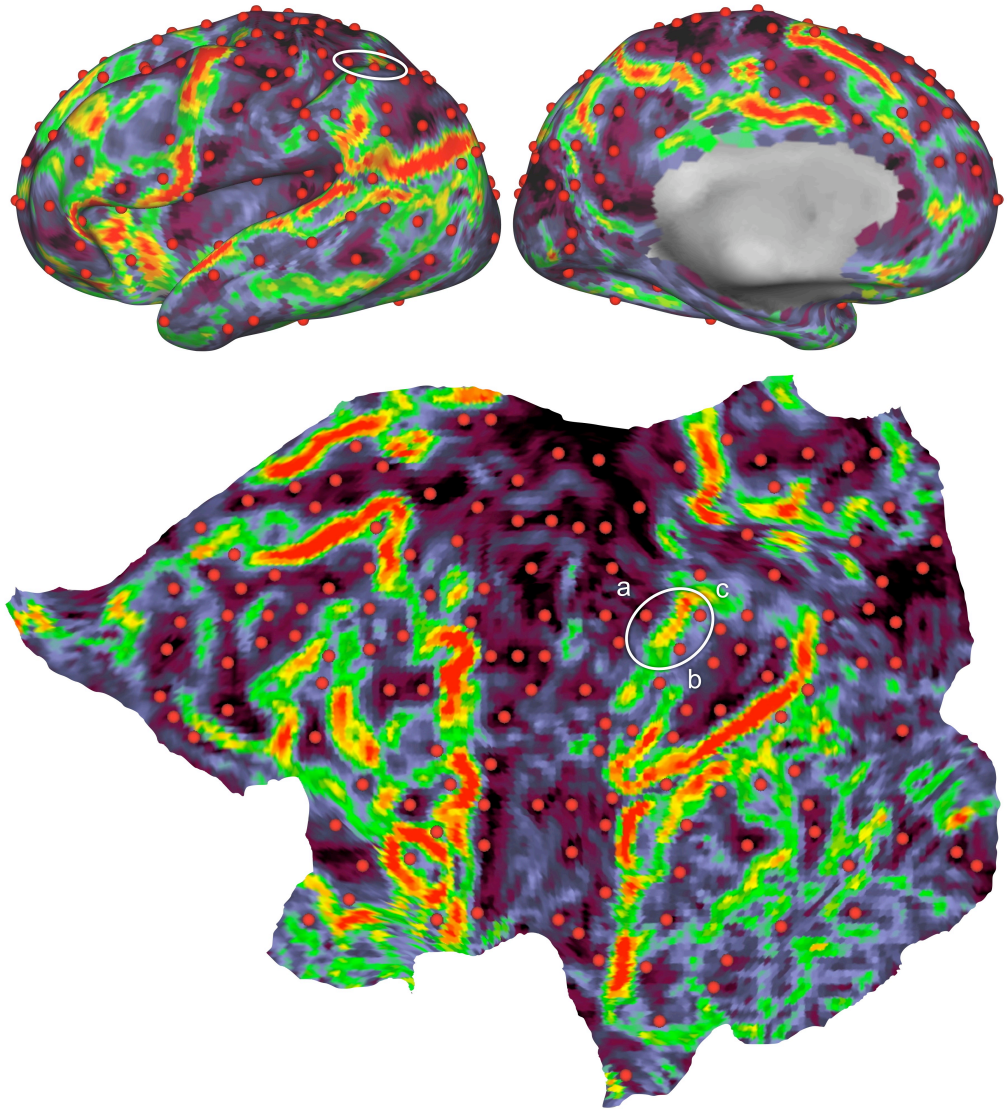

Figure 3.9: Three putative areas in lateral parietal cortex in an individual subject

Shown are lateral, medial, and flat views of the left hemisphere for a single subject's gradient magnitude-based rs-fcMRI contour map derived from the gradient magnitude maps with demarcated putative area locations derived from the Canny-based rs-fcMRI contour map in red (Layout is identical to Figure 3.2, Panel A). Highlighted in white are three putative areas in lateral parietal cortex, with a region denoted 'a' separated from regions 'b' and 'c' by a strong rs-fcMRI boundary. 'Hot' colors represent stronger gradient values, while 'cool' colors represent weaker gradient values.

This is demonstrated by visual inspection (Figure 3.10, Panel A) and spatial correlation calculations (Figure 3.10, Panel B) shown below in Figure 3.10 for three putative areas roughly near each other in lateral parietal cortex.

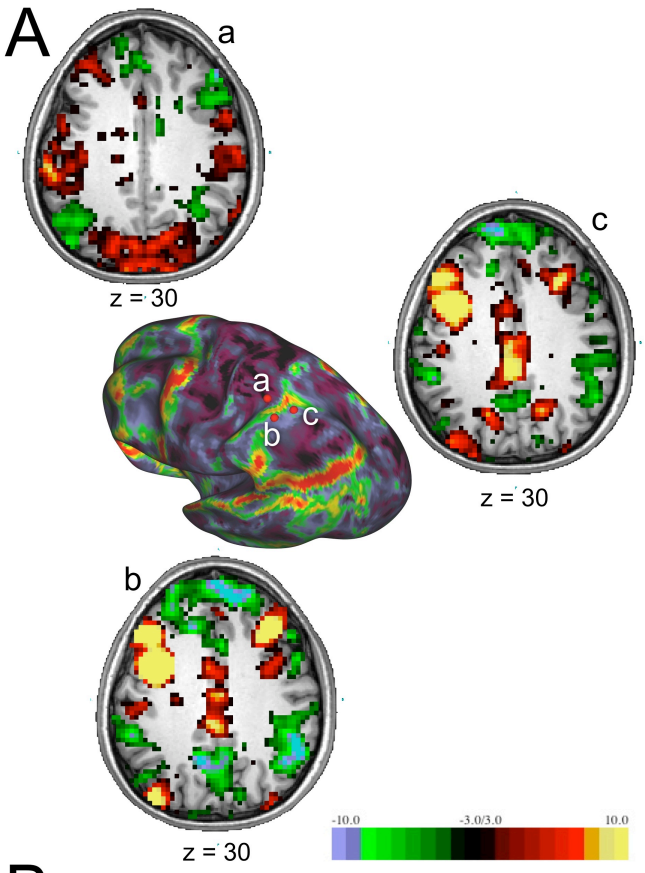

Figure 3.10: Comparison of three putative areas in lateral parietal cortex in an individual subject

Panel A shows a representative slice of each of the three putative areas' (from Figure 3.9) rs-fcMRI correlation maps arranged around a rotated postero-lateral view of an inflated left hemisphere. Panel B shows the volumetric distances between the three putative areas and the pair-wise spatial correlations of the rs-fcMRI correlation maps shown in Figure 3.9 and Panel A. In Panel A, 'hot' colors represent positive Z-converted correlations, and 'cool' colors represent negative Z-converted correlations.

Gradient magnitude-based rs-fcMRI contour maps produce higher spatial correlation across time within an individual subject.

Computing the spatial correlation across time for the three rs-fcMRI contour maps shown above in Figure 3.8 finds that the non-maxima suppressed contour maps are more correlated (r=0.60) across day than the Canny-based contour maps (r=.52), and the gradient magnitude contour maps show the highest correlations across day (r=0.75) (Figure 3.11). While this may appear to be due to the seemingly lower-resolution (i.e., greater blur/less contrast) of the average gradient magnitude maps, the values at each point in the average gradient maps actually more accurately represent the rate of change in rs-fcMRI correlation patterns at that point. As such, while the Canny edge detection maps clearly ease the delineation of putative functional areas, the gradient magnitude maps produce a more reliable measure of the underlying dynamics and are more useful for quantitative comparisons involving the entire cortex across time or subject.

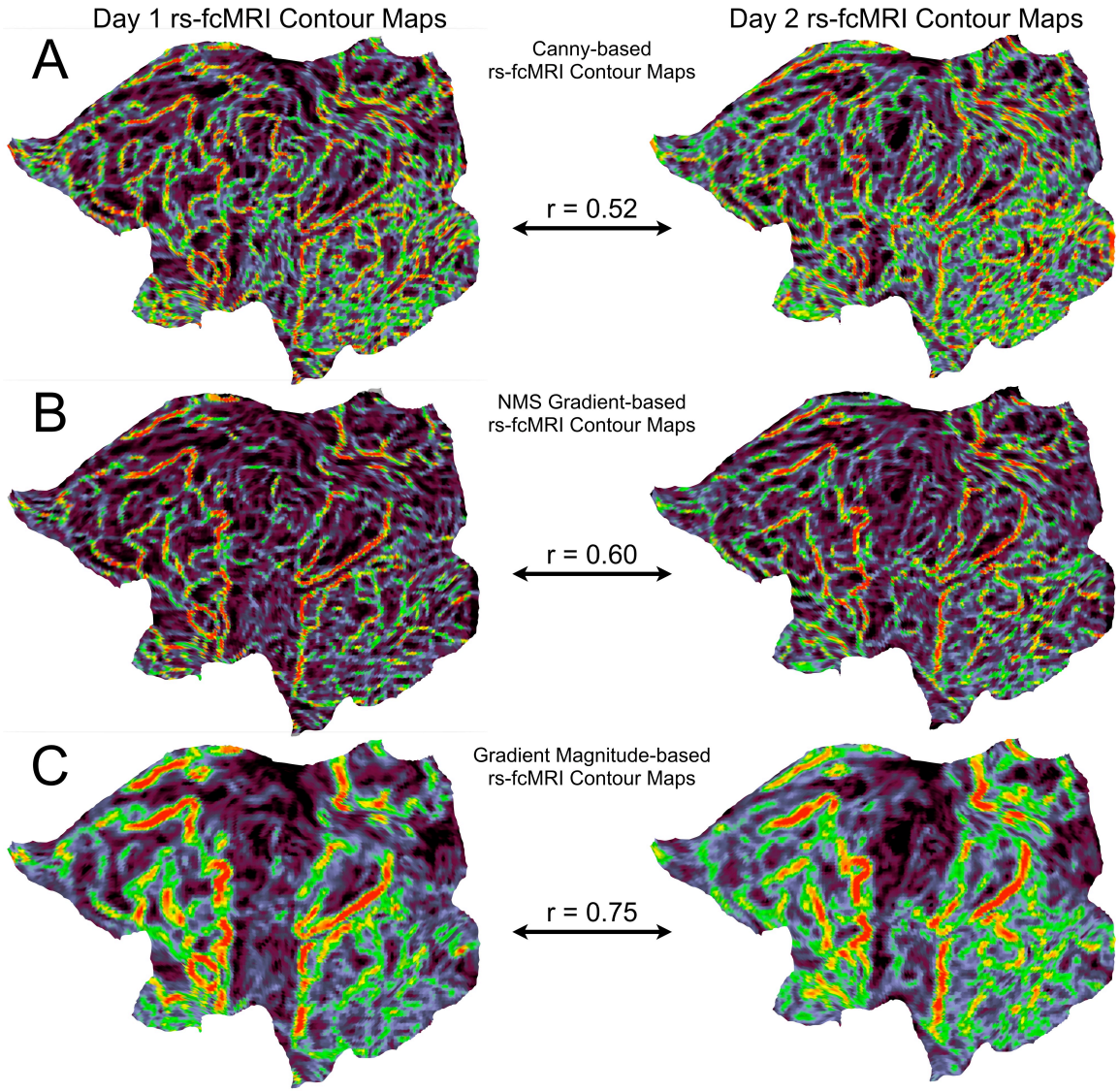

Figure 3.11: Comparison of the three rs-fcMRI contour map types across time in an individual subject

Shown are flat views of the left hemisphere for a single subject, processed to various points of our current algorithm and then combined into a single rs-fcMRI contour map for both Day 1 (left column) and Day 2 (right column), demonstrating the increase in measured spatial correlation across time from Canny-based contour maps (Panel A) to the non-maxima suppressed (NMS) gradient-based contour maps (Panel B) to the

gradient magnitude-based maps (Panel C) for this subject. In these representations, 'hot' colors represent stronger gradient values, while 'cool' colors represent weaker gradient values, or higher and lower probabilities of being detected as an edge for the Canny edge detection method.

The consistency of gradient magnitude-based rs-fcMRI contour maps across time within individuals is generalizable to multiple subjects.

To generalize the observation that rs-fcMRI contour maps are consistent across time within subject, seven additional subjects were analyzed with resting state data from two separate days with at least one week between sessions (avg. interval ~20 days, range 7d-53d). Since the gradient magnitude-based rs-fcMRI contour maps provide the least processed view of the underlying profiles, i.e., most accurately represent the strength of the gradients across the brain, and appear to have the strongest consistency across time for the single individual above (Figure 3.11), gradient magnitude rs-fcMRI contour maps are used here to examine cross-day consistency for multiple subjects.

In all cases, a strong spatial correlation was found between each subject's rs-fcMRI contour maps generated from the first and second days (Figure 3.12). For comparison, each subject's 'Day 1' rs-fcMRI contour map was also spatially correlated with the other seven subject's 'Day 2' scan as well as his or her own 'Day 2' scan. The results from this comparison are shown in Figure 3.12, demonstrating the higher degree of spatial correlation within subject across time than between subject (see Chapter 4 for a further analysis comparing rs-fcMRI contour maps across subjects).

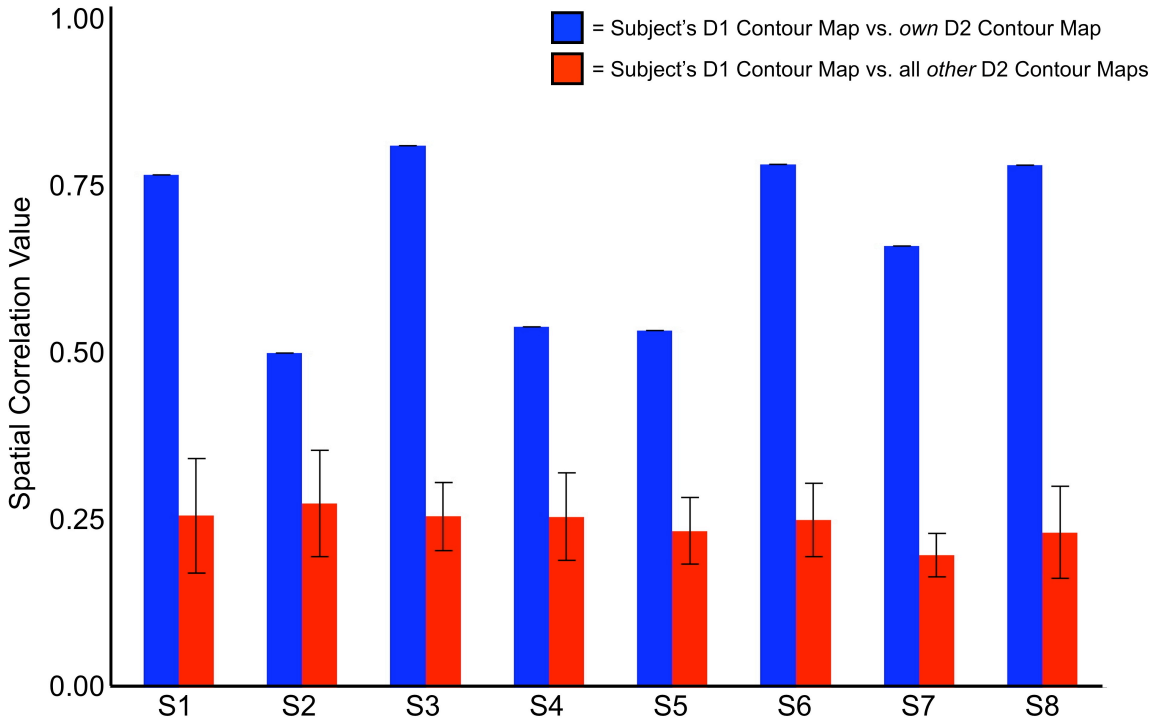

Figure 3.12: Spatial correlations between rs-fcMRI contour maps generated on two separate days for eight individual subjects

Each set of bars along the X-axis represent the amount of spatial correlation between a given subject's Day 1 rs-fcMRI contour map with his/her own Day 2 rs-fcMRI contour map (shown in blue) and with the other seven subjects' Day 2 contour maps (mean value shown in red, with error bars represent standard deviation of the spatial correlations).

An alternative approach to assessing the consistency of each subject's rs-fcMRI contour map over time is to ask whether maps generated from the same subject on two different days can be matched from a set of unlabeled maps, i.e., given a group of subject-labeled Day 1 maps, can a set of Day 2 maps be correctly labeled as belonging to the appropriate subject. This brief test was performed using the Hungarian algorithm

(Kuhn, 1955), an assignment algorithm that attempts to minimize the overall cost of assigning a set of tasks to a set of agents with a pre-existing cost for each possible task-agent assignment. In this case, Day 2 maps were assigned to Day 1 maps using spatial correlations as a cost function. As shown in Figure 3.13 below, the Hungarian algorithm easily finds the appropriate matching maps for each subject. In fact, the subjects are consistent enough within subject for this assignment to be done by eye. However, with increases in number of subjects and data, an algorithmic approach is more rapid and potentially more accurate.

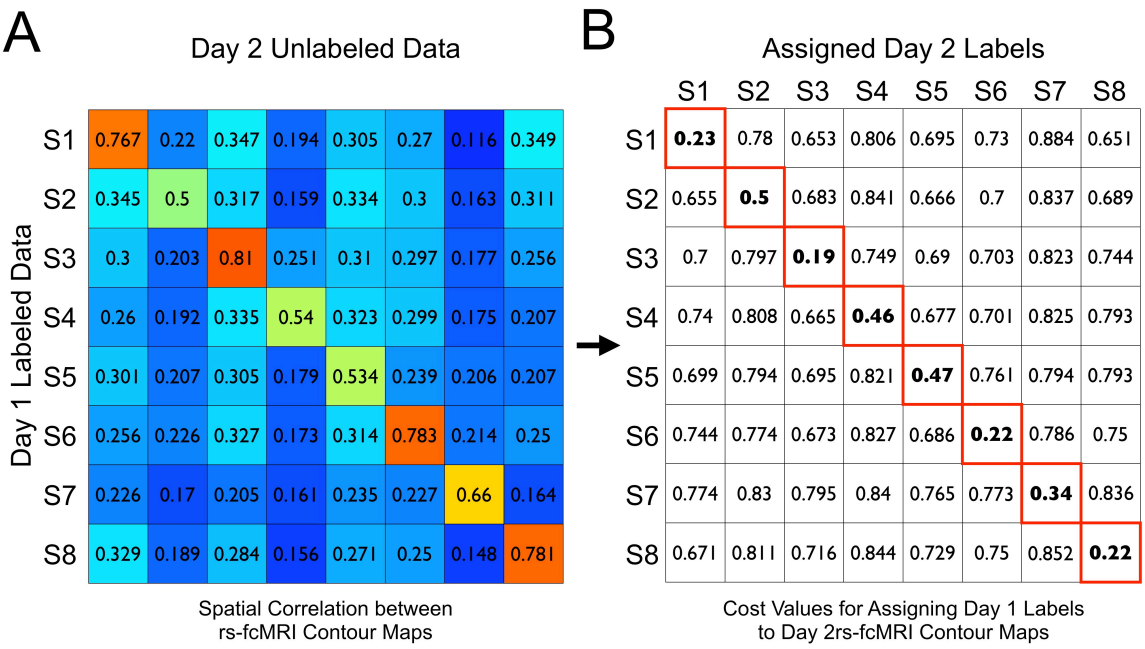

Figure 3.13: Assignment of second day scans to first day labels from eight subjects using the Hungarian algorithm

In Panel A is shown a correlation matrix comparing each of eight subjects' Day 1 rs-fcMRI contour maps, along vertical axis, to all subjects' unlabeled Day 2 map, along

horizontal axis. In Panel B is the corresponding cost matrix (where each value is 1-r) along with the output of the Hungarian algorithm shown as bold entries with red outlines in the matrix, assigning each of the Day 2 maps to a subject. In Panel A, warm colors represent higher pair-wise correlation values, and cool colors represent cooler pair-wise correlation values.

Discussion

Significance of extending previous results to generate rs-fcMRI contour maps across full hemispheric surfaces in single individuals based on resting data alone

The methodology described here, if extensible to other subjects and validated against other techniques, provides a framework for examining functional area organization in living humans in a rapid, non-invasive fashion. Functional area location, size, and placement could thus be measured and compared against task-evoked fMRI data or used to provide potential source location information to ease the analysis of EEG data. Additionally, the methods described here may eventually unburden neuroimaging from the need for extensive data collection to examine functional areas within single subjects. Perhaps even more profound is the possibility of a true function-based registration of functional areas across subject, moving beyond volumetric and/or surface-based registration of data across subjects, a possibility to be more specifically examined in the following chapters.

The use of focused 'patch' analyses vs. full cortical contour mapping

While functional areas in the the brain appear to be organized into large-scale distributed networks with long-range connections between anatomically separated regions (Bullmore and Sporns, 2009; Posner and Petersen, 1990; Sporns et al., 2004), it is often the case that functional areas involved in similar processing demands are located relatively near each other on the cortical surface, e.g., many areas involved in vision and visual attention (DeYoe et al., 1996; Felleman and Van Essen, 1991), or as seen for many functional areas in childhood (Church et al., 2008b; Fair et al., 2007a; Kelly et al., 2008). Thus, distinctions between functionally-similar adjacent regions might only be elicited by focused, analyses of 'patches' to test specific hypotheses of parcellation in a portion of the cortex.

While the 'patch'-based approach provides some additional gains in fine-scale cortical parcellation, we do not theorize that the additional distinctions created represent partitioning below the level of functional areas, and likely represent enhancement of the method's ability to distinguish adjacent but functionally similar putative functional areas. However, exceptions may exist in specific cases, such as the delineation of the motor mouth representation from surrounding motor cortex (see Chapter 4).

Resiliency of rs-fcMRI contour to functional dynamics over time

Recent work has shown that the rs-fcMRI correlations between functional areas evolve over childhood development (Fair et al., 2008; Fair et al., 2009; Fair et al., 2007a; Supekar et al., 2009) and relatively quickly (~months) given intense training on novel tasks (Lewis et al., 2009). However, since the spatial differentiation of cortex into functional areas is thought to be complete and relatively static after the first several years

of life (Sur and Leamey, 2001), the locations of boundaries around or between functional areas should also remain constant over the course of a lifetime. However, if two adjacent functional areas slowly become differentially specialized for particular processes, i.e., will start to have less correlated co-activation histories due to experience or training, the detected gradient between them would likely change in *strength*, but not *location*. As such, the extension of the methodology described here to younger ages is solely dependent on the presence of correlated low-frequency spontaneous activity as used here, which has been observed to be already established in infants (Fransson et al., 2007; Gao et al., 2009), and the ability to acquire resting state data on children of various age ranges.

Exploiting the different types of information gained from gradient magnitude-based and Canny-based rs-fcMRI contour maps may help extend these methods to younger populations and for study of chronic patient populations. It may hopefully be the case that putative area boundary locations can be stably detected and tracked across development or training/disease trajectory, while simultaneously measuring the strengthening or weakening of boundaries as spatially-adjacent functional areas become more or less differentially specialized.

Large spatial domains of functional similarity seen in gradient magnitude-based rs-fcMRI contour maps

The gradient-based rs-fcMRI contour maps often contain several large regions with very low gradient magnitudes throughout. These large low-gradient spatial domains bounded by strong gradients, seen above as 'cool' plateaus/valleys in Figure 3.9 and Figure 3.11 (Panel C), may represent several functional 'domains' across the cortex, i.e.,

multiple adjacent functional areas that are involved in similar processing demands. Within these domains, putative functional area boundaries are still detected with Canny edge detections, but since these boundaries are tentatively between functionally-related putative areas, they appear much weaker than boundaries between functionally-distinct, but spatially adjacent cortical regions. There have been many previous attempts to ascribe general 'domain'-level labels to separate extended regions of the cortex, e.g., 'association cortex' (Sakata et al., 1997), but these have by necessity been very general and typically describe some anatomically region larger than a functional area, but not precisely a functional 'system' either (Sejnowski et al., 1988). The methods described here may allow the actual locations, boundaries, and functional involvements of these domain-level partitions, and of the functional areas *within* each to be more accurately described than previously capable.

The creation of regions of interest or nodes for network analysis of individual differences in fMRI activity and rs-fcMRI correlations

Recent work has analyzed the network organization of regions known to be involved across many different tasks in normal adults (Dosenbach et al., 2006), across development (Fair et al., 2007a), in aging (Wig et al., 2009), and in disease (Church et al., 2008b). The network organization of these regions in normal adults readily recapitulates many of the relationships seen as co-activations, or as sets of regions containing particular sets of signals, across a range of tasks (Dosenbach et al., 2006). Comparing task-evoked activity in sets of regions with the differential correlations/connections seen

between sets of regions, it is predicted that rs-fcMRI correlations represent the statistical co-activation history between regions over a long period of time.

Given that the relationships between different functional areas appears to change over development, in aging, as well as in clinical populations, task-evoked activity should be interpreted not only in the context of the specific functional areas involved, but also in the context of the specific network relationships each functional area has with the rest of the brain (Church et al., submitted). Since rs-fcMRI mapping obtains regions that by definition have consistent patterns of rs-fcMRI correlations, and can be used to extract fMRI activity from tasks within individuals, the nodes and networks generated will have increased stability and potentially increased validity for each individual. Thus, individual differences in network relationships can be easily studied as well as the differential task-evoked activity from each region, or node, of the network. Specific group differences in both the location and size of nodes, as well as the relationships between them, will also be accessible with this type of analysis.

Conclusion

The results presented here demonstrate the potential benefits of applying the methods from Cohen et al., 2008 in describing the entire cortical surface. It is possible to use resting state data to both locate and characterize locations of rapid change in rs-fcMRI patterns, that thus likely represent functional area boundaries. The rs-fcMRI contour maps generated following the procedures discussed in this chapter are highly stable within individuals over time, and are consistent enough within subject to be

uniquely identifiable, indicating that not only are these maps potentially meaningful, but they are also practicable for analysis and use in other domains.

CHAPTER 4: COMPARING RS-FCMRI CONTOUR MAPS ACROSS INDIVIDUAL SUBJECTS, INDEPENDENT COHORTS, AND DATASOURCE

Introduction

The study of functional areas in humans requires the comparison of observations across many subjects and groups, yet appropriate alignment is still an evolving process.

Studies in non-human primates, as well as other model organisms, often leverage the ability to perform multiple serial experiments in a single animal to localize and characterize functional areas across the brain with minimal ambiguity as to which functional area is being studied. Given the prerequisite for non-invasive procedures in humans and the desire to minimize the requirement of multiple studies within individuals, most neuroimaging studies combine data across multiple subjects, and/or groups. While volumetric registration is typically used to align neuroimaging data, cortical surface alignment and task-based localization of functional areas are also becoming increasingly available:

Interrogating cortical function within and across subjects and groups is primarily done by volumetrically registering subjects to a common stereotactic space using anatomical information.

Functional data derived from single subjects, or from groups of subjects, are primarily referred to using stereotatic coordinates resulting from volumetric registration, i.e., translating, rotating, and scaling the data from each subject to match a common

stereotactic space (Lancaster et al., 1995). This allows for the comparison of functional distinctions within and between subjects and groups by comparing their stereotactic coordinates within this shared space (Lancaster et al., 1995; Ojemann et al., 1997; Snyder, 1996; Talairach and Tournoux, 1988). Since each subject's alignment to a common volumetric space is based on the shape and orientation of their brain, differences in folding pattern, as well as variability in functional area shape and size, remain in the data. As such, a set of coordinates may represent a single functional area, or a potential mixture of different functional areas in each subject. Additionally, stereotactic coordinates differ depending on the chosen stereotactic space, i.e., MNI 305/152 average, colin27, Talairach T88, WU-NIL 711-2B, etc. This can cause confusion when comparing reported coordinates in the literature if the differences between spaces are not taken into account (Bohland et al., 2009).

However, with appropriate care concerning stereotaxis, and since anatomical variation in the population is finite, combining data from a sufficient number of subjects results in a predictable amount of anatomical 'blurring' and similarly registered and combined group data can be easily compared (Burgund et al., 2002; Fox et al., 1988; Friston et al., 1991). Additionally, volumetric registration techniques are presently quite straightforward, and a small number of stereotactic atlas spaces are becoming accepted as standard in the literature. Combined with the ability to bypass concerns of individual anatomical variation by increasing the size of the study population, volumetric registration is a very attractive method for aligning neuroimaging data across subjects and

is still the standard for the majority of neuroimaging studies currently being performed (Devlin and Poldrack, 2007).

Surface-based registration can identify locations in relation to each individual's own cortical structures, but still does not account for variation in the actual size and location of functional areas.

It has recently become possible, using freely available software, e.g., Freesurfer, Caret/SUREfit, etc. (Dale et al., 1999; Dale and Sereno, 1993; Fischl et al., 2001; Fischl et al., 1999; Ségonne et al., 2004; Ségonne et al., 2005; Van Essen et al., 2001), to rapidly segment the cortical surface from anatomical MRI data. This has resulted in the preliminary ability to align surface features, such as specific gyri and sulci labels, or sulcal depth at all points, across the brain to find potentially corresponding cortical locations across subjects (Lyttelton et al., 2007; Van Essen, 2005; Van Essen and Dierker, 2007a). Analyses can thus be performed on a 'surface-based atlas space', with corresponding points on each subjects' cortical surface, which likely each have differing volumetric coordinates. This has the potential for improving the alignment of functional data from neuroimaging studies by accounting for folding differences across subject, but still does not address the variation in the relationship between folding landmarks and functional areas (Amunts et al., 2000; Amunts et al., 1999; Andrews et al., 1997; Uylings et al., 2005; Van Essen et al., 1984). While methods for surface-based analyses are still being developed, it is hoped that by partially accounting for individual variability in folding patterns, functional observations may be compared across subject more

appropriately, reducing the amount of uncertainty about which functional area is being observed.

Identifying functional area locations within single subjects with task-evoked activity currently requires extensive data collection and is often incomplete.

A functional area's location within individuals can be directly assessed if 'localizer' tasks have been developed which reliably activate a particular functional area more than the surrounding cortex (Swallow et al., 2003). While these tasks do not exist for the majority of functional areas across the brain, there have been efforts to generate batteries of tasks that can identify multiple areas in individual subjects (Drobyshevsky et al., 2006). These batteries, however, still do not identify a majority of functional areas and often require significant subject involvement which may preclude their application to developmental and clinical populations.

Recent work has shown that it may be possible to perform additional registration based on extended task-related activity within subjects (Sabuncu et al., 2010). This line of methodology, however, relies on the similarity of neural responses across subjects to a long-duration (~1hr) stimulus. As such, the potential individual variation in response and the large amounts of functional data required, still provide challenges for this type of 'functional' registration based on task-related activity.

rs-fcMRI mapping of individual subjects appears to find consistent contours and putative functional areas within subject that may allow direct assessment and comparison of functional areas within and across subjects.

Given the remaining potential ambiguity in anatomical registration methods such as volumetric and surface registration at the individual level, and the limited applicability of functional localizers, a method for generating accurate functional area locations within individuals would prove very useful in comparing functional distinctions across subjects. As described in the previous chapter, rs-fcMRI mapping can generate contour maps that cover the full hemispheric surface and can be used to generate putative functional area and boundary locations. Since these contour maps appear to respect many known functional distinctions and are relatively stable across time, they may be useful for finding functional areas in individual subjects, as well as as allow for improved cross-subject comparison of putative functional areas. Additionally, since resting state data is easily acquired in a wide range of populations with minimal time requirements and demands on subject compliance, rs-fcMRI based methods are particularly appealing.

rs-fcMRI mapping is here performed individually on a group of subjects as well as on group-averaged data from two matched cohorts and the resulting rs-fcMRI contour maps compared for consistency across subject, cohort, and scanning parameters.

The analyses presented below provide an initial proof of principle that: (i) rs-fcMRI mapping produces similar patterns across individual subjects. (ii) Highly salient large-scale features are seen in individual and group-averaged contour maps and appear to demarcate large-scale functional ‘domains’. (iii) These results also appear stable to differences in group, MRI field strength, and resolution of acquisition.

Methods

Overview

The analysis stream presented here is an extension of that presented in the previous chapters, adding statistical testing across a group of rs-fcMRI contour maps, and a modified 'group-average' procedure to analyze data from groups of subjects that do not yet have individual fiducial surfaces available.

Subjects

Either 16.1 or 21.3 minutes of rs-fcMRI data were collected on a set of 29 subjects (16F, age 21.3-28.8 years). 11 subjects were instructed to relax and fixate on a black crosshair against a white background for four runs of 2.5s TR, 132 frames per run, while 18 subjects were instructed to relax and fixate on a white crosshair against a black background for three runs of 2.5s TR, 133 frames per run, for a total average of 434 usable frames/subject acquired with a 3.0T Siemens MAGNETOM Trio Scanner (Erlangen, Germany).

For an additional set of 28 subjects scanned with a 1.5T Siemens MAGNETOM Vision Scanner (Erlangen, Germany), 10.7 minutes of (256 frames of 2.5TR) rs-fcMRI data was extracted from previously acquired task data by excising and concatenating the resting fixation-blocks from before, between, and after task blocks in mixed blocked/ event-related studies. The procedure for doing this has been recently described and validated with a dataset including these subjects (Fair et al., 2007b).

Informed consent was obtained in a manner approved by the Institutional Review Board of Washington University School of Medicine and subjects were compensated for their time.

Data acquisition

3.0T Trio resting state acquisition

Images were acquired as in Chapter 3 for 3.0T Trio data.

1.5T Vision task-interleaved resting state acquisition

Images were acquired as in Chapter 2 for 1.5T Vision data.

Data preprocessing

Standard fMRI preprocessing

Imaging data from each subject were pre-processed as in previous chapters.

rs-fcMRI specific preprocessing

Additional pre-processing for functional connectivity analyses was carried out as in previous chapters.

Surface preprocessing

Cortical surface generation from anatomical MRI data using Freesurfer

Individual cortical surfaces were generated for each of the 29 subjects scanned on the 3.0T Trio scanner as in Chapter 3.

Surface-based registration to the PALS atlas using Caret

Registration of each subject to the PALS surface atlas was carried out as in Chapter 3.

Alternative 'PALS fiducial-based' approach for group-average non-individually segmented data

To analyze group data where the individual subject fiducial surfaces were not available, i.e., a group of subjects for whom pre-existing resting state data was available but segmented surfaces were not, rs-fcMRI contour maps were generated and analyzed using an alternative, albeit less ideal, method. For these subjects, the PALS atlas fiducial surface was transformed to the appropriate atlas space and used to obtain probable surface coordinates for the present group-averaged datasets (Van Essen, 2005). This automates the procedure originally used to generate a 'line' of seed locations between angular gyrus and supramarginal gyrus in Chapter 2.

The PALS atlas fiducial surface represents the average of 12 individual grey mid-thickness surfaces each volumetrically registered to the 711-2B atlas, and while it does not represent the actual fiducial surface of any specific individual, can be used to approximate average fiducial surface locations in group-averaged data in the same volumetric atlas space.

Cortical seed and rs-fcMRI correlation map generation

A set of cortical seeds that covered a full hemisphere was created as in Chapter 3.

Generation of group average rs-fcMRI correlation maps for 'group-average' analysis

For 'group-average' data, a set of average volumetric correlation maps were made for a group of subjects, using the seed locations from the PALS atlas fiducial surface and averaging the set of subjects' correlation maps generated from each seed. This set of average rs-fcMRI correlation maps and the PALS atlas fiducial surface itself were then used for the remaining analysis of this data.

eta^2 matrix creation for each seed

eta^2 matrices for each rs-fcMRI seed location were then made for each subject or group-average dataset as in Chapter 3.

Analysis of contrast information in eta^2 matrices

Gradient map derivation

Gradient magnitude maps were computed from each eta^2 matrix as in Chapter 3.

Construction of cortical contour maps based on compiled contrast information

Direct averaging of contrast maps

To explore the consistency of rs-fcMRI mapping across subjects, gradient magnitude-based rs-fcMRI contour maps were used here, and computed as the average of the underlying gradient magnitude maps, as described in Chapter 3.

Analysis of similarity and variation in rs-fcMRI contour maps across 29 individual subjects

To analyze the similarity and amount of variance across the subjects, a surface-registered average rs-fcMRI contour map was created from the individual contour maps of 29 subjects, and the spatial correlation between each subject's contour map and the average contour map computed. One-sample t-tests were also computed for each location across the group of 29 subjects against the median of average rs-fcMRI contour map to find locations containing statistically stronger or weaker gradient values. This would typically be done by performing a one-sample t-test at each location against the *mean* of the total dataset, but since the distribution of gradient values is non-normally distributed (there is a slight skew towards higher gradient values), we here performed one sample t-tests at each location against the median of the average rs-fcMRI contour map, a potentially more reliable metric of the central tendency of the dataset. The observed p-value distribution was used to calculate a False Discovery Rate threshold, controlling for the expected proportion of false positives among suprathreshold locations (Genovese et al., 2002).

Comparison of rs-fcMRI contour maps between two age-, sex-, and resting length-matched cohorts acquired on different scanners

To examine potential effects of resolution, field strength, resting state type, and other scanner-dependent parameters, two independent cohort group-average datasets were constructed containing subjects matched for age, sex, movement, and approximate amount of data (n = 28, 15F, avg. age 25.4 years, avg. 360 frames from each subject in both groups). These subjects were then processed using the alternative PALS-fiducial

method described above to generate single rs-fcMRI contour maps representing the gradients detected from the two sets of group-average rs-fcMRI correlation maps.

These two cohorts were constructed to be closely matched in age, sex, and amount of data per subject to the data, and thus required the inclusion of some subjects who were among those used for the individual analyses described above (18 of the 29) acquired on the 3.0T Trio scanner.

Results

While the Canny-based rs-fcMRI contour maps shown in Chapter 3 performed well at delineating putative area locations across the cortical surface, gradient magnitude-based rs-fcMRI contour maps retain significantly more information at any given point concerning the spatial dynamics of the rs-fcMRI patterns. Gradient magnitude-based rs-fcMRI contour maps are thus used for the remainder of this thesis as they are more suited for point-by-point comparisons made across the entire surface.

rs-fcMRI mapping produces a statistically reliable large-scale contour pattern across a group of individuals.

If rs-fcMRI contour maps reflect the spatial organization of functional areas in each individual, contour maps should not only be consistent across time (Chapter 3), but also moderately similar across subjects, barring the amount of expected variation in their functional area locations. As an initial test of the similarity of rs-fcMRI contour maps across subject, we created an average rs-fcMRI contour map from 29 subjects (Figure 4.1, Panel A) and computed FDR-corrected one-sample t-tests (Figure 4.1, Panel B) at each location against the median gradient value of the average rs-fcMRI contour map.

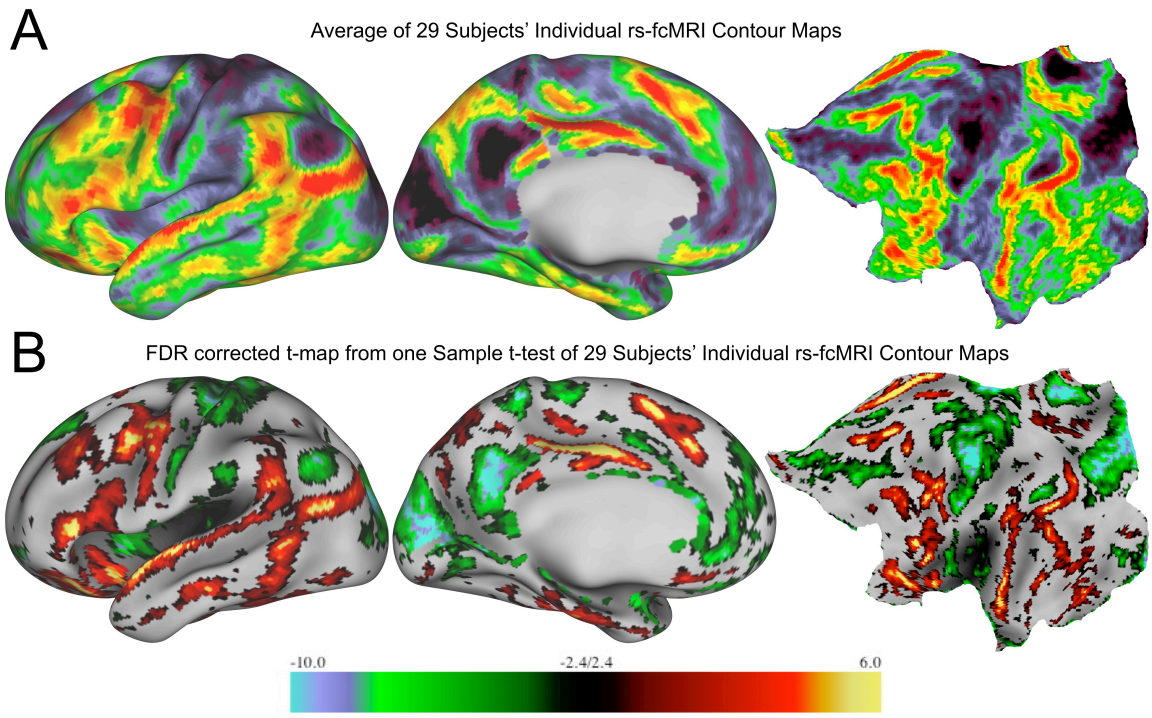

Figure 4.1: Average rs-fcMRI contour map and one-sample t-test results of 29 subjects

Shown are lateral, medial, and flat views of the left hemisphere of data from a group of 29 subjects, with the average gradient magnitude-based rs-fcMRI contour map in Panel A, and a statistical t-map testing the reliability of each location across the subjects in Panel B. In Panel A, 'hot' colors represent stronger gradient values, while 'cool' colors represent weaker gradient values, while in Panel B, 'hot' colors represent gradient values statistically higher than the overall distribution, while 'cool' colors represent gradient values statistically lower than the overall distribution. Using a False Discovery Rate of 0.05 results in a t-score threshold of >+/-2.4 for significance. Underlying inflated surfaces are generated from the average fiducial surface of the group of 29 subjects.

As can be seen in Figure 4.1, there are several strong and consistent putative boundaries and functional areas that are significantly reliable in both strength and

location. It is important to note, however, that significance, or lack thereof, at any particular location in this map is the result of the reliability of gradient values at a surface-registered location, and thus is a convolution of the variability in gradient strength *and* the variability in anatomical location.

There is a measurable degree of fine-grain variation across subjects, yet strong rs-fcMRI features remain detectable.

To examine the amount of variation and similarity of rs-fcMRI contour maps across this set of 29 subjects, we computed the spatial correlation between each individual's rs-fcMRI contour map and the group's average rs-fcMRI contour map. This provides a straightforward way to determine the consistency of the group, as outliers will be dramatically less correlated with the group average. As shown in Figure 4.2, there is a relatively narrow range of spatial correlation between each individual subject's rs-fcMRI contour map and the group average rs-fcMRI contour map (average spatial $r = 0.50$). It should be noted that due to the inherent contrast difference between the group average map and each individual's contour map, the maximum possible correlation is significantly less than 1. Additionally, as indicated by white and yellow arrows in the final flat map of Figure 4.2, even the individual contour maps least correlated with the group average still contain strong features seen in all other subjects.

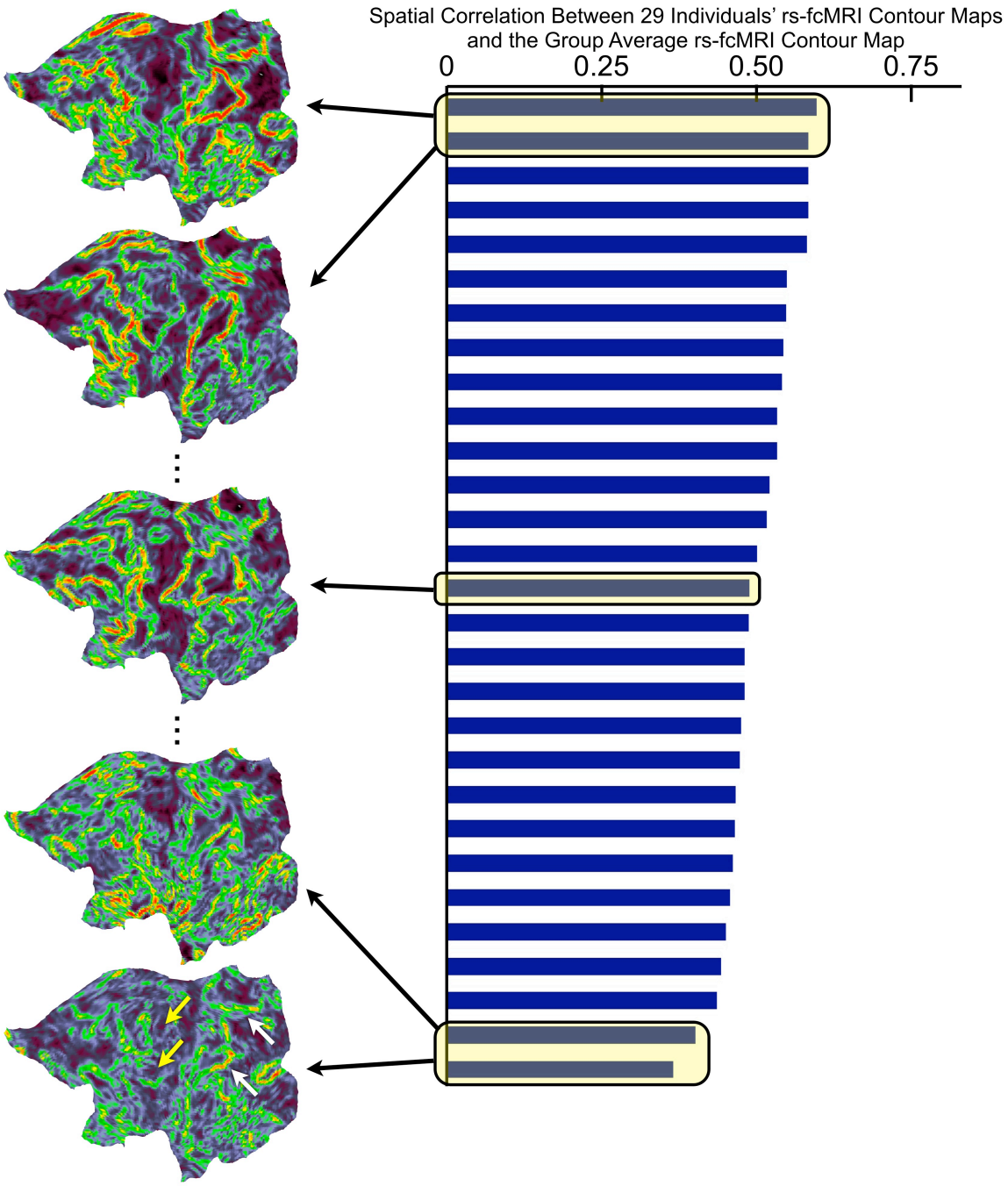

Figure 4.2: Spatial correlations between each of 29 individual subjects' rs-fcMRI contour map and the group average rs-fcMRI contour map

Spatial correlations between each of the 29 subjects' own rs-fcMRI contour map and the group's average rs-fcMRI contour map, ordered by decreasing spatial correlation. To the

left of the spatial correlation values are selected individual's rs-fcMRI contour maps, to illustrate the range of similarity with the group average and to each other. Of note, the final subject, having the lowest spatial correlation with the mean map, still contains many of the features reliably seen in the other subjects, such as boundaries in posterior cingulate and lateral parietal cortex indicated by white arrows, and consistent putative areas indicated by yellow arrows (see next section for a more thorough description of the many consistent features).

Several strong, salient, and potentially functionally important features are consistently observed in rs-fcMRI contour maps, regardless of source.

There are several salient features that have been observed in many of the individual subjects' rs-fcMRI contour maps, including particularly strong boundaries and stable putative functional area locations. As demarcated below in Figure 4.3 (Panel A), on the average rs-fcMRI contour map replicated from Figure 4.1, as well as on two separate matched cohorts of subjects scanned on two separate scanners (Figure 4.3, Panels B-C), these strong and consistently detected putative 'landmark' features include:

- A strong boundary that appears to separate dorsal /anterior from ventral/posterior anterior cingulate cortex, then extends onto lateral prefrontal cortex dividing motor-related territory anterior to the central sulcus from territory in dorsal lateral frontal cortex. This boundary appears to continue ventrally to separate anterior insula from middle and posterior insula, dividing putative control-related areas in anterior insula

from putative interoceptive/homeostasis-related areas in the insula (Craig, 2009; Singer et al., 2009).

- Additional strong boundaries appear to extend around strong stable regions in the posterior cingulate cortex, lateral parietal cortex, and to a lesser extant ventral medial prefrontal cortex, all three of which are of appropriate locations and size to represent regions members of the default network (Raichle et al., 2001).
- In temporal cortex, a boundary runs the length of the superior temporal gyrus, paralleled by a boundary extending along the inferior temporal gyrus to posteriorly, together partially bounding regions observed to be related to semantic content (Wig et al., 2009) as well as sub-lexical/phonological processing (Hickok and Poeppel, 2007) from surrounding cortex.
- Another boundary in posterior temporal cortex circumscribes territory that, based on anatomical location and available functional data (see Chapter 5), are likely to be visual processing areas extending from occipital cortex, including MT+, and continuing to the ventral 'stream' of functional areas (Connor et al., 1994; Mishkin et al., 1982; Mishkin and Ungerleider, 1982).
- Localized regions of increased *stability* appear in multiple locations across the cortex, particularly along the central sulcus, spanning the somatomotor representation. Two of these are of particular note, being of the right location and size to potentially be the somatomotor representations of hand (Grafton et al., 1993; Ramsey et al., 1996) and mouth (Fox et al., 2001; Petersen et al., 1988).

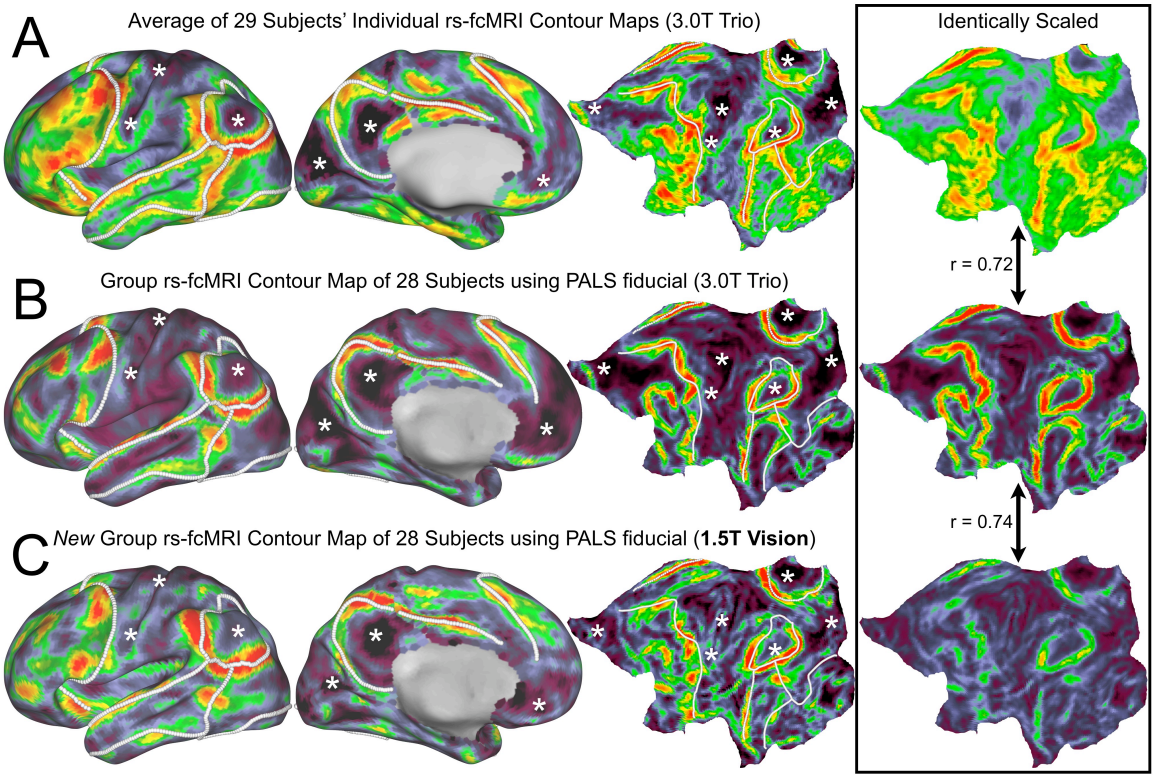

Figure 4.3: Consistent features seen across rs-fcMRI contour maps

Shown are lateral, medial, and flat views of the left hemisphere for an average of 29 subjects' individual rs-fcMRI contour maps (Panel A), and two group datasets using the PALS-fiducial and data from two different scanners. (Panel B represents data collected at 3.0T, while Panel C represents data collected at 1.5T). Demarcated in solid white lines are boundaries consistently seen across datasets, while white stars denote locations of consistent stability across datasets. The boxed panel to the right demonstrates the relative strength of the different contour maps when identically scaled, while for the remainder of the figure, the datasets are independently scaled to visualize the dynamic range of the data. In all Panels, 'hot' colors represent stronger gradient values, while 'cool' colors represent weaker gradient values. Underlying inflated surfaces in Panel A are generated

from the average fiducial surface of the group of 29 subjects, while the underlying inflated surfaces in Panels B and C are from the PALS atlas surface set.

Extending the comparison of individual rs-fcMRI contour maps described above, two matched cohorts of 28 subjects were processed using a PALS fiducial-alternative method which locates boundaries (Figure 4.3, Panels B-C) based on a group's *volumetrically-averaged* rs-fcMRI correlation maps, as opposed to individual subjects' rs-fcMRI correlation maps. As described in the introduction above, volumetric registration over a significant number of subjects should 'average'. For purely group comparisons, this has the advantage of requiring a fraction of the processing time, does not require each subject to undergo cortical segmentation and registration, and limited existent amounts of resting state fMRI data per subject can be countered by increasing the number of subjects within the group.

As can be seen in Figure 4.3 Panels B-C, rs-fcMRI contour maps generated from two independent groups still appeared quite similar despite the greatly different acquisition parameters, scanner MR field strengths (1.5T vs. 3.0T), resolutions of acquisition (3.75mm x 3.75mm x 8mm vs. 4mm x 4mm x 4mm), and differences in SNR due to headcoil and software between the Vision and Trio scanners. While the spatial correlation between the two rs-fcMRI contour maps was quite high (r=0.74), rs-fcMRI contour maps generated from subjects scanned on the 3T scanner (Figure 4.3, Panels A-B) had higher dynamic range and apparent increases in the strength of boundaries

(demonstrated in boxed panel in Figure 4.3), as could be expected from higher resolution data with improved SNR.

Discussion

Applicability and comparability of rs-fcMRI mapping across subject populations

rs-fcMRI contour maps appear to be relatively consistent across subjects and across groups denoting the applicability of the techniques described here to a wide variety of subject populations. Indeed, the spatial distribution of boundaries and putative areas are similar enough that strong features can be seen as landmarks, as demarcated in Figure 4.3. The remaining variability in rs-fcMRI contour maps likely represent the combination of the considerable remaining variability not accounted for by volumetric and surface landmark-based alignment, the variable relationship between functional area locations and registration landmarks across subjects. As such, while there remains a great deal of work in reducing registration error across subjects, rs-fcMRI mapping does appear to produce relatively consistent contour maps across subjects, potentially allowing the ability to compare results across subject, group, and study.

Interpretation of some of the most reliable strong spatial patterns seen across rs-fcMRI contour maps

Paralleling the finding that seed-based rs-fcMRI correlation maps appear to replicate many observed functional co-activation patterns seen in task-related fMRI, many of the strongest boundaries seen here also appear to delineate the locations between and around observed task-evoked regions. For instance, dorsal and ventral anterior

cingulate cortex appear to be separated by a strong transition in rs-fcMRI patterns, mirroring a spatial segregation in the literature of regions involved in cognitive processes being found more dorsally while regions shown to be involved in emotional processes have tended to be found more ventrally (Bush et al., 2000; Critchley et al., 2003).

Strong boundaries can also be found separating regions known to deactivate during goal-directed tasks, i.e, the default network, and surrounding functional areas (Raichle et al., 2001). Specifically, a strong boundary is seen separating a region in lateral parietal cortex/angular gyrus from supramarginal gyrus and inferior parietal lobule while other boundaries circumscribe posterior cingulate and ventral medial prefrontal regions.

There are additional strong boundaries that appear to delineate the ventral pathway of visual attention, separating this section of lateral and inferotemporal cortex from surrounding territory (Connor et al., 1994). More anteriorly, along lateral temporal cortex, this boundary replicates a division seen between regions sensitive to perceptual content ventro-posteriorly and regions sensitive to semantic content dorso-anteriorly, consistent with recent descriptions using task-related and seed-based rs-fcMRI data in Wig et al (Wig et al., 2009), and elsewhere (Martin, 2007; Simmons et al., 2009).

Conversely, topographically organized areas that are spatially adjacent do not appear to be strongly distinguished from one another by abrupt changes in rs-fcMRI patterns. For instance the succession of visual areas ranging outwards from the calcarine sulcus typically seen using retinotopic paradigms appears to be not detected here (DeYoe et al., 1996; Warnking et al., 2002). Relatedly, it appears that functional areas known to have a strongly correlated history of co-activation are also not strongly distinguished

from one another by abrupt changes in rs-fcMRI patterns. As a prime example, there is no strong rs-fcMRI boundary running down the central sulcus between primary motor cortex and primary sensory cortex, yet smaller distinctions appear to differentiate the hand and mouth representations from surrounding sensory and motor cortex (Fox et al., 2001; Grafton et al., 1993; Petersen et al., 1988; Ramsey et al., 1996). This observation is consistent with task-related fMRI studies often finding high levels of co-activation between motor and somatosensory regions as well (Porro et al., 1996).

Conclusion

The results described here demonstrate that not only can rs-fcMRI contour maps be reliably produced for multiple individual subjects, but that these contour maps are relatively similar across subject and are also similar across data of differing quality. Many of the strong and resilient patterns repeatably seen across subjects and groups in rs-fcMRI contour maps appear to represent previously observed functional distinctions across the cortex, yet are here created purely from resting state data. These landmark features open the door for a 'functional-registration' of functional areas across subjects and groups, based purely on task-independent scan data. The ability to generate rs-fcMRI contour maps on single individuals also allows for numerous analyses comparing the size, shape, and distribution of putative functional areas to individual differences in a rapid and tractable fashion.

CHAPTER 5: INITIAL VALIDATION AND COMPARISON OF RS-FCMRI MAPPING WITH FMRI FUNCTIONAL ACTIVATION DATA

Introduction

rc-fcMRI analyses have become a useful tool in neuroimaging due to the fact that rs-fcMRI correlations appear to align with many task-related fMRI patterns in describing functional distinctions across the brain.

Typically, functional neuroimaging uses differential activity between conditions to identify specific information processing operations occurring in separate functional areas (Posner et al., 1988). Over the past several decades, numerous reproducible task-evoked responses have been observed in a broad number of 'regions' that may include all of, or more than one, functional area. One of the major motivations behind the increasingly widespread use of rs-fcMRI analyses is that the patterns seen in seed-based analyses (Biswal et al., 1995; Fox et al., 2006a; Greicius et al., 2003; Hampson et al., 2006b; Mencl et al., 2000; Raichle and Snyder, 2007), independent component analyses (ICA) (Calhoun et al., 2005; Calhoun et al., 2008; Esposito et al., 2008; Kiviniemi et al., 2009; Stevens et al., 2009; Zuo et al., 2009), and network analyses (Bullmore and Sporns, 2009; Church et al., 2008b; Dosenbach et al., 2007; Fair et al., 2008; Fair et al., 2009; Honey et al., 2009) of rs-fcMRI correlations all appear to replicate, inform, and/or extend patterns seen in task-evoked fMRI studies (Damoiseaux et al., 2006; Dosenbach et al., 2007; Dosenbach et al., 2006; Raichle et al., 2001) as well as those seen in connectional anatomy studies (Honey et al., 2009), without the necessity for task performance. This consistency in the observed patterns make it highly likely that rs-fcMRI correlations

represent relationships between the same functional areas or regions involved in task-related fMRI. Indeed, since the relationships in rs-fcMRI are not based on the performance of particular tasks, it is hoped that rs-fcMRI correlations may more closely represent the overall statistical history of co-activation between two functional areas, as opposed to merely the co-activation of two functional areas during a single, or small number of, tasks.

rs-fcMRI mapping reliably detects many putative functional areas and boundaries that also appear to correspond with known distinctions obtainable with task-evoked fMRI.

As discussed in Chapter 4, many of the putative areas and boundaries most reliably detected with rs-fcMRI mapping appear to be in the same locations as many known fMRI-defined regions and functional boundaries (Chapter 4, discussion). However, this attempt as labeling putative areas with labels derived from other studies requires more information than simply anatomical colocation, both coordinate and surface alignment, and the spatial arrangement of borders across the cortex. This is particularly true, given the potential use of rs-fcMRI mapping as a way to rapidly delineate large numbers of functional areas.

Since both task-related fMRI activity and rs-fcMRI correlations appear to similarly reflect the underlying spatial organization of functional areas, these two analyses should be relatively consistent. Acquiring both task-related fMRI data and rs-fcMRI data in the same group of subjects should allow the potential validation of putative area labels for involved task-related regions. Given the consistency of rs-fcMRI contour

maps across subjects, it is hopeful that once functional area identities of detected areas are known and replicated for a few groups of subjects, the labels themselves may be transferrable based on the rs-fcMRI contour maps alone, i.e., functional areas could be localized in new subjects, *without* having to perform localization studies.

Here, we perform an initial comparison of the spatial patterns of rs-fcMRI mapping and fMRI task-related activity at the individual and group level for two tasks.

The analyses presented below demonstrate that: (i) Group-level statistics for an extended retrieval task in many cases align with rs-fcMRI mapping results from the same group of subjects. (ii) Averaged within-subject statistics from a saccade localizer task align with averaged individual within-subject rs-fcMRI contour maps from the same group of subjects. (iii) Within-subject statistics for a saccade localizer in a single individual, while more variable, also align with rs-fcMRI mapping performed on the same individual subject.

Methods

Overview

The analysis stream presented here is an extension of the methodology presented in the previous chapters, allowing for comparison of rs-fcMRI and task-evoked fMRI data from individual subjects on their own surfaces, as well as for group averages of subjects through surface-registration. For tasks where only group-level statistical maps are available, the average fiducial surface of the group is used to sample the cortical voxels of the group map.

Data acquisition

Images were acquired as in previous chapter for 3.0T Trio data with the exception of differences between the two groups of subjects listed below.

Saccade Localizer Subjects

rs-fcMRI and fMRI data were collected on a set of subjects (n = 11, 6F, age 21.8-26.8 years) who were instructed to either relax while fixating on a black cross against a white background (four runs) or to perform a saccadic eye-movement task (two runs) as described below (2.5s TR, 132 frames per run). Data were acquired for each subject on a 3.0T Siemens MAGNETOM Trio Scanner (Erlangen, Germany).

Extended Retrieval Subjects

rs-fcMRI and fMRI data were collected on a set of subjects (n = 21, 11F, age 21.3-28.8 years, including three subjects that overlap with the saccade localizer group) who were instructed to either relax while fixating on a white cross against a black background (three runs of 2.5s TR, 133 frames per run) or to perform an extended retrieval task (six runs of 2.0s TR, 212 frames per run) as described below. Data were acquired for each subject on a 3.0T Siemens MAGNETOM Trio Scanner (Erlangen, Germany).

Experimental Design

Saccade Localizer

Subjects completed two runs of a saccade task in which they were instructed to fixate on a small (<1 degree) black crosshair presented on a white background. Each 5.5

min run began with 35s of fixation, followed by five 30s blocks of saccades separated by 27.5 s of fixation. Within each block of saccades, the crosshair randomly shifted horizontally to +/- 3, 6, 9, or 12 degrees off-axis for 500 ms and then returned to the center for 500 ms (i.e., subjects made saccades at 2 Hz). Each run concluded with 35s of fixation. Visual stimuli were generated on an Apple iMac (Intel Core 2 Duo, OSX 10.4) with PsyScope X and projected onto a magnet-compatible rear-projection screen (CinePlex) positioned at the head of the magnet bore using a Boxlight CP730e digital multimedia projector (1024 x 768 pixels) via a mirror attached to the head coil (usable visual field = 24 degs wide x 14 degs high). The iMac used a PsyScope Button Box to detect when an MR scanner frame occurred and therefore synchronized stimulus presentation to the timing of the MR scanner.

Extended Retrieval

Stimuli

Subjects were shown pictures from a set of 200 grayscale images (Rossion and Pourtois, 2004) reformatted into a standard 284 x 284 pixel image with a white background (e.g., pictures in Figure 5.1). The images subtended, on average, 10.3 degrees of visual angle. Visual stimuli were generated as above for the saccade localizer task. Subject key press responses in the scanner were made using a fiber optic button pad connected to the computer via an interface unit (Current Designs, Inc; Philadelphia, PA).

Encoding Task (Study)

The experiment consisted of two unscanned runs in which the subjects were asked to make a living/non-living judgment on a randomly chosen set of 100 pictures. Stimuli appeared for 1.5s and were presented every 2.5s (Figure 5.1, Panel A). Subjects were not given explicit instructions that they would need to remember this material at any time in the future, but were simply told to decide if the object is living or non-living.

Retrieval Task (Test)

In the retrieval task, subjects were asked to determine if a presented picture was "old" or "new", depending on whether they had seen it during the encoding phase of the experiment (old) or had not (new). The presentation order of the pictures was counterbalanced across subjects.

At trial onset, pictures were covered by a black mask that partially dissolved at each successive 2s interval (i.e., revelation step) until pictures were completely revealed (Figure 5.1, Panel B). Participants were instructed to press a button when they could determine whether the item was old or new while the object was being unmasked. Neither speed nor accuracy were emphasized in the instruction, and participants were not specifically encouraged to respond prior to full revelation. After stimuli were unmasked, subjects were instructed that they could respond a second time, making the same response as they had done during unmasking or changing their response.

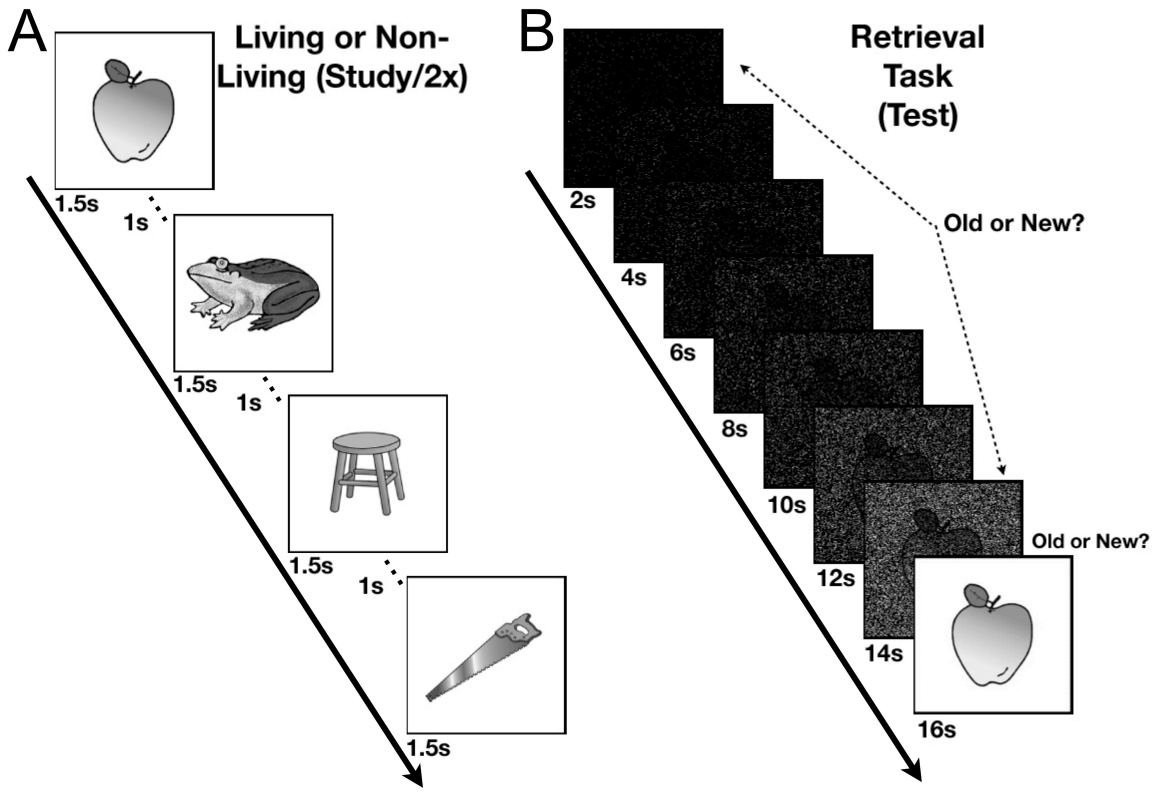

Figure 5.1: Extended retrieval behavioral paradigm

(A) The study phase consisted of 2 presentations of an item that subjects judged either living or non-living. Items were presented for 1.5s with an interval of 1s. (B) The test phase consisted of a retrieval task, during which, pictures were revealed gradually from a mask of noise at intervals of 2s. Subjects pressed a button when they felt they could decide whether they had seen the item during the living/non-living judgment ("old" item) or whether they had not ("new" item). When the picture was fully unmasked, subjects were asked to either confirm their initial response or change their initial response if after the unmasking they thought they had responded incorrectly. (Adapted from (Nelson et al., In Preparation))

Data preprocessing

Standard fMRI preprocessing

Imaging data from each subject were pre-processed as in previous chapters.

rs-fcMRI specific preprocessing

Pre-processing for functional connectivity analyses was carried out as in previous chapters.

Functional MRI data analysis using the general linear model

Pre-processed data were analyzed at the voxel level using a general linear model (GLM) approach (Friston et al., 1994; Miezin et al., 2000). Details of this procedure are described by Ollinger and colleagues (Ollinger et al., 2001). Briefly, the model treats the data at each timepoint (in each voxel) as the sum of all effects present at that timepoint. Effects can be produced by events in the model and by a residual term which represents the non-modeled signal, i.e., noise and unconstrained events. Estimates of the timecourse of effects were derived from the model for each response category by coding timepoints as a set of delta functions immediately following onset of the coded event (Ollinger et al., 2001). While saccades were modeled as blocks of activity, fifteen timepoints were modeled in the GLM for the extended retrieval events. Over each run, a trend term accounted for linear changes in signal, and a constant term was used to model the baseline signal. Effects are computed in terms of percent signal change, defined as signal magnitude divided by a constant term. This approach makes no assumptions about the specific shape of the BOLD response, but does assume that all events included in a

category are associated with the same BOLD response (Ollinger et al., 2001). Thus, we could extract timecourses without placing constraints on their shape. Image processing and analyses were carried out using in-house software written in IDL (Research Systems, Inc.).

Statistical map creation

For the extended retrieval task, group z-statistical maps were derived from the GLMs using voxelwise repeated measures ANOVA with time as a repeated factor (Winer et al., 1991). The ANOVA implementation produces a set of main effect and interactions images determined by the factors in the design (Schlaggar et al., 2002). The main effect of time image identifies voxels in which the temporal profile over the analyzed time period is not flat, i.e., no change in signal. Interaction by time images identify voxels in which activity differs across levels of factors as a function of time. Here, we computed a bin x time interaction image and a response x time interaction image. The bin x time image (4 levels of bin (subject responded during the 8s, 10s, 12s, or 14s bin) and 15 levels of time) represents voxels that showed significantly different activity depending on the reveal step, i.e., bin, in which the subject responded. The response x time image (2 levels of response, i.e., hit vs correct rejection, and 15 levels of time) represents voxels that showed significantly different activity depending on whether the item was correctly identified as being old (hit) or new (correct rejection).

For the saccade localizer task, individual z-statistical maps were derived from each subject's GLM by computing the average z-score of the main effect of saccade across the runs. The group saccade z-statistical map used here is the surface-registered

average of these within-subject saccade maps to potentially better locate saccade-related regions within this group.

Surface preprocessing

Cortical surface generation from anatomical MRI data using Freesurfer

Individual cortical surfaces were generated for each subject as in Chapter 3.

Surface-based registration to the PALS atlas using Caret

Registration of each subject to the PALS surface atlas was carried out as in Chapter 3.

Group-average fiducial surface generation for sampling volumetrically-averaged group statistical data

For the extended retrieval task, only group-level statistical maps are available, due to the low number of specific trial types within individuals. Therefore, to produce surface-based statistical maps that can be compared to the rs-fcMRI contour maps, the group-level volumetric statistical maps were sampled by generating a group-average fiducial surface to approximate the common cortical location for the group and extracting the values of the intersecting voxels. Thus, a group-average fiducial surface was created for the 21 extended retrieval subjects by averaging the 21 individual grey mid-thickness surfaces each volumetrically registered to the 711-2B atlas space. While not as accurate for directly sampling and analyzing any single individual, the generated surface can be appropriately used to sample the group's own statistical maps as it approximates the average fiducial surface location across the subjects.

Cortical seed and rs-fcMRI correlation map generation

A set of cortical seeds that covered a full hemisphere was created as in Chapter 3.

eta^2 matrix creation for each seed

eta^2 matrices for each rs-fcMRI seed location were then made for each subject, or group average, as in Chapter 3.

Analysis of contrast information in eta^2 matrices

Gradient map derivation

Gradient magnitude maps were computed from each eta^2 matrix as in Chapter 3.

Construction of cortical contour maps based on compiled contrast information

Direct averaging of contrast maps

For similar reasons to those stated in Chapter 4, gradient magnitude-based rs-fcMRI contour maps were used here and were computed as the average of the underlying gradient magnitude maps, as described in Chapter 3.

Results

Group-level functional activation maps from an extended retrieval task reveal regions of consistency with the group average rs-fcMRI contour map made from the same group of 21 subjects.

Chapter 4 demonstrated that individual rs-fcMRI contour maps are generally stable across multiple subjects. However, if rs-fcMRI contour maps represent the spatial organization of functional areas in each individual, task-evoked activations from the same

group of subjects should also be largely consistent with rs-fcMRI contour maps, i.e., peaks of activations should avoid strong putative functional boundaries and tend to align with putative functional areas. To perform an initial comparison, an average rs-fcMRI contour map was generated from the gradient magnitude-based rs-fcMRI contour maps of 21 subjects (Figure 5.2, Panel A) who were also scanned while performing an extended retrieval task. As mentioned previously, the amount of task-related data collected per subject only allowed for statistical testing of conditions at the group-level, and thus, group volumetric statistical images were intersected with the group's average fiducial surface to obtain surface-based statistical maps. This produced several main effect and effect x time statistical maps, two of which are shown here in Figure 5.2. A bin x time interaction map(identifying regions showing differential activity depending on when, i.e., in which 'bin', subjects responded to the task) is displayed in Panel B, while a response x time interaction map (indicating regions differentially involved when a presented item was correctly identified as previously studied or new) is shown in Panel C. Note that while there are a few regions that overlap between the two interaction maps, there are many regions that are statistically involved in one interaction and not the other. To demonstrate the general consistency between these two maps with the rs-fcMRI contour map, strong 'landmark' rs-fcMRI boundaries and putative areas are overlaid on this group's average rs-fcMRI contour map (Figure 5.2, Panel A), as in Chapter 4, and transferred onto the two statistical maps, shown in Figure 5.2, Panels B and C.

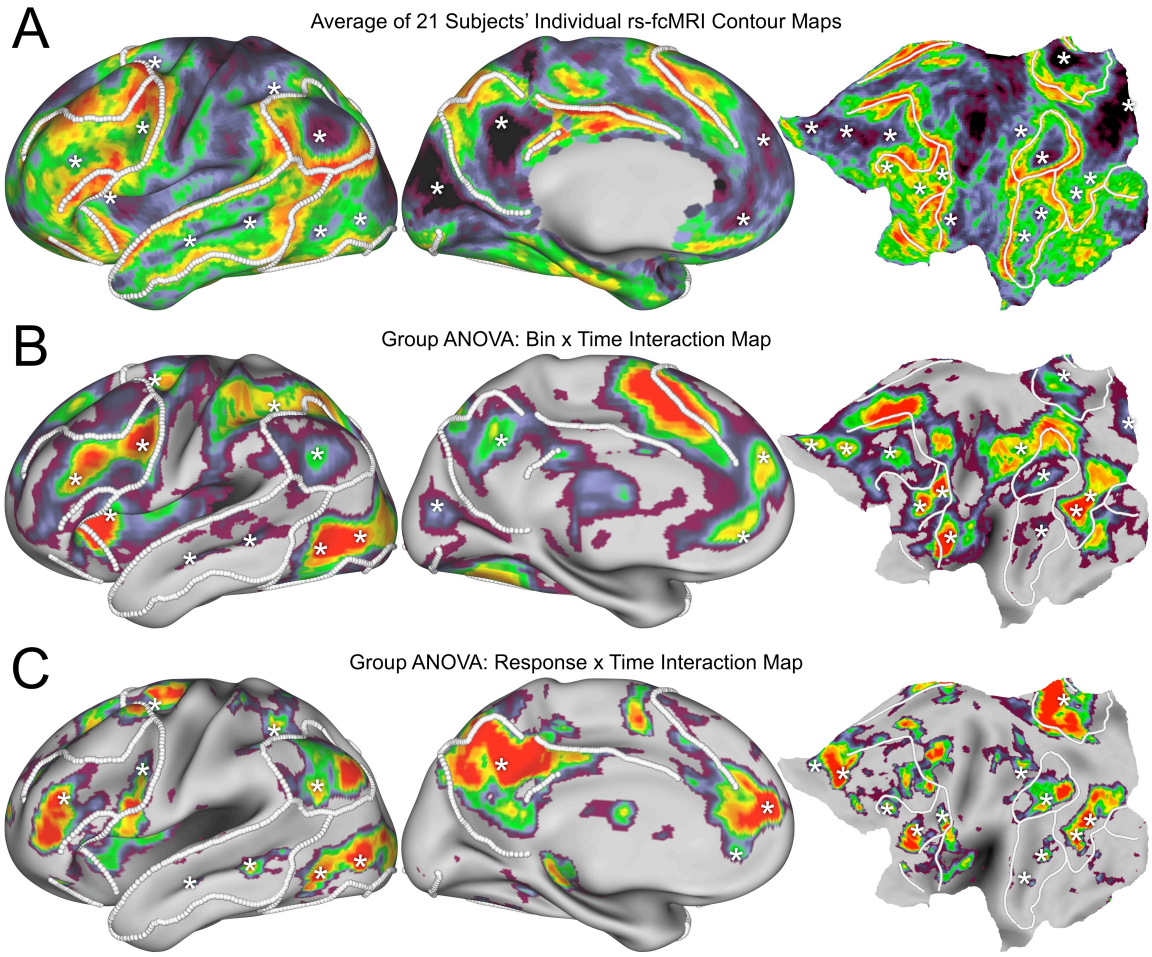

Figure 5.2: Comparison of rs-fcMRI contour maps with memory retrieval statistical maps within a group of 21 subjects

Shown in Panel A are lateral, medial, and flat views of the left hemisphere average gradient magnitude-based rs-fcMRI contour map for a group of 21 subjects who also performed an extended retrieval task, with solid white lines demarcating boundaries consistently seen across subjects and white stars denoting locations of consistent stability across subjects that later appear as significant locations in the statistical maps. Panel B contains surface representations of a group-level bin x time statistical image, i.e, what regions contain differential activity based on when subjects respond to the task, for the

group of 21 subjects performing an extended retrieval task. Panel C contains surface representations of a group-level response x time statistical image,i.e., what regions contain differential activity based on whether the presented item was correctly judged 'old' or 'new', for the group of 21 subjects performing an extended retrieval task. In Panel A, 'hot' colors represent stronger gradient values, while 'cool' colors represent weaker gradient values, while in Panel B, 'hot' colors represent regions containing activity that is statistically affected by the conditions tested. Statistical maps are thresholded above the level of statistical significance to localize peaks of activation/ deactivation. Displayed inflated surfaces are generated from the average fiducial surface of the group of 21 subjects.

Averaged within-subject functional activation maps from a saccade localizer task reveal regions of consistency with the averaged within-subject rs-fcMRI contour maps from the same group of 11 subjects.

As was done for the group of 21 subjects above, a group average gradient magnitude-based rs-fcMRI contour map was generated for a group of 11 subjects (Figure 5.3, Panel A), who were also scanned while performing a block-design saccade localizer task, powered to generate significant within-subject activation maps. Thus, within-subject surface-based statistical maps were created by intersecting each subject's own fiducial surface with his or her own volumetric saccade effect map. Since the subjects have undergone surface-registration to the PALS atlas, The resultant surface-based statistical maps can be registered together and averaged to produced a group average statistical map

across the surface, where the z-score at each point represents the average within-subject z-score, *not* the group-level statistic (Figure 5.3, Panel B). This parallels the group average rs-fcMRI contour map which represents the average within-subject gradients, *not* the gradients of group-averaged rs-fcMRI correlation maps. As was done in Figure 5.2, strong 'landmark' rs-fcMRI boundaries and putative areas were overlaid on this group's average rs-fcMRI contour map and transferred onto the group's average effect of saccade statistical map, shown in Figure 5.3, Panel B.

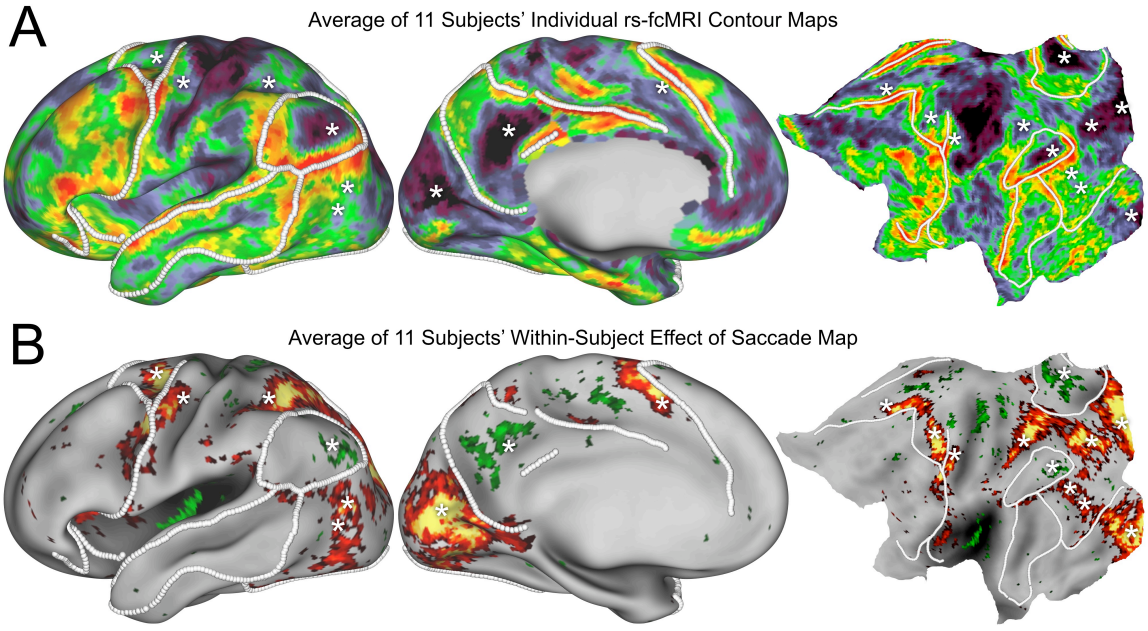

Figure 5.3: Comparison of rs-fcMRI contour maps with saccade-related statistical maps within a group of 11 subjects

Shown in Panel A are lateral, medial, and flat views of the left hemisphere average gradient magnitude-based rs-fcMRI contour map for a group of 11 subjects, with solid white lines demarcating boundaries consistently seen across subjects and white stars denoting locations of consistent stability across subjects. Panel B contains surface

representations of the average within-subject effect of saccade statistical image for the group of 11 subjects performing a saccade localizer task, with the consistent boundaries and putative areas from Panel A overlaid in white. In Panel A, 'hot' colors represent stronger gradient values, while 'cool' colors represent weaker gradient values, while in Panel B, 'hot' colors represent regions that are statistically more activated during the block of saccades, while 'cool' colors represent locations that are statistically more deactivated during the block of saccades. Statistical maps are thresholded above normal significance levels to localize peaks of activation/deactivation. Displayed inflated surfaces are generated from the average fiducial surface of the group of 11 subjects.

Single-subject functional activation maps from a saccade localizer task, while more variable, also largely respect the spatial boundaries seen within the same subject's rs-fcMRI contour map.

Saccade localizer task data was acquired for the individual subject used to illustrate rs-fcMRI contour map generation in Chapter 3. Here, we again show the average gradient magnitude-based rs-fcMRI contour map for this subject (Figure 5.4, Panel A), as well as this subject's own within-subject saccade activation map, converted to a surface representation from a volumetric statistical map as above for Figure 5.3. As was done in Figure 5.2 and Figure 5.3, strong 'landmark' rs-fcMRI boundaries and putative areas were generated from this subject's rs-fcMRI contour map and transferred onto his or her own saccade activation map, shown in Figure 5.4, Panel B.

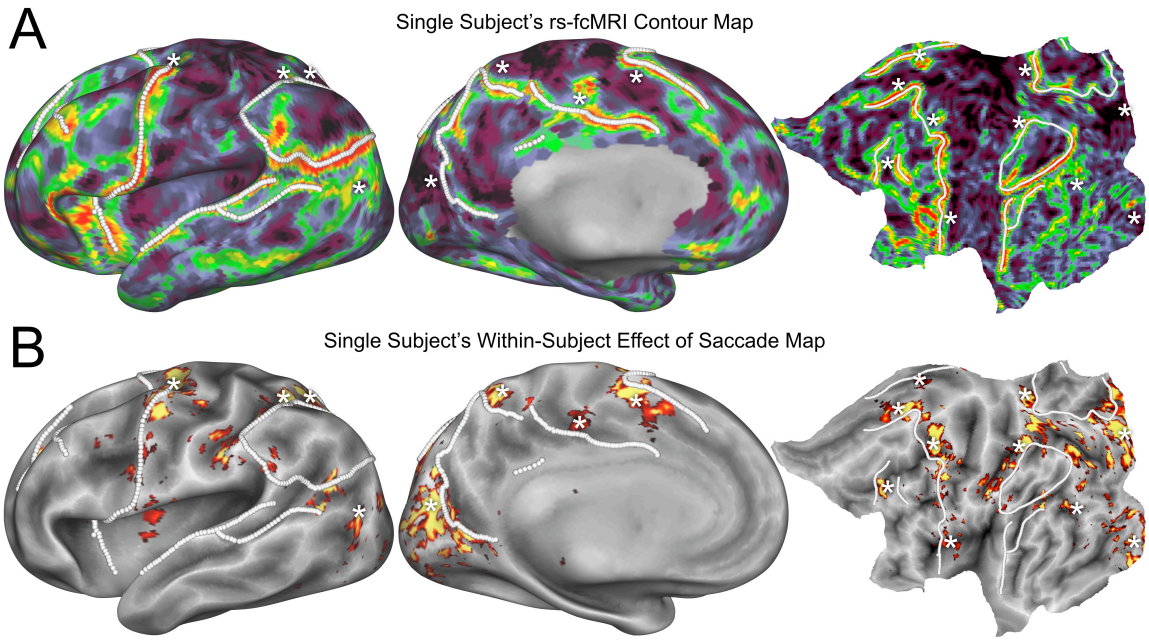

Figure 5.4: Comparison of a single subject's rs-fcMRI contour map with his or her own saccade-related activation map

Shown in Panel A are lateral, medial, and flat views of the left hemisphere of a gradient magnitude-based rs-fcMRI contour map for a single subject, with solid white lines demarcating strong rs-fcMRI boundaries. White stars denote locations of consistent stability in rs-fcMRI patterns that also appear as saccade-related regions in Panel B, which contains surface representations of a within-subject saccade activation map for this subject. In Panel A, 'hot' colors represent stronger gradient values, while 'cool' colors represent weaker gradient values, while in Panel B, 'hot' colors represent regions that are statistically activated during the blocks of saccades. Activation map is thresholded above normal significance levels to localize peaks of activation. Displayed inflated surfaces are generated from the fiducial surface of this subject.

Discussion

An initial validation of rs-fcMRI contour maps by comparison with task-related fMRI activity from the same cohort of subjects

rs-fcMRI contour maps are fairly consistent across time (Chapter 3) and across subjects (Chapter 4), with many consistently seen contours that appear to describe some known functional distinctions. Here we demonstrate that for two independent tasks in two separate groups, task-related fMRI and rs-fcMRI contour maps do in fact appear to align, with multiple instances of task-related functional distinctions respecting rs-fcMRI boundaries and aligning with putative area locations. While the specific analyses presented above are largely qualitative in nature, there does appear to be an above chance level of consistency for several of the task-related regions. This serves as a proof of principle that rs-fcMRI contour maps do, in fact, reflect the underlying spatial organization of functional areas. Statistical analyses were not shown here, since while multiple standard and novel quantitative approaches have been explored, most of which indicate greater than chance consistency, more rigorous development is still required to generate statistical tests that appropriately take into account the different character of these two datatypes.

Several issues have made finding the best strategy for direct statistical testing of this consistency quite difficult. For instance, while rs-fcMRI mapping produces contours covering the entire hemisphere, a specific task or contrast typically only differentially involves specific areas to significant levels, i.e., comparing ‘sparse’ statistical activations vs. ‘full’ cortical contour maps. Additionally, since the performance of specific tasks may

involve spatially adjacent functional areas, activation/deactivation patterns may be detected spanning rs-fcMRI putative boundaries, resulting from functional areas on either side of the boundary being involved, with a resultant 'peak' of activation found between the involved functional areas, instead of separately centered on each.

Using rs-fcMRI mapping to differentiate specific locations of functional involvement, potentially improving fMRI activation analyses

Within the results shown here are several demonstrations that some regions typically seen in task-related fMRI studies appear to also be reliably seen in rs-fcMRI contour maps generated from groups of subjects or even from single individuals. As one example, the region typically referred to as the "frontal eye fields" (FEF) in superior lateral frontal cortex (Berman et al., 1999; Corbetta et al., 1998), can be seen above in both Figures 5.3 and 5.4, i.e., group and individual rs-fcMRI contour maps (Figures 5.3 and 5.4, Panels A), and is verified here by the localization of saccade-related activity to the same location, again in both group and individual data (Figures 5.3 and 5.4, Panels B).

A parallel analysis has recently used rs-fcMRI mapping in combination with graph theoretic approaches to distinguish multiple regions in left lateral parietal cortex known to be involved in memory retrieval (Nelson et al., In Preparation). rs-fcMRI mapping-derived putative areas in left lateral parietal cortex were found to belong to several distinct long-range communities of regions across the brain, each of which carried distinct timecourses with significant memory-retrieval effects. Shown in Figure 5.5 is a visual summary of that body of work:

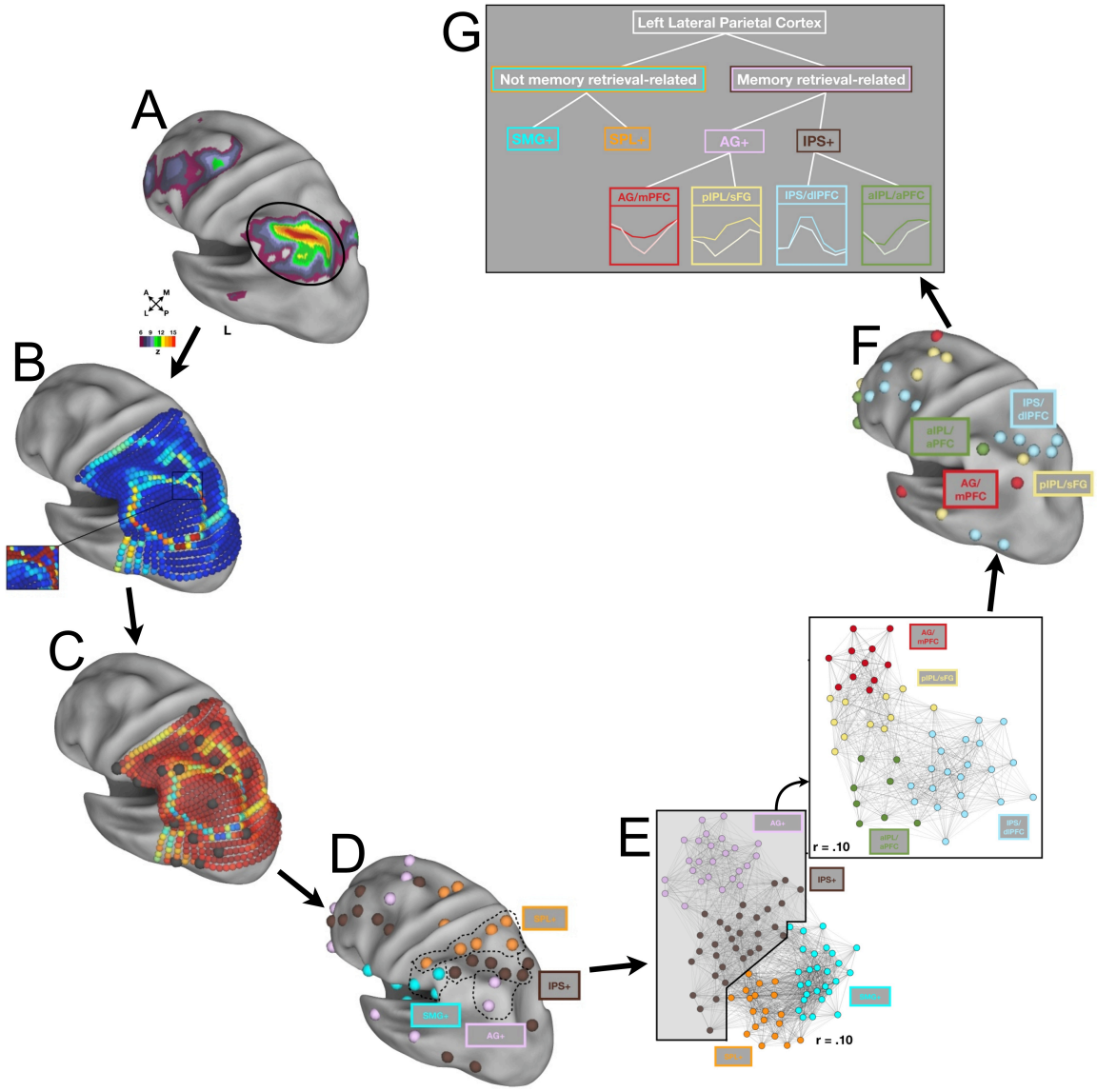

Figure 5.5: Delineation and characterization of memory retrieval-related regions in a 'patch' of left lateral parietal cortex using rs-fcMRI mapping and graph theoretic tools

(A) A fixed-effect statistical map from a meta-analysis of memory retrieval-related studies finds reliable involvement of left lateral parietal cortex (LLPC). (B) A 'patch' rs-fcMRI contour map was generated over LLPC to analyze this region. (Inset contains a boundary near posterior inferior parietal lobule (pIPL) more easily seen with different thresholds.) (C) Putative areas were generated and 10mm diameter ROIs created at each location,

shown as grey spheres on the inflated surface. (D) The 15 putative areas within LLPC were found to belong to distinct communities based on modularity optimization of the pair-wise correlations between these 15 putative areas and the regions, or 'neighbors' in graph theory terms, they most correlate with across the brain. Regions are color-coded by the communities' parietal lobe members, i.e., SMG+ (cyan), SPL+ (orange), IPS+ (brown), and AG+ (purple). Dotted lines are shown for the purposes of more easily visualizing the distinctions. (E) Shown is a graph layout of pair-wise correlations between the 15 detected putative areas in LLPC and their most correlated 'neighbors'. The placement of each node is determined by the relationships between nodes using a spring-embedding algorithm that takes into account both the presence and strength of inter-node connections (rs-fcMRI correlations). The graph is shown at a threshold (r = . 10) with all connections relaxed into a low energy state. Further modularity optimization of the IPS+ and AG+ communities (the two communities containing memory retrieval-related effects) finds that the AG+ community (purple, left) has separated further (yellow and red, right) as has the IPS+ community (brown, left; green and blue, right). (F) Memory retrieval-related putative areas in LLPC are parcellated into four components that show distinctions based on their distribution of functional connections, shown in (E), and timecourse profiles, summarized in (G), all of which show significant effects of retrieval success. (G) A summary of the detected communities of putative areas in LLPC, indicating the likely presence of at least six separate functional areas. (Adapted from (Nelson et al., In Preparation))

As mentioned in Chapter 4 and as used in the example study of Figure 5.5, these predicted functional area locations can be used to generate regions of interest are *not* dependent on any particular task-evoked fMRI activation, and thus the extracted functional timecourses can be analyzed for significance without bias (Poldrack and Mumford, 2009) as well as analyzed for increased statistical power and reduced variation across subjects as compared to the common volumetric centroid of activation.

Conclusion

The results described here demonstrate that rs-fcMRI contour maps do, in fact, appear to be consistent with task-related fMRI results for two separate tasks in two groups of subjects. Additionally, several described functional regions of interest can already be located using rs-fcMRI contour maps for groups as well as within individual subjects. These results provide a proof-of-concept for using resting state data to not only describe the putative functional distribution of functional areas and the boundaries between them, but also to improve task-related studies through the independent delineation of regions that can be compared across subjects, across groups, and across studies without relying on specific coordinate-based or anatomically-defined labels.

CHAPTER 6: DISCUSSION AND FUTURE DIRECTIONS FOR RS-FCMRI MAPPING

Using rs-fcMRI mapping to study the structure and function of the human brain

The past century has seen significant advancement in our understanding of cognition and behavior and the ascription of function to neural structures at multiple levels of organization. Indeed, the ability to use PET and fMRI, among other techniques, to study function non-invasively in humans in the past few decades has allowed much of this work to be performed on a broad scale in humans. This has supported the investigation into the normal function, developmental profiles, recovery after injury, and modification or loss due to disease of specific cognitive processes supported by the nervous system.

The present work represents a step towards rapid and non-invasive functional area mapping in humans.

The body of work presented here adds to the current abilities of neuroimaging by facilitating the rapid consideration of the spatial dynamics in rs-fcMRI, i.e., correlated and continuous low-frequency spontaneous activity seen in the BOLD signal. To summarize:

Chapter 1 outlined the current understanding of the organization of the nervous system relative to the importance of studying functional areas, and the current limits in defining functional areas non-invasively in humans. Chapter 1 also introduced rs-fcMRI as a potential tool that may allow for rapid, non-invasive, and broadly applicable functional area localization on an individual basis.

Chapter 2 demonstrated that rs-fcMRI correlation patterns can change rapidly over short spatial distances across the cortex, that these rapid transitions can be identified quantitatively, and that these transitions appear to form continuous contours across the cortical surface of an appropriate shape and size to be putative functional area boundaries.

Chapter 3 extended these observations into a method for the rapid generation of full hemispheric rs-fcMRI contour maps. Chapter 3 also demonstrated that these rs-fcMRI contour maps can be used to generate volumetric regions of interest that represent putative functional areas, that these maps and putative areas are stable over time within individual subjects, and that rs-fcMRI mapping can produce significant information about the strength of rs-fcMRI putative 'boundaries', corresponding to how similar or different neighboring putative areas' correlation maps are to one another.

Chapter 4 illustrated an initial comparison of rs-fcMRI contour maps across subjects, finding that many of the strongest features are similar across subjects, independent groups, and acquisition.

Chapter 5 demonstrated a preliminary validation of rs-fcMRI mapping via comparison with task-related fMRI data acquired from the same subjects, indicating that task-related activity does appear to respect putative areas and boundaries seen in rs-fcMRI contour maps.

Yet substantial work remains.

The current work demonstrates the potential utility of rs-fcMRI mapping techniques as a practicable approach to non-invasive functional mapping, while recent

parallel work has provided an example of using rs-fcMRI mapping to gain insight into the spatial organization of functional signals (Nelson et al., In Preparation). However, there is still much to be done in refining, extending, and validating the methods described here, as well as actual utilization and application of rs-fcMRI mapping to multiple lines of research.

Logical progressions for rs-fcMRI mapping

During the investigation into and development of rs-fcMRI mapping as described in this thesis, multiple logical 'next-step' projects have presented themselves, organized into three broad themes: (1) The refinement of the currently described rs-fcMRI mapping techniques and extension to sub-cortical structures, (2) the comparison of rs-fcMRI mapping with other available mapping techniques, both at a group level and on an individual basis, and (3) the application of rs-fcMRI mapping to gain traction for several specific questions in neuroscience.

Refinement and extension of current rs-fcMRI mapping techniques

Separating adjacent topographically-organized functional areas from one another

During the development of the presented rs-fcMRI mapping methods, it was observed that strong gradients were not frequently detected at predicted locations of boundaries between topographically organized functional areas, specifically, between V1-V2, V2-V3, or between S1 and M1. Since the borders between these topographic regions do not represent a stark difference in activation histories, this likely represents a fundamental limitation of rs-fcMRI mapping based purely on gradient calculation. One

possible adaptation to rs-fcMRI mapping that may allow the delineation of this category of boundaries may be to use the underlying rs-fcMRI correlation maps in a fashion more closely similar to task-related fMRI phase-encoded topographic mapping (Warnking et al., 2002), i.e., specifically looking for repeating peaks and troughs of correlation across the surface of the occipital lobe, as opposed to looking for abrupt transitions as was done here.

Refining the underlying methodology of rs-fcMRI mapping to reduce distortion and increase accuracy of generated maps

Currently, generating a grid that covers a significant portion of the cortex requires using a half-flattened spherical representation, or a 'cut' flattened representation. While both of these surfaces are made with as minimal distortion as possible, generating equally spaced grids using either surface will distort the distance relationships between nodes on the fiducial surface. Thus, there may be some advantage to adapting rs-fcMRI mapping to operate on arbitrary closed topologies, i.e., generating grids that are equally spaced on the fiducial surface yet still easily parameterized. Recent work describing cortical parameterization without cutting may soon become applicable to the methods described here (Clouchoux et al., 2009). This would potentially reduce distortion as well as remove some difficulty in obtaining reliable results around the 'cuts' of a flat representation.

As demonstrated in Chapter 3, using patches with restricted spatial extent across the cortex reveals additional fine-grain detail. This observation could potentially be generalized into a full hemispheric mapping procedure to improve the sensitivity of rs-

fcMRI contour maps, i.e., combining the results from multiple overlapping patches into a larger extensive contour map with a higher level of detail.

Combining rs-fcMRI mapping, based on gradient calculations, with a parallel method that reflects the observed peaks of rs-fcMRI correlation maps

Given that each functional area is likely to correlate with multiple other functional areas, the 'peaks' of correlation in each rs-fcMRI correlation map may represent the centers of distant, but related, functional areas. Thus, an alternative analysis procedure has been developed which uses the same set of underlying cortical seeds and rs-fcMRI correlation maps as used here for rs-fcMRI contour mapping, to instead obtain the set of commonly seen 'peaks' of correlation across the set of correlation maps. These rs-fcMRI peak maps may provide an approach for interval validation of the rs-fcMRI contour mapping described here.

Performing rs-fcMRI mapping in non-cortical, i.e., volumetrically-organized structures

Obtaining gradient information across the cortical surface allows for rapid calculation and delineation across a large portion of the potential full collection of functional areas in the brain. However, there are a significant number of brain structures that are *not* organized as folded sheets and require the extension of these methods into 3D. In particular, the thalamus and basal ganglia are both known to contain multiple functionally distinct entities, and while some of these distinctions can be made using anatomical data, additional insight can be found using rs-fcMRI mapping, as has recently been done for the thalamus (Zhang et al., 2009b). Preliminary studies towards this end

using the presently described methods are already underway with promising results (Barnes et al., 2009).

Using left and right hemispheric rs-fcMRI contour maps within subject to generate laterality metrics for putative functional areas

It has been repeatedly observed since the first uses of rs-fcMRI (Biswal et al., 1995) that the strongest correlations seen in any given rs-fcMRI correlation map are often the homotopic region to the seed in the contralateral hemisphere. Calculating the strength of correlations between each location of a left hemispheric grid (~10,000 seeds) and the set of putative homotopic locations in the right hemisphere, found by reflecting the stereotactic coordinates along the x-axis, has preliminarily found several interesting patterns. This indicates a potential use of rs-fcMRI to measure the degree of functional laterality of putative areas across the cortex. Some parallel work has performed examining this phenomenon using anatomically-defined volumetric regions of interest and group data (Stark et al., 2008). Due to the known folding differences between the left and right hemispheres and the variation across individuals, however, correctly analyzing this data will require using appropriately registered cortical surfaces from both sides and obtaining putative area locations, followed by calculation and analysis of the contralateral correlations on an individual basis.

Generating metrics to determine the reliability/confidence of delineated putative areas

While chapters 4 and 5 addressed the overall consistency of rs-fcMRI contour maps both across subjects and with task-related fMRI data, the generalized creation of putative areas from Canny-based rs-fcMRI contour maps and the subsequent parallel

comparisons are a logical progression of the presented results. A current difficulty in proceeding to this next analysis is a lack of an internal metric of the confidence or reliability of derived putative areas based on single sessions of data. As shown in Chapter 3, reliability across multiple sessions of resting state data can be used to isolate stable putative area locations, however this is often not available. Further work is needed to generate metrics that can be used to accept or reject delineated putative areas.

Rapidly identifying putative areas within and across subjects, likely based on rs-fcMRI correlation map 'signatures'

Related to the generation of confidence metrics for each putative area, an automated or interactive procedure for 'labeling' a set of putative areas within single individuals, with previously observed patterns in other subjects and/or group-level data, will greatly ease the interpretation of generated results. It is this ability that will allow for significantly less ambiguous labeling and comparison of functionally-involved regions generated from a study's individual subjects or from new group data. Several putative areas can already be tentatively labeled by eye due to their relative positions to anatomical and rs-fcMRI landmarks (see Chapter 4, Discussion), however, a more structured approach will likely reveal a larger set of reliably identifiable putative areas.

Additionally, since the generation of rs-fcMRI putative areas/regions of interest are *not* dependent on any particular task-evoked fMRI activation, extracted functional timecourses for performed tasks can be analyzed for significance without biasing the analysis by the necessity of creating regions from statistical maps (Poldrack and Mumford, 2009; Vul and Pashler, 2008).

Great clinical utility would also arise from the rapid delineation of functional areas across the cortex, in both pre-surgical planning and epilepsy treatment, among others. Some recent work has been performed using rs-fcMRI towards this end, but requires a great deal of technical intervention and is currently limited to regions with very stereotyped location and rs-fcMRI correlation pattern, e.g., primary motor cortex (Zhang et al., 2009a).

Comparison of rs-fcMRI mapping with other available mapping techniques

Comparing rs-fcMRI mapping to electrophysiology, connectional tracing, and histological patterns in non-human primates

The ability to obtain and analyze comparable rs-fcMRI data in non-human primates (Vincent et al., 2007) presents the opportunity to compare patterns seen using rs-fcMRI mapping with spatial delineation detected using electrophysiological recordings, connectional tracer injections, and histological measures of changes in cell type and distributions between functional areas. While not explicated here, adapting the present methods to be compatible with non-human primate data does not present any conceptual or prohibitive technical challenges.

Comparing rs-fcMRI mapping to atlases of architectonic, connectional, and lesion data in humans

While architectonic data is typically not available for normal subjects, there are ongoing efforts (Kurth et al., 2009; Schleicher et al., 2009; Zilles and Amunts, 2009) to import high-resolution architectonic data from multiple subjects into neuroimaging

stereotactic space, generating a population-based architectonic atlas with greater generalizability than the current Talairach and Tournoux stereotactic appellations (Talairach and Tournoux, 1988). Additionally, datasets of lesion data with associated deficits and population-based measures of connectivity are obvious candidates for comparison with rs-fcMRI mapping results (Agosta et al., 2009; Bates et al., 2003; Borovsky et al., 2007; Dronkers et al., 2007; Turken et al., 2008).

Comparing rs-fcMRI mapping to within-subject anatomical information, e.g., cortical thickness and diffusion imaging metrics

Of particular interest for cross-modal validation is the possibility that comparisons between rs-fcMRI mapping and diffusion imaging-based mapping are rapidly becoming feasible (Skudlarski et al., 2008). These two imaging techniques, can also be compared with surface-registered anatomical measures such as cortical thickness or grey matter volume (Winkler et al., 2009) potentially allowing for increased understanding of the relationship between anatomical structure, connectional patterns, and functional involvement of functional areas across the cortex.

Applications of rs-fcMRI mapping

While there are likely more potential uses of rs-fcMRI mapping than can be described here, several specific applications seem particularly apropos, including the generation of large-scale networks of putative areas, the functional registration of data across subjects, and the dual analyses of examining differences across subjects, and across temporally dynamic processes.

Analyzing large-scale cortical networks of functional areas within individual subjects

As has been done to great advantage with selected functionally-defined or anatomically-defined regions of interest (Dosenbach et al., 2007; Fair et al., 2008; Hagmann et al., 2008), constructing large-scale networks based on the pair-wise correlations between putative areas, both at the group-level and on an individual basis presents a tremendous opportunity for understanding the organization of the brain's interconnected functional networks, i.e, the level *above* 'maps' in the original Churchland and Sejnowski diagram (Chapter 1, Figure 1.1, (Sejnowski et al., 1988)). Since both putative area definition with rs-fcMRI mapping and pair-wise connection computation are both done with rs-fcMRI data, this would allow for dataset-tailored nodes to be used for analysis, lessoning registration and cohort concerns as well as removing the need for task-related localization, and should additionally provide a larger number of nodes than would be available from task-related data (Petersen et al., 2009). As an added benefit, the generation of large-scale networks would also assist in the identification of putative functional areas across individuals and datasets through putative area membership in recognizable communities and patterns of connections with the rest of the network.

Functional registration using rs-fcMRI mapping

Strong and consistently detected rs-fcMRI boundaries may provide a tractable extension to volumetric and surface-based registration techniques: first aligning each subject's brain into a target stereotactic space, then aligning cortical surfaces based on anatomically stable landmarks, and finally using rs-fcMRI mapping results to align the data with further deformations. A 'functional' registration could be performed by either

trying to align the full rs-fcMRI contour map, as has been done with extended functional timecourses (Sabuncu et al., 2010), or by trying to align strong resilient 'landmark' boundaries as described above, mirroring what is done with surface anatomical landmarks in PALS atlas registration (Van Essen, 2005). While these two alternatives each have potential trade-offs (Pantazis et al., 2009), either could be performed prior to defining putative functional areas, as they use the rs-fcMRI contour maps themselves. Alternatively, putative areas could first be delineated across each individual's surface, as in Chapter 3, with registration occurring at a later step in a region to region fashion without surface deformation.

An additional method has been explored that starts with either a set of putative areas based on rs-fcMRI mapping of group data or a set of task-related regions of interest for a group, creates group volumetrically-averaged 'fingerprint' rs-fcMRI correlation maps for each putative areas or region, then looks for the locations *across each individual's own surface* that have correlation maps most similar to the group's putative areas' correlation maps. This generates a set of unique coordinates for each subject for each putative area. This is akin to the cross-day alignment technique demonstrated in Chapter 3 for one subject, but uses group-defined putative areas, or even task-related regions as a starting point.

Studying individual differences using rs-fcMRI mapping

Given that there is some variability across subjects in both their rs-fcMRI contour maps, and thus also in their putative areas beyond that induced by differential folding patterns, exploring the individual differences in putative area/contour map patterns poses

an interesting question in it's own right. Additionally, determining the correlates, both biological and behavioral, with putative area size, shape, and distribution will likely entail a full research effort of it's own. Separately, obtaining individually-defined large-scale networks also provides the opportunity for finding correlates with network-level metrics, putative area memberships, and differences in network relationships between subjects.

Studying developmental, treatment/recovery, and other temporally dynamic phenomenon using rs-fcMRI mapping

The currently presented results are all obtained from a young typical adult population. Of tremendous scientific interest is the specialization of functional areas across normal and altered development (Church et al., 2008b; Fair et al., 2009) and the elaboration and evolution of large-scale cortical networks across the normal life-span (Andrews-Hanna et al., 2007; Gong et al., 2009). Since rs-fcMRI data can be easily acquired on a wide-range of ages, rs-fcMRI mapping is aptly suited for assisting the study of functional area differentiation from surrounding cortex, the reconfiguration of networks of defined putative areas (Fair et al., 2009), and potentially the evolution of the large-scale 'domains' seen in rs-fcMRI contour maps (Chapter 4, Discussion).

In addition to studying the effects of normal development and aging, there is also the opportunity to enhance the study of interventions likely to affect cortical network composition or configuration by acquiring resting state data prior and/or subsequent to surgical procedures, medical treatments, behavior modifications, or simply training paradigms. Assessment of recovery from injuries such as strokes and other traumatic

brain injuries may also be tractable using measures of changes seen in rs-fcMRI mapping or within large-scale networks and compared to models of network recovery dynamics (Alstott et al., 2009; Honey and Sporns, 2008). Some recent work has been performed examining specific diffusion parameters post-injury with correlations to behavioral performance (MacDonald et al., 2008; Perlbarg et al., 2009; Sidaros et al., 2008), potential gains may be possible through combination with the methods described here.

Conclusions

The body of work presented here has shown that resting state functional connectivity MRI can be used to quickly and non-invasively generate maps across individual human cortical surfaces that are reliable, consistent, and appear to align with many known functional distinctions, yet are based solely on resting state data. It is our hope that these methods will assist the investigation of the spatial organization of functional areas as well as the more appropriate ascription of processing to functional areas in general.

BIBLIOGRAPHY

Achard, S., Salvador, R., Whitcher, B., Suckling, J., and Bullmore, E. (2006). A resilient, low-frequency, small-world human brain functional network with highly connected association cortical hubs. J Neurosci *26*, 63-72.

Agosta, F., Henry, R.G., Migliaccio, R., Neuhaus, J., Miller, B.L., Dronkers, N.F., Brambati, S.M., Filippi, M., Ogar, J.M., Wilson, S.M., and Gorno-Tempini, M.L. (2009). Language networks in semantic dementia. Brain.

Aguilera, C.A.V. (2005). EXTREMA2: Extrema point detection from a surface. A MATLAB file. [WWW document]. http://www.mathworks.com/matlabcentral/fileexchange/loadFile.do?objectId=12275

Allman, J.M., Newsome, W.T., Baker, J.F., and Petersen, S.E. (1981). Visual topography and function: the cortical visual areas of the owl monkey. In Multiple Cortical Somatic, Sensory-motor, Visual and Auditory Areas and their Connectivities, C. Woolsey, ed. (Humana Press), pp. 171-185.

Alstott, J., Breakspear, M., Hagmann, P., Cammoun, L., and Sporns, O. (2009). Modeling the impact of lesions in the human brain. PLoS Comput Biol *5*, e1000408.

Amunts, K., Malikovic, A., Mohlberg, H., Schormann, T., and Zilles, K. (2000). Brodmann's areas 17 and 18 brought into stereotaxic space-where and how variable? Neuroimage *11*, 66-84.

Amunts, K., Schleicher, A., Burgel, U., Mohlberg, H., Uylings, H.B., and Zilles, K. (1999). Broca's region revisited: cytoarchitecture and intersubject variability. J Comp Neurol *412*, 319-341.

Amunts, K., and Zilles, K. (2001). Advances in cytoarchitectonic mapping of the human cerebral cortex. Neuroimaging Clin N Am *11*, 151-169, vii.

Andrews, T.J., Halpern, S.D., and Purves, D. (1997). Correlated size variations in human visual cortex, lateral geniculate nucleus, and optic tract. J Neurosci *17*, 2859-2868.

Andrews-Hanna, J.R., Snyder, A.Z., Vincent, J.L., Lustig, C., Head, D., Raichle, M.E., and Buckner, R.L. (2007). Disruption of large-scale brain systems in advanced aging. Neuron *56*, 924-935.

Barnes, K.A., Cohen, A.L., Power, J.D., Nelson, S.M., Miezin, F.M., Petersen, S.E., and Schlaggar, B.L. (2009). Identifying functional distinctions in individuals' basal ganglia using resting state functional connectivity MRI. In Society for Neuroscience (Chicago, IL).

Bates, E., Wilson, S.M., Saygin, A.P., Dick, F., Sereno, M.I., Knight, R.T., and Dronkers, N.F. (2003). Voxel-based lesion-symptom mapping. Nat Neurosci *6*, 448-450.

Beckmann, C.F., DeLuca, M., Devlin, J.T., and Smith, S.M. (2005). Investigations into resting-state connectivity using independent component analysis. Philos Trans R Soc Lond B Biol Sci *360*, 1001-1013.

Beckmann, M., Johansen-Berg, H., and Rushworth, M.F.S. (2009). Connectivity-based parcellation of human cingulate cortex and its relation to functional specialization. J Neurosci *29*, 1175-1190.

Behrens, T.E., Jenkinson, M., Robson, M.D., Smith, S.M., and Johansen-Berg, H. (2006). A consistent relationship between local white matter architecture and functional specialisation in medial frontal cortex. Neuroimage *30*, 220-227.

Berman, R.A., Colby, C.L., Genovese, C.R., Voyvodic, J.T., Luna, B., Thulborn, K.R., and Sweeney, J.A. (1999). Cortical networks subserving pursuit and saccadic eye movements in humans: an FMRI study. Human brain mapping *8*, 209-225.

Biswal, B., Yetkin, F.Z., Haughton, V.M., and Hyde, J.S. (1995). Functional connectivity in the motor cortex of resting human brain using echo-planar MRI. Magn Reson Med *34*, 537-541.

Bohland, J.W., Bokil, H., Allen, C.B., and Mitra, P.P. (2009). The brain atlas concordance problem: quantitative comparison of anatomical parcellations. PLoS ONE *4*, e7200.

Bokde, A.L., Lopez-Bayo, P., Meindl, T., Pechler, S., Born, C., Faltraco, F., Teipel, S.J., Moller, H.J., and Hampel, H. (2006). Functional connectivity of the fusiform gyrus during a face-matching task in subjects with mild cognitive impairment. Brain *129*, 1113-1124.

Borovsky, A., Saygin, A.P., Bates, E., and Dronkers, N. (2007). Lesion correlates of conversational speech production deficits. Neuropsychologia *45*, 2525-2533.

Broca, P. (1861). Nouvelle observation d'aphémie produite par une lésion de la troisième circonvolution frontale. Bulletins de la Société d'anatomie (Paris) *2e serie*, 398-407.

Brodmann, K. (1909). Vergleichende lokalisationslehre der grosshirnrinde in ihren prinzipien dargestellt auf grund des zellenbaues (Leipzig: J. A. Barth).

Brugge, J.F., and Reale, R.A. (1985). Auditory cortex. In Cerebral Cortex. Volume 4. Association and Auditory Cortices, A. Peters, and E.G. Jones, eds. (New York: Plenum Press).

Buckner, R.L., Head, D., Parker, J., Fotenos, A.F., Marcus, D., Morris, J.C., and Snyder, A.Z. (2004). A unified approach for morphometric and functional data analysis in young, old, and demented adults using automated atlas-based head size normalization: reliability and validation against manual measurement of total intracranial volume. Neuroimage *23*, 724-738.

Buckner, R.L., and Vincent, J.L. (2007). Unrest at rest: Default activity and spontaneous network correlations. Neuroimage *37*, 1091-1096.

Bullmore, E., and Sporns, O. (2009). Complex brain networks: graph theoretical analysis of structural and functional systems. Nat Rev Neurosci.

Burgund, E.D., Kang, H.C., Kelly, J.E., Buckner, R.L., Snyder, A.Z., Petersen, S.E., and Schlaggar, B.L. (2002). The feasibility of a common stereotactic space for children and adults in fMRI studies of development. Neuroimage *17*, 184-200.

Bush, G., Luu, P., and Posner, M.I. (2000). Cognitive and emotional influences in anterior cingulate cortex. Trends Cogn Sci *4*, 215-222.

Calhoun, V.D., Adali, T., Stevens, M.C., Kiehl, K.A., and Pekar, J.J. (2005). Semi-blind ICA of fMRI: A method for utilizing hypothesis-derived time courses in a spatial ICA analysis. Neuroimage *25*, 527-538.

Calhoun, V.D., Kiehl, K.A., and Pearlson, G.D. (2008). Modulation of temporally coherent brain networks estimated using ICA at rest and during cognitive tasks. Human brain mapping *29*, 828-838.

Canny, J. (1986). A computational approach to edge detection. IEEE Transactions on Pattern Analysis and Machine Intelligence *PAMI-8*, 679-698.

Carmichael, S.T., and Price, J.L. (1994). Architectonic subdivision of the orbital and medial prefrontal cortex in the macaque monkey. Journal of Comparative Neurology *346*, 366-402.

Castellanos, F.X., Margulies, D.S., Kelly, A.M.C., Uddin, L.Q., Ghaffari, M., Kirsch, A., Shaw, D., Shehzad, Z., Di Martino, A., Biswal, B.*, et al.* (2008). Cingulate-precuneus interactions: A new locus of dysfunction in adult attention-deficit/ hyperactivity disorder. Biological Psychiatry *63*, 332-337.

Church, J.A., Coalson, R.S., Lugar, H.M., Petersen, S.E., and Schlaggar, B.L. (2008a). A developmental fMRI study of reading and repetition reveals changes in phonological and visual mechanisms over age. Cerebral Cortex *18*, 2054-2065.

Church, J.A., Fair, D.A., Dosenbach, N.U., Cohen, A.L., Miezin, F.M., Petersen, S.E., and Schlaggar, B.L. (2008b). Control networks in paediatric Tourette syndrome show immature and anomalous patterns of functional connectivity. Brain.

Church, J.A., Petersen, S.E., and Schlaggar, B.L. (submitted). Issues in developmental neuroimaging. Human Brain Mapping.

Churchland, P.S., and Sejnowski, T.J. (1991). Perspectives on cognitive neuroscience. In Perspectives on cognitive neuroscience, R.G. Lister, and H.J. Weingartner, eds. (Oxford: Oxford University Press).

Clark, S.A., Allard, T., Jenkins, W.M., and Merzenich, M.M. (1988). Receptive fields in the body-surface map in adult cortex defined by temporally correlated inputs. Nature *332*, 444-445.

Clouchoux, C., Rivière, D., Mangin, J.-F., Operto, G., Régis, J., and Coulon, O. (2009). Model-driven parameterization of the cortical surface for localization and inter-subject matching. Neuroimage.

Cohen, A.L., Fair, D.A., Dosenbach, N.U., Miezin, F.M., Dierker, D., Van Essen, D.C., Schlaggar, B.L., and Petersen, S.E. (2008). Defining functional areas in individual human brains using resting functional connectivity MRI. NeuroImage *41*, 45-57.

Connor, C.E., Gallant, J.L., and Van Essen, D.C. (1994). Representation of stimulus position relative to attented objects in Macaque Area V4. Society for Neuroscience Abstracts *20*, 1054.

Corbetta, M., Akbudak, E., Conturo, T.E., Snyder, A.Z., Ollinger, J.M., Drury, H.A., Linenweber, M.R., Petersen, S.E., Raichle, M.E., Van Essen, D.C., and Shulman, G.L. (1998). A common network of functional areas for attention and eye movements. Neuron *21*, 761-773.

Cordes, D., Haughton, V., Carew, J.D., Arfanakis, K., and Maravilla, K. (2002). Hierarchical clustering to measure connectivity in fMRI resting-state data. Magn Reson Imaging *20*, 305-317.

Craig, A.D.B. (2009). How do you feel--now? The anterior insula and human awareness. Nat Rev Neurosci *10*, 59-70.

Critchley, H.D., Mathias, C.J., Josephs, O., O'Doherty, J., Zanini, S., Dewar, B.-K., Cipolotti, L., Shallice, T., and Dolan, R.J. (2003). Human cingulate cortex and autonomic control: converging neuroimaging and clinical evidence. Brain *126*, 2139-2152.

Croxson, P.L., Johansen-Berg, H., Behrens, T.E., Robson, M.D., Pinsk, M.A., Gross, C.G., Richter, W., Richter, M.C., Kastner, S., and Rushworth, M.F. (2005). Quantitative investigation of connections of the prefrontal cortex in the human and macaque using probabilistic diffusion tractography. J Neurosci *25*, 8854-8866.

Dale, A.M., Fischl, B., and Sereno, M.I. (1999). Cortical surface-based analysis. I. Segmentation and surface reconstruction. Neuroimage *9*, 179-194.

Dale, A.M., and Sereno, M.I. (1993). Improved localization of cortical activity by combining EEG and MEG with cortical surface reconstruction: A linear approach. Journal of Cognitive Neuroscience *5*, 162-176.

Damoiseaux, J.S., Rombouts, S.A., Barkhof, F., Scheltens, P., Stam, C.J., Smith, S.M., and Beckmann, C.F. (2006). Consistent resting-state networks across healthy subjects. Proc Natl Acad Sci U S A *103*, 13848-13853.

Devlin, J.T., and Poldrack, R.A. (2007). In praise of tedious anatomy. Neuroimage *37*, 1033-1041; discussion 1050-1038.

DeYoe, E., Carman, G., Bandettini, Glickman, S., Wieser, J., Cox, R., Miller, D., and Neitz, J. (1996). Mapping striate and extrastriate visual areas in human cerebral cortex. Proceedings of the National Academy of Sciences of the United States of America *93*, 2382-2386.

DeYoe, E.A., Neitz, J., Carman, G., MIller, D., Schmit, P., Glickman, S., and Weiser, J. (1995). Topographic mapping of striate and extrastriate visual areas in human cerebral cortex using an active visual task. Human Brain Mapping *1*, 27.

Dosenbach, N.U., Fair, D.A., Miezin, F.M., Cohen, A.L., Wenger, K.K., Dosenbach, R.A.T., Fox, M.D., Snyder, A.Z., Vincent, J.L., Raichle, M.E.*, et al.* (2007). Distinct brain networks for adaptive and stable task control in humans. Proc Natl Acad Sci U S A *104*, 11073-11078.

Dosenbach, N.U., Visscher, K.M., Palmer, E.D., Miezin, F.M., Wenger, K.K., Kang, H.C., Burgund, E.D., Grimes, A.L., Schlaggar, B.L., and Petersen, S.E. (2006). A core system for the implementation of task sets. Neuron *50*, 799-812.

Drevets, W.C., Burton, H., Videen, T.O., Snyder, A.Z., Simpson, J.R.J., and Raichle, M.E. (1995). Blood flow changes in human somatosensory cortex during anticipated stimulation. Nature *373*, 249-252.

Drobyshevsky, A., Baumann, S.B., and Schneider, W. (2006). A rapid fMRI task battery for mapping of visual, motor, cognitive, and emotional function. Neuroimage *31*, 732-744.

Dronkers, N.F., Plaisant, O., Iba-Zizen, M.T., and Cabanis, E.A. (2007). Paul Broca's historic cases: high resolution MR imaging of the brains of Leborgne and Lelong. Brain *130*, 1432-1441.

Eisen, M.B., Spellman, P.T., Brown, P.O., and Botstein, D. (1998). Cluster analysis and display of genome-wide expression patterns. Proc Natl Acad Sci U S A *95*, 14863-14868.

Esposito, F., Aragri, A., Pesaresi, I., Cirillo, S., Tedeschi, G., Marciano, E., Goebel, R., and Di Salle, F. (2008). Independent component model of the default-mode brain function: combining individual-level and population-level analyses in resting-state fMRI. Magn Reson Imaging *26*, 905-913.

Fair, D.A., Cohen, A.L., Dosenbach, N.U., Church, J.A., Miezin, F.M., Barch, D.M., Raichle, M.E., Petersen, S.E., and Schlaggar, B.L. (2008). The maturing architecture of the brain's default network. PNAS *105*, 4028-4032.

Fair, D.A., Cohen, A.L., Power, J.D., Dosenbach, N.U.F., Church, J.A., Miezin, F.M., Schlaggar, B.L., and Petersen, S.E. (2009). Functional brain networks develop from a "local to distributed" organization. PLoS Computational Biology *5*.

Fair, D.A., Dosenbach, N.U.F., Church, J.A., Cohen, A.L., Brahmbhatt, S., Miezin, F.M., Barch, D.M., Raichle, M.E., Petersen, S.E., and Schlaggar, B.L. (2007a). Development of distinct control networks through segregation and integration. Proc Natl Acad Sci U S A *104*, 13507-13512.

Fair, D.A., Schlaggar, B.L., Cohen, A.L., Miezin, F.M., Dosenbach, N.U., Wenger, K.K., Fox, M.D., Snyder, A.Z., Raichle, M.E., and Petersen, S.E. (2007b). A method for

using blocked and event-related fMRI data to study "resting state" functional connectivity. Neuroimage *35*, 396-405.

Felleman, D.J., and Van Essen, D.C. (1991). Distributed hierarchical processing in the primate cerebral cortex. Cerebral Cortex *1*, 1-47.

Fischl, B., Liu, A., and Dale, A.M. (2001). Automated manifold surgery: constructing geometrically accurate and topologically correct models of the human cerebral cortex. IEEE Trans Med Imaging *20*, 70-80.

Fischl, B., Sereno, M.I., and Dale, A.M. (1999). Cortical surface-based analysis. II: Inflation, flattening, and a surface-based coordinate system. Neuroimage *9*, 195-207.

Fox, M.D., Corbetta, M., Snyder, A.Z., Vincent, J.L., and Raichle, M.E. (2006a). Spontaneous neuronal activity distinguishes human dorsal and ventral attention systems. Proc Natl Acad Sci U S A *103*, 10046-10051.

Fox, M.D., Snyder, A.Z., Vincent, J.L., Corbetta, M., Van Essen, D.C., and Raichle, M.E. (2005). The human brain is intrinsically organized into dynamic, anticorrelated functional networks. Proc Natl Acad Sci U S A *102*, 9673-9678.

Fox, M.D., Snyder, A.Z., Zacks, J.M., and Raichle, M.E. (2006b). Coherent spontaneous activity accounts for trial-to-trial variability in human evoked brain responses. Nat Neurosci *9*, 23-25.

Fox, P.T., Huang, A., Parsons, L.M., Xiong, J.H., Zamarippa, F., Rainey, L., and Lancaster, J.L. (2001). Location-probability profiles for the mouth region of

human primary motor-sensory cortex: model and validation. Neuroimage *13*, 196-209.

Fox, P.T., Mintun, M.A., Reiman, E.M., and Raichle, M.E. (1988). Enhanced detection of focal brain responses using intersubject averaging and change-distribution analysis of subtracted PET images. Journal of Cerebral Blood Flow and Metabolism *8*, 642-653.

Fransson, P. (2005). Spontaneous low-frequency BOLD signal fluctuations: an fMRI investigation of the resting-state default mode of brain function hypothesis. Hum Brain Mapp *26*, 15-29.

Fransson, P., Skiold, B., Horsch, S., Nordell, A., Blennow, M., Lagercrantz, H., and Aden, U. (2007). Resting-state networks in the infant brain. Proc Natl Acad Sci U S A *104*, 15531-15536.

Friston, K., Jezzard, P., and Turner, R. (1994). Analysis of functional MRI time-series. Human Brain Mapping *1*, 153-171.

Friston, K.J., Frith, C.D., Liddle, P.F., and Frackowiak, R.S.J. (1991). Comparing functional (PET) images: The assessment of significant change. Journal of Cerebral Blood Flow and Metabolism *11*, 690-699.

Gao, W., Zhu, H., Giovanello, K.S., Smith, J.K., Shen, D., Gilmore, J.H., and Lin, W. (2009). Evidence on the emergence of the brain's default network from 2-week-old to 2-year-old healthy pediatric subjects. Proc Natl Acad Sci USA *106*, 6790-6795.

Genovese, C.R., Lazar, N.A., and Nichols, T. (2002). Thresholding of statistical maps in functional neuroimaging using the false discovery rate. Neuroimage *15*, 870-878.

Gong, G., Rosa-Neto, P., Carbonell, F., Chen, Z.J., He, Y., and Evans, A.C. (2009). Age- and gender-related differences in the cortical anatomical network. J Neurosci *29*, 15684-15693.

Grafton, S.T., Woods, R.P., and Mazziotta, J.C. (1993). Within-arm somatotopy in human motor areas determined by positron emission tomography imaging of cerebral blood flow. Experimental Brain Research *95*, 172-176.

Greicius, M. (2008). Resting-state functional connectivity in neuropsychiatric disorders. Curr Opin Neurol *21*, 424-430.

Greicius, M.D., Flores, B.H., Menon, V., Glover, G.H., Solvason, H.B., Kenna, H., Reiss, A.L., and Schatzberg, A.F. (2007). Resting-State Functional Connectivity in Major Depression: Abnormally Increased Contributions from Subgenual Cingulate Cortex and Thalamus. Biol Psychiatry.

Greicius, M.D., Krasnow, B., Reiss, A.L., and Menon, V. (2003). Functional connectivity in the resting brain: a network analysis of the default mode hypothesis. Proc Natl Acad Sci U S A *100*, 253-258.

Greicius, M.D., Srivastava, G., Reiss, A.L., and Menon, V. (2004). Default-mode network activity distinguishes Alzheimer's disease from healthy aging: evidence from functional MRI. Proc Natl Acad Sci U S A *101*, 4637-4642.

Grinvald, A., and Hildesheim, R. (2004). VSDI: a new era in functional imaging of cortical dynamics. Nat Rev Neurosci *5*, 874-885.

Hagmann, P., Cammoun, L., Gigandet, X., Meuli, R., Honey, C.J., Wedeen, V.J., and Sporns, O. (2008). Mapping the structural core of human cerebral cortex. PLoS Biol *6*, e159.

Hampson, M., Driesen, N.R., Skudlarski, P., Gore, J.C., and Constable, R.T. (2006a). Brain connectivity related to working memory performance. J Neurosci *26*, 13338-13343.

Hampson, M., Tokoglu, F., Sun, Z., Schafer, R.J., Skudlarski, P., Gore, J.C., and Constable, R.T. (2006b). Connectivity-behavior analysis reveals that functional connectivity between left BA39 and Broca's area varies with reading ability. Neuroimage *31*, 513-519.

Handl, J., Knowles, J., and Kell, D.B. (2005). Computational cluster validation in post-genomic data analysis. Bioinformatics *21*, 3201-3212.

He, Y., Wang, J., Wang, L., Chen, Z.J., Yan, C., Yang, H., Tang, H., Zhu, C., Gong, Q., Zang, Y., and Evans, A.C. (2009). Uncovering intrinsic modular organization of spontaneous brain activity in humans. PLoS ONE *4*, e5226.

Hickok, G., and Poeppel, D. (2007). The cortical organization of speech processing. Nat Rev Neurosci *8*, 393-402.

Honey, C.J., and Sporns, O. (2008). Dynamical consequences of lesions in cortical networks. Hum Brain Mapp *29*, 802-809.

Honey, C.J., Sporns, O., Cammoun, L., Gigandet, X., Thiran, J.P., Meuli, R., and Hagmann, P. (2009). Predicting human resting-state functional connectivity from structural connectivity. Proc Natl Acad Sci USA *106*, 2035-2040.

Hua, K., Oishi, K., Zhang, J., Wakana, S., Yoshioka, T., Zhang, W., Akhter, K.D., Li, X., Huang, H., Jiang, H.*, et al.* (2009). Mapping of functional areas in the human cortex based on connectivity through association fibers. Cereb Cortex *19*, 1889-1895.

Imig, T.J., Ruggero, M.A., Kitzes, L.M., Javel, E., and Brugge, J.F. (1977). Organization of auditory cortex in the owl monkey (Aotus trivirgatus). Journal of Comparative Neurology *171*, 111-128.

Jack, A.I., Shulman, G.L., Snyder, A.Z., McAvoy, M., and Corbetta, M. (2006). Separate modulations of human V1 associated with spatial attention and task structure. Neuron *51*, 135-147.

Jackson, J.H. (1870). A study of convulsions. In Selected writings of John Hughlings Jackson. On epilepsy and epileptiform convulsions Vol. 1, 1958, J. Taylor, ed. (London: Staples Press), pp. 8-36.

Johansen-Berg, H., Behrens, T.E., Robson, M.D., Drobnjak, I., Rushworth, M.F., Brady, J.M., Smith, S.M., Higham, D.J., and Matthews, P.M. (2004). Changes in connectivity profiles define functionally distinct regions in human medial frontal cortex. Proc Natl Acad Sci U S A *101*, 13335-13340.

Johansen-Berg, H., Behrens, T.E., Sillery, E., Ciccarelli, O., Thompson, A.J., Smith, S.M., and Matthews, P.M. (2005). Functional-anatomical validation and individual variation of diffusion tractography-based segmentation of the human thalamus. Cereb Cortex *15*, 31-39.

Kaas, J.H., Nelson, R.J., Sur, M., Lin, C.S., and Merzenich, M.M. (1979). Multiple representations of the body within the primary somatosensory cortex of primates. Science *204*, 521-523.

Kelly, A.M., Di Martino, A., Uddin, L.Q., Shehzad, Z., Gee, D.G., Reiss, P.T., Margulies, D.S., Castellanos, F.X., and Milham, M.P. (2008). Development of Anterior Cingulate Functional Connectivity from Late Childhood to Early Adulthood. Cereb Cortex.

Kerns, J.G. (2006). Anterior cingulate and prefrontal cortex activity in an FMRI study of trial-to-trial adjustments on the Simon task. Neuroimage *33*, 399-405.

Kim, J.-H., Lee, J.-M., Jo, H.J., Kim, S.H., Lee, J.H., Kim, S.T., Seo, S.W., Cox, R.W., Na, D.L., Kim, S.I., and Saad, Z.S. (2009). Defining functional SMA and pre-SMA subregions in human MFC using resting state fMRI: Functional connectivity-based parcellation method. Neuroimage.

Kiviniemi, V., Starck, T., Remes, J., Long, X., Nikkinen, J., Haapea, M., Veijola, J., Moilanen, I., Isohanni, M., Zang, Y.-F., and Tervonen, O. (2009). Functional segmentation of the brain cortex using high model order group PICA. Human brain mapping *30*, 3865-3886.

Klein, J.C., Behrens, T.E., Robson, M.D., Mackay, C.E., Higham, D.J., and Johansen-Berg, H. (2007). Connectivity-based parcellation of human cortex using diffusion MRI: Establishing reproducibility, validity and observer independence in BA 44/45 and SMA/pre-SMA. Neuroimage *34*, 204-211.

Kuhn, H.W. (1955). The Hungarian method for the assignment problem. Naval Res. Logist. Quart. *2*, 83-97.

Kurth, F., Eickhoff, S.B., Schleicher, A., Hoemke, L., Zilles, K., and Amunts, K. (2009). Cytoarchitecture and Probabilistic Maps of the Human Posterior Insular Cortex. Cereb Cortex.

Lancaster, J.L., Glass, T.G., Lankipalli, B.R., Downs, H., Mayberg, H., and Fox, P.T. (1995). A Modality-Independent Approach to Spatial Normalization of Tomographic Images of the Human Brain. Hum Brain Mapp *3*, 209-223.

Langers, D.R., Backes, W.H., and van Dijk, P. (2007). Representation of lateralization and tonotopy in primary versus secondary human auditory cortex. Neuroimage *34*, 264-273.

Leopold, D.A., Murayama, Y., and Logothetis, N.K. (2003). Very slow activity fluctuations in monkey visual cortex: implications for functional brain imaging. Cereb Cortex *13*, 422-433.

Levitt, P. (2003). Structural and functional maturation of the developing primate brain. J Pediatr *143*, S35-45.

Lewis, C.M., Baldassarre, A., Committeri, G., Romani, G.L., and Corbetta, M. (2009). Learning sculpts the spontaneous activity of the resting human brain. Proc Natl Acad Sci USA *106*, 17558-17563.

Lewis, J.W., and Van Essen, D.C. (2000a). Corticocortical connections of visual, sensorimotor, and multimodal processing areas in the parietal lobe of the macaque monkey. Journal of Comparative Neurology *428*, 112-137.

Lewis, J.W., and Van Essen, D.C. (2000b). Mapping of architectonic subdivisions in the macaque monkey, with emphasis on parieto-occipital cortex. Journal of Comparative Neurology *428*, 79-111.

Lim, J.S. (1990). Two-dimension signal and image processing (Englewood Cliffs, NJ: Prentice Hall).

Lowe, M.J., Mock, B.J., and Sorenson, J.A. (1998). Functional connectivity in single and multislice echoplanar imaging using resting-state fluctuations. Neuroimage *7*, 119-132.

Luks, T.L., Simpson, G.V., Dale, C.L., and Hough, M.G. (2007). Preparatory allocation of attention and adjustments in conflict processing. Neuroimage.

Lyttelton, O., Boucher, M., Robbins, S., and Evans, A. (2007). An unbiased iterative group registration template for cortical surface analysis. Neuroimage *34*, 1535-1544.

MacDonald, C.L., Schwarze, N., Vaishnavi, S.N., Epstein, A.A., Snyder, A.Z., Raichle, M.E., Shimony, J.S., and Brody, D.L. (2008). Verbal memory deficit following traumatic brain injury: assessment using advanced MRI methods. Neurology *71*, 1199-1201.

Margulies, D.S., Kelly, A.M.C., Uddin, L.Q., Biswal, B.B., Castellanos, F.X., and Milham, M.P. (2007). Mapping the functional connectivity of anterior cingulate cortex. Neuroimage *37*, 579-588.

Martin, A. (2007). The representation of object concepts in the brain. Annu Rev Psychol *58*, 25-45.

Maunsell, J.H.R., and Van Essen, D.C. (1983). The connections of the middle temporal visual ara (MT) and their relationship to a cortical hierarchy in the macaque monkey. Journal of Neuroscience *3*, 2563-2586.

Mencl, W.E., Pugh, K.R., Shaywitz, S.E., Shaywitz, B.A., Fulbright, R.K., Constable, R.T., Skudlarski, P., Katz, L., Marchione, K.E., Lacadie, C., and Gore, J.C. (2000). Network analysis of brain activations in working memory: behavior and age relationships. Microsc Res Tech *51*, 64-74.

Merzenich, M.M., Nelson, R.J., Kaas, J.H., Stryker, M.P., Jenkins, W.M., Zook, J.M., Cynader, M.S., and Schoppmann, A. (1987). Variability in hand surface representations in areas 3b and 1 in adult owl and squirrel monkeys. J Comp Neurol *258*, 281-296.

Miezin, F., Maccotta, L., Ollinger, J., Petersen, S., and Buckner, R. (2000). Characterizing the hemodynamic response: Effects of presentation rate, sampling procedure, and the possibility of ordering brain activity based on relative timing. NeuroImage *11*, 735-759.

Mishkin, M., Lewis, M.E., and Ungerleider, L.G. (1982). Equivalence of parieto-preoccipital subareas for visuospatial ability in monkeys. Behavioural brain research *6*, 41-55.

Mishkin, M., and Ungerleider, L.G. (1982). Contribution of striate inputs to the visuospatial functions of parieto-preoccipital cortex in monkeys. Behavioural brain research *6*, 57-77.

Mugler, J.P., and Brookeman, J.R. (1990). Three-dimensional magnetization-prepared rapid gradient-echo imaging (3D MP RAGE). Magnetic Resonance in Medicine *15*, 152-157.

Nelson, S.M., Cohen, A.L., Power, J.D., Wig, G.S., Miezin, F.M., Wheeler, M.E., Velanova, K., Donaldson, D.I., Schlaggar, B.L., and Petersen, S.E. (In Preparation). An integrated approach to studying parietal cortex and memory retrieval.

Nir, Y., Hasson, U., Levy, I., Yeshurun, Y., and Malach, R. (2006). Widespread functional connectivity and fMRI fluctuations in human visual cortex in the absence of visual stimulation. Neuroimage *30*, 1313-1324.

O'Leary, D.D., Schlaggar, B.L., and Tuttle, R. (1994). Specification of neocortical areas and thalamocortical connections. Annu Rev Neurosci *17*, 419-439.

Ojemann, J.G., Akbudak, E., Snyder, A.Z., McKinstry, R.C., Raichle, M.E., and Conturo, T.E. (1997). Anatomic localization and quantitative analysis of gradient refocused echo-planar fMRI susceptibility artifacts. Neuroimage *6*, 156-167.

Ollinger, J.M., Shulman, G.L., and Corbetta, M. (2001). Separating processes within a trial in event-related functional MRI I. The method. Neuroimage *13*, 210-217.

Pantazis, D., Joshi, A., Jiang, J., Shattuck, D.W., Bernstein, L.E., Damasio, H., and Leahy, R.M. (2009). Comparison of landmark-based and automatic methods for cortical surface registration. Neuroimage.

Parker, J.R. (1997). Algorithms for image processing and computer vision (New York: John Wiley & Sons, Inc.).

Passingham, R.E., Stephan, K.E., and Kotter, R. (2002). The anatomical basis of functional localization in the cortex. Nat Rev Neurosci *3*, 606-616.

Perlbarg, V., Puybasset, L., Tollard, E., Lehéricy, S., Benali, H., and Galanaud, D. (2009). Relation between brain lesion location and clinical outcome in patients with severe traumatic brain injury: a diffusion tensor imaging study using voxel-based approaches. Human brain mapping *30*, 3924-3933.

Petersen, S.E., Fox, P.T., Posner, M.I., Mintun, M., and Raichle, M.E. (1988). Positron emission tomographic studies of the cortical anatomy of single-word processing. Nature *331*, 585-589.

Petersen, S.E., Power, J.D., Cohen, A.L., Nelson, S.M., Wig, G.S., Miezin, F.M., Vogel, A.C., Church, J.A., and Schlaggar, B.L. (2009). Functionally defined regions across the brain organize into distinct community structures. In Society for Neuroscience (Chicago, IL).

Poldrack, R.A., and Mumford, J.A. (2009). Independence in ROI analysis: where is the voodoo? Social Cognitive and Affective Neuroscience *4*, 208-213.

Porro, C.A., Francescato, M.P., Cettolo, V., Diamond, M.E., Baraldi, P., Zuiani, C., Bazzocchi, M., and di Prampero, P.E. (1996). Primary motor and sensory cortex activation during motor performance and motor imagery: a functional magnetic resonance imaging study. J Neurosci *16*, 7688-7698.

Posner, M.I., and Petersen, S.E. (1990). The attention system of the human brain. Annual Review of Neuroscience *13*, 25-42.

Posner, M.I., Petersen, S.E., Fox, P.T., and Raichle, M.E. (1988). Localization of cognitive operations in the human brain. Science *240*, 1627-1631.

Raichle, M.E., MacLeod, A.M., Snyder, A.Z., Powers, W.J., Gusnard, D.A., and Shulman, G.L. (2001). A default mode of brain function. Proc Natl Acad Sci U S A *98*, 676-682.

Raichle, M.E., and Snyder, A.Z. (2007). A default mode of brain function: a brief history of an evolving idea. NeuroImage *37*, 1083-1090.

Ramsey, N.F., Kirkby, B.S., Van Gelderen, P., Berman, K.F., Duyn, J.H., Frank, J.A., Mattay, V.S., Van Horn, J.D., Esposito, G., Moonen, C.T., and Weinberger, D.R. (1996). Functional mapping of human sensorimotor cortex with 3D BOLD fMRI correlates highly with H2(15)O PET rCBF. J Cereb Blood Flow Metab *16*, 755-764.

Rombouts, S., and Scheltens, P. (2005). Functional connectivity in elderly controls and AD patients using resting state fMRI: a pilot study. Curr Alzheimer Res *2*, 115-116.

Rossion, B., and Pourtois, G. (2004). Revisiting Snodgrass and Vanderwart's object pictorial set: the role of surface detail in basic-level object recognition. Perception *33*, 217-236.

Roy, A.K., Shehzad, Z., Margulies, D.S., Kelly, A.M.C., Uddin, L.Q., Gotimer, K., Biswal, B.B., Castellanos, F.X., and Milham, M.P. (2009). Functional connectivity of the human amygdala using resting state fMRI. Neuroimage *45*, 614-626.

Rushworth, M.F., Behrens, T.E., and Johansen-Berg, H. (2006). Connection patterns distinguish 3 regions of human parietal cortex. Cereb Cortex *16*, 1418-1430.

Sabuncu, M.R., Singer, B.D., Conroy, B., Bryan, R.E., Ramadge, P.J., and Haxby, J.V. (2010). Function-based intersubject alignment of human cortical anatomy. Cereb Cortex *20*, 130-140.

Sakata, H., Mikami, A., and M. Fuster, J. (1997). The association cortex: structure and function. 317.

Salvador, R., Suckling, J., Schwarzbauer, C., and Bullmore, E. (2005). Undirected graphs of frequency-dependent functional connectivity in whole brain networks. Philos Trans R Soc Lond B Biol Sci *360*, 937-946.

Scheperjans, F., Hermann, K., Eickhoff, S.B., Amunts, K., Schleicher, A., and Zilles, K. (2007). Observer-Independent Cytoarchitectonic Mapping of the Human Superior Parietal Cortex. Cereb Cortex.

Schlaggar, B.L., Brown, T.T., Lugar, H.M., Visscher, K.M., Miezin, F.M., and Petersen, S.E. (2002). Functional neuroanatomical differences between adults and school-age children in the processing of single words. Science *296*, 1476-1479.

Schlaggar, B.L., and O'Leary, D.D. (1991). Potential of visual cortex to develop an array of functional units unique to somatosensory cortex. Science *252*, 1556-1560.

Schleicher, A., Morosan, P., Amunts, K., and Zilles, K. (2009). Quantitative architectural analysis: a new approach to cortical mapping. J Autism Dev Disord *39*, 1568-1581.

Schubotz, R.I., Anwander, A., Knösche, T.R., von Cramon, D.Y., and Tittgemeyer, M. (2009). Anatomical and functional parcellation of the human lateral premotor cortex. Neuroimage.

Ségonne, F., Dale, A.M., Busa, E., Glessner, M., Salat, D., Hahn, H.K., and Fischl, B. (2004). A hybrid approach to the skull stripping problem in MRI. Neuroimage *22*, 1060-1075.

Ségonne, F., Grimson, E., and Fischl, B. (2005). A genetic algorithm for the topology correction of cortical surfaces. Inf Process Med Imaging *19*, 393-405.

Sejnowski, T.J., Koch, C., and Churchland, P.S. (1988). Computational Neuroscience. Science *241*, 1299-1306.

Sereno, M.I., Dale, A.M., Reppas, J.B., Kwong, K.K., Belliveau, J.W., Brady, T.J., Rosen, B.R., and Tootell, R.B.H. (1995). Borders of multiple visual areas in humans revealed by functinal magnetic resonance imaging. Science *268*, 889-893.

Sidaros, A., Engberg, A.W., Sidaros, K., Liptrot, M.G., Herning, M., Petersen, P., Paulson, O.B., Jernigan, T.L., and Rostrup, E. (2008). Diffusion tensor imaging during recovery from severe traumatic brain injury and relation to clinical outcome: a longitudinal study. Brain *131*, 559-572.

Silver, M.A., and Kastner, S. (2009). Topographic maps in human frontal and parietal cortex. Trends Cogn Sci (Regul Ed) *13*, 488-495.

Simmons, W.K., Reddish, M., Bellgowan, P.S.F., and Martin, A. (2009). The Selectivity and Functional Connectivity of the Anterior Temporal Lobes. Cereb Cortex.

Singer, T., Critchley, H.D., and Preuschoff, K. (2009). A common role of insula in feelings, empathy and uncertainty. Trends Cogn Sci (Regul Ed) *13*, 334-340.

Skudlarski, P., Jagannathan, K., Calhoun, V.D., Hampson, M., Skudlarska, B.A., and Pearlson, G. (2008). Measuring brain connectivity: diffusion tensor imaging validates resting state temporal correlations. Neuroimage *43*, 554-561.

Snyder, A.Z. (1996). Difference image vs. ratio image error function forms in PET-PET realignment. In Quantification of Brain Function Using PET, R. Myer, V.J. Cunningham, D.L. Bailey, and T. Jones, eds. (San Diego, CA: Academic Press), pp. 131-137.

Sporns, O., Chialvo, D.R., Kaiser, M., and Hilgetag, C.C. (2004). Organization, development and function of complex brain networks. Trends Cogn Sci *8*, 418-425.

Stark, D.E., Margulies, D.S., Shehzad, Z.E., Reiss, P., Kelly, A.M.C., Uddin, L.Q., Gee, D.G., Roy, A.K., Banich, M.T., Castellanos, F.X., and Milham, M.P. (2008). Regional variation in interhemispheric coordination of intrinsic hemodynamic fluctuations. J Neurosci *28*, 13754-13764.

Stevens, M.C., Pearlson, G.D., and Calhoun, V.D. (2009). Changes in the interaction of resting-state neural networks from adolescence to adulthood. Human brain mapping *30*, 2356-2366.

Strick, P.L. (1988). Anatomical organization of multiple motor areas in the frontal lobe: Implications for recovery of function. In Advances in Neurology, S.G. Waxman, ed. (New York: Raven Press), pp. 293-312.

Supekar, K., Musen, M., and Menon, V. (2009). Development of Large-Scale Functional Brain Networks in Children. PLoS Biology *7*, e1000157.

Sur, M., and Leamey, C.A. (2001). Development and plasticity of cortical areas and networks. Nat Rev Neurosci *2*, 251-262.

Swallow, K.M., Braver, T.S., Snyder, A.Z., Speer, N.K., and Zacks, J.M. (2003). Reliability of functional localization using fMRI. Neuroimage *20*, 1561-1577.

Talairach, J., and Tournoux, P. (1988). Co-Planar Stereotaxic Atlas of the Human Brain (New York: Thieme Medical Publishers, Inc.).

Tian, L., Jiang, T., Wang, Y., Zang, Y., He, Y., Liang, M., Sui, M., Cao, Q., Hu, S., Peng, M., and Zhuo, Y. (2006). Altered resting-state functional connectivity patterns of anterior cingulate cortex in adolescents with attention deficit hyperactivity disorder. Neurosci Lett *400*, 39-43.

Turken, A., Whitfield-Gabrieli, S., Bammer, R., Baldo, J.V., Dronkers, N.F., and Gabrieli, J.D.E. (2008). Cognitive processing speed and the structure of white matter pathways: convergent evidence from normal variation and lesion studies. Neuroimage *42*, 1032-1044.

Uylings, H.B., Rajkowska, G., Sanz-Arigita, E., Amunts, K., and Zilles, K. (2005). Consequences of large interindividual variability for human brain atlases: converging macroscopical imaging and microscopical neuroanatomy. Anat Embryol (Berl) *210*, 423-431.

Van Dijk, K.R.A., Hedden, T., Venkataraman, A., Evans, K.C., Lazar, S.W., and Buckner, R.L. (2009). Intrinsic Functional Connectivity As a Tool For Human Connectomics: Theory, Properties, and Optimization. J Neurophysiol.

Van Essen, D.C. (1985). Functional organization of primate visual cortex. In Cerebral Cortex, A. Peters, and E.G. Jones, eds. (New York: Plenum Press), pp. 259-329.

Van Essen, D.C. (2004a). Organization of visual areas in macaque and human cerebral cortex. In The visual neurosciences, L.M. Chalupa, and J.S. Werner, eds. (MIT Press), pp. 507-521.

Van Essen, D.C. (2004b). Origin of visual areas in macaque and human cerebral cortex. In Visual Neuroscience, L.M. Chalupa, and J.S. Werner, eds. (Cambridge, MA: MIT Press), pp. 507-521.

Van Essen, D.C. (2005). A Population-Average, Landmark- and Surface-based (PALS) Atlas of Human Cerebral Cortex. Neuroimage *28*, 635-662.

Van Essen, D.C., Dickson, J., Harwell, J., Hanlon, D., Anderson, C.H., and Drury, H.A. (2001). An integrated software suite for surface-based analyses of cerebral cortex. J Am Med Inform Assoc *41*, 1359-1378. See also http://brainmap.wustl.edu/caret.

Van Essen, D.C., and Dierker, D. (2007a). On navigating the human cerebral cortex: Response to 'in praise of tedious anatomy'. Neuroimage *37*, 1050-1054.

Van Essen, D.C., and Dierker, D.L. (2007b). Surface-based and probabilistic atlases of primate cerebral cortex. Neuron *56*, 209-225.

Van Essen, D.C., and Drury, H.A. (1997). Structural and functional analyses of human cerebral cortex using a surface-based atlas. Journal of Neuroscience *17*, 7079-7102.

Van Essen, D.C., Newsome, W.T., and Maunsell, J.H. (1984). The visual field representation in striate cortex of the macaque monkey: asymmetries, anisotropies, and individual variability. Vision Res *24*, 429-448.

Vincent, J.L., Patel, G.H., Fox, M.D., Snyder, A.Z., Baker, J.T., Van Essen, D.C., Zempel, J.M., Snyder, L.H., Corbetta, M., and Raichle, M.E. (2007). Intrinsic functional architecture in the anesthetized monkey brain. Nature *447*, 46-47.

Vincent, J.L., Snyder, A.Z., Fox, M.D., Shannon, B.J., Andrews, J.R., Raichle, M.E., and Buckner, R.L. (2006). Coherent spontaneous activity identifies a hippocampal-parietal memory network. J Neurophysiol *96*, 3517-3531.

Vincent, L., and Soille, P. (1991). Watersheds in digital spaces: an efficient algorithm based on immersion simulations. IEEE Transactions of Pattern Analysis and Machine Intelligence *13*, 583-598.

Vul, E., and Pashler, H. (2008). Measuring the crowd within: probabilistic representations within individuals. Psychol Sci *19*, 645-647.

Warnking, J., Dojat, M., Guerin-Dugue, A., Delon-Martin, C., Olympieff, S., Richard, N., Chehikian, A., and Segebarth, C. (2002). fMRI retinotopic mapping--step by step. Neuroimage *17*, 1665-1683.

Wernicke, C. (1874). Der aphasische Symptomenkomplex: eine psychologische Studie auf anatomomischer Basis. In Wernicke's work on aphasia, 1977, G.H. Eggert, ed. (The Hague: Mouton), pp. 219-283.

Whalley, H.C., Simonotto, E., Marshall, I., Owens, D.G., Goddard, N.H., Johnstone, E.C., and Lawrie, S.M. (2005). Functional disconnectivity in subjects at high genetic risk of schizophrenia. Brain *128*, 2097-2108.

Wig, G.S., Buckner, R.L., and Schacter, D.L. (2009). Repetition priming influences distinct brain systems: evidence from task-evoked data and resting-state correlations. J Neurophysiol *101*, 2632-2648.

Winer, B.J., Brown, D.R., and Michels, K.M. (1991). Statistical Principles in Experimental Design, Third edn (Boston, Massachusetts: McGraw-Hill).

Winkler, A.M., Kochunov, P., Blangero, J., Almasy, L., Zilles, K., Fox, P.T., Duggirala, R., and Glahn, D.C. (2009). Cortical thickness or grey matter volume? The importance of selecting the phenotype for imaging genetics studies. Neuroimage.

Zhang, D., Johnston, J.M., Fox, M.D., Leuthardt, E.C., Grubb, R.L., Chicoine, M.R., Smyth, M.D., Snyder, A.Z., Raichle, M.E., and Shimony, J.S. (2009a). Preoperative sensorimotor mapping in brain tumor patients using spontaneous fluctuations in neuronal activity imaged with functional magnetic resonance imaging: initial experience. Neurosurgery *65*, 226-236.

Zhang, D., Snyder, A.Z., Shimony, J.S., Fox, M.D., and Raichle, M.E. (2009b). Noninvasive Functional and Structural Connectivity Mapping of the Human Thalamocortical System. Cereb Cortex.

Zilles, K., and Amunts, K. (2009). Receptor mapping: architecture of the human cerebral cortex. Curr Opin Neurol *22*, 331-339.

Zilles, K., Schleicher, A., Palomero-Gallagher, N., and Amunts, K. (2002). Quantitative analysis of cyto- and receptor architecture of the human brain. In Brain Mapping: The Methods, J.C. Mazziotta, and A. Toga, eds. (Academic Press), pp. 573-602.

Zuo, X.-N., Kelly, C., Adelstein, J.S., Klein, D.F., Castellanos, F.X., and Milham, M.P. (2009). Reliable intrinsic connectivity networks: Test-retest evaluation using ICA and dual regression approach. Neuroimage.